UNIVERSITÉ DE SHERBROOKE
Faculté de génie
Département de génie civil

INFLUENCE DE LA TAILLE ET DE LA GRADATION DES PARTICULES SUR LA RÉSISTANCE AU CISAILLEMENT ET LE COMPORTEMENT DILATANT DES MATÉRIAUX GRANULAIRES

Thèse de doctorat
Spécialité : génie civil

Samaneh AMIRPOUR HAREHDASHT

Jury : Mourad KARRAY (directeur)
Mathieu Nuth (rapporteur)
Michael James (membre externe)
Simon Grenier (membre externe)
Anna.Chiaradonna (membre externe)

Sherbrooke (Québec) Canada Novembre 2016

To my family
my wonderful parents
my gorgeous sisters Sara, and Solaleh

RÉSUMÉ

Cette étude examine l'impact de la taille et de la gradation de particules sur les corrélations théoriques et empiriques existantes les plus connues entre la résistance au cisaillement et le comportement dilatatant des matériaux granulaires en condition de déformation plane et en compression triaxiale drainée. À cette fin, 276 tests de cisaillements symétriques directs et 35 tests de compressions triaxiales drainées ont été menés sur des échantillons composés de billes de basalte (particules rondes), et de sables constitués de particules angulaires (sable de Péribonka et sable d'Eastmain) sur une échelle de 63 μm à 2000 μm afin d'évaluer leur résistance au cisaillement et leur comportement de dilatance sur une vaste échelle de pressions normales et de densités relatives initiales.

Premièrement, la fiabilité et l'applicabilité des limites de mesure à l'aide de tests physiques de cisaillements symétriques directs dans l'interprétation de la résistance au cisaillement frictionnel en déformation plane des matériaux granulaires ont été discutées et confirmées par l'usage du code informatique DEM, SiGran. L'accent a été particulièrement mis sur la validation du modèle DEM au moyen de comparaison des résultats des simulations DEM avec leurs équivalents physiques à une échelle macro. Les résultats virtuels DSA sont abordés du point de vue de la coaxialité entre les principales tensions et les principales directions des paliers de pression ainsi que de la déviation de la direction d'extension nulle à partir de la direction horizontale. Les résultats numériques fournissent également des données quantitatives sur les différentes formes d'énergie consommées durant le cisaillement confirmées par d'autres résultats physiques et numériques publiés.

Sur la base des postulats précédents, un examen minutieux des résultats des essais de cisaillements directs et de données issues de la littérature a été accompli afin d'évaluer la fiabilité des formules empiriques bien connues de Bolton et Collins *et al.* avec leurs constantes couramment employées en condition de déformation plane. L'étude montre qu'une application des relations empiriques de force-dilatation de cisaillement avec les constantes proposées par Bolton (1986) et Collins *et al.* (1992) aux sables ayant une distribution de taille de particules différente peut conduire à surestimer leurs valeurs en terme de force de cisaillement. Dans cette étude, les coefficients des équations de Bolton et Collins *et al.* ont donc été ajustée afin de prendre en compte les caractéristiques des particules, en particulier le diamètre médian, D_{50}.

De manière analogue, les effets microstructuraux imposés par la géométrie interne des particules (par exemple la taille, la forme et la gradation des particules) sur la relation tension-dilatation très connue, celle de Rowe (1962), et son ajustement empirique en condition triaxiale drainée ont été examinés dans cette étude. Une comparaison des prédictions des formules proposées avec les données de force de cisaillement issues de la littérature fournit de nombreuses preuves en faveur des contraintes mises en place au sein des relations existantes de force-dilatation de cisaillement en condition de déformation plane et triaxiale. Ces comparaisons prouvent également que la prise en compte de la taille des grains conduit à des résultats plus tangibles que lorsque la taille de la particule n'est pas considérée. Les formules de force-dilatation ajustées peuvent se révéler avantageuses pour évaluer indépendamment la cohérence des forces de cisaillement déterminées expérimentalement et pour introduire des lois d'écoulement plus précises dans les analyses géotechniques analytiques et numériques.

Mots-clés: la taille de la particule, la forme, la force de cisaillement, le comportement de dilatation, analyse numérique, assais expérimentale

ABSTRACT

The present study examines more closely the potential impact of particle size and gradation on the most famous existing theoretical and empirical correlations between the shear strength and the dilation behavior of granular materials in plane strain and drained triaxial compression conditions. For this purpose, 276 symmetrical direct shear and 35 drained triaxial compression tests have been carried out on samples made up of basalt beads (rounded particles), and sands consisting of angular particles (Péribonka sand and Eastmain sand) in the range of 63 μm to 2000 μm to evaluate their shear resistance and dilation behavior over a wide range of normal pressures and initial relative densities.

First, the reliability and applicability of boundary measurements in physical symmetrical direct shear tests to interpret the plane strain frictional shearing resistance of granular material have been discussed and confirmed using DEM computer code SiGran. Particular emphasis is placed on the validation of the DEM model by comparing the results of DEM simulations with their physical counterparts at the macro-scale. The virtual DSA results are discussed in terms of the coaxiality between the principal stresses and the principal strains increments directions as well as the deviation of the zero extension direction from the horizontal direction. The numerical results also provide quantitative data on different forms of energy consumed during shearing confirming other published physical and numerical results found in the literature.

Following the assumptions above, a close scrutiny of symmetrical direct shear test results and strength and dilation data from the literature have been done to evaluate the reliability of well-known empirical Bolton's and Collins et al.'s formulations with their commonly used constants in plane strain condition. The study shows that an application of empirical shear strength-dilation relationships with the constants proposed by Bolton (1986) and Collins et al. (1992) to sands with different particle-size distribution may strongly over-predict their shear strength values. In this study, the coefficients of Bolton's and Collins et al.'s equations have been, therefore, adjusted to account for particle characteristics, in particular for D_{50}.

Similarly, the microstructural effects imposed by internal particle geometry (e.g. particle-size, particle shape, and particle gradation) on most popular stress-dilatancy relationship of Rowe (1962), and its empirical adjustment in drained triaxial condition have been investigated in this study. A comparison of the predictions by the proposed formulas with shear strength data from the literature provides evidences in support of the implemented constraints into existing shear strength-dilation relations in plane strain and drained triaxial conditions. These comparisons also proves that accounting for the grain size yields more authentic results than when particle size is not considered. The adjusted strength-dilation formulas may be beneficial for independently assessing the consistency of the experimentally-determined shear strengths, and introducing more refined flow rules into analytical and numerical geotechnical analyses.

Key words: Particle size, Shape, Shear strength, Dilation, Numerical simulation, Experimental tests

REMERCIEMENTS

This dissertation could not have been finished without the help and support from many professors, research staff, graduate students, colleagues and my family. It is my great pleasure to acknowledge people who have given me guidance, help and encouragement.

First and foremost, I would like to express my sincere gratitude to my mentor, Prof. Mourad Karray for his patience, motivation, enthusiasm, immense knowledge and continuous support throughout my research. His guidance helped me in my research and writing of this thesis at all times. I could not have imagined having a better advisor and mentor for my PhD study. His timely advice, meticulous scrutiny, scholarly acumen and scientific approach has helped me in every way to accomplish this task.

I am grateful to Dr. Mahmoud N. Hussien for sharing his expertise during data analysis and interpretation. Despite his busy schedule, he spared the much needed time to finish my project on time. My special appreciation goes also to Dr. Mohamed Chekired and Dr. Varvara Roubtsova in Institut de Recherche d'Hydro-Québec, who provided me with valuable computer codes. They also gave me much information and discussion in this respect. I would like to extend my gratitude to the rest of my thesis committee, Prof. Mathieu Nuth, Prof. Michael James, Dr. Simon Grenier and Dr. Anna Chiaradonna for their encouragement, insightful comments, and timely suggestions.

I am also very grateful to all my colleagues in Civil Engineering Department of Université de Sherbrooke who helped me in numerous ways during various stages of my research. I take this opportunity to express my gratitude to Valérie Dumoulin for her helps and supports during my work in geotechnical and geo-environmental engineering laboratory.

Finally, I would express my gratitude to my parents, my sisters Sara and Solaleh, whose support and constant encouragement helped me through the hard times of this program. My deepest appreciation is expressed to them for their love, understanding, and inspiration. Without their blessings and encouragement, I would not have been able to finish this work.

TABLE DES MATIÈRES

LISTE DES FIGURES

LISTE DES TABLEAUX

LISTE DES SYMBOLES

Symbol	Definition
τ	Average horizontal shear stress
σ_n	Average vertical normal stress
σ_1, σ_3	major and minor principal stresses
R	Stress ratio, σ_1/σ_3
$d\varepsilon_v$, $d\varepsilon_a$	plastic components of the volumetric strain and axial strai
D	$d\varepsilon_v/d\varepsilon_a$
ϕ_μ	Inter-particle friction angle
ϕ_{ds}	Direct shear friction angle
ϕ_{ps}	Plane strain friction angle
ϕ_f	The mobilized friction angle at the onset of dilation
ψ	Dilation angle measured in boundaries
D_{50}	Mean particle size
C_u	Coefficient of uniformity
e_{max}, e_{min}	Maximum and minimum void ratios
e, e_{cr}	current and critical void ratios
ξ	state parameter (Been and Jefferies 1985) $(e-e_{cr})$
D_R	Relative density
q_{ult}	ultimate bearing capacity
$d\upsilon_y$, $d\upsilon_x$	Rate of change of vertical and horizontal displacements
$\Delta\theta$	Angle between principal stress and principal strain incremental directions
$\Delta\psi$	Difference in the computed dilation angle in boundaries to that inside the shear band
a	Second-order coefficient of contact normal anisotropy
a_n	Second-order coefficient of average contact normal force anisotropy

a_s , a_w	Second-order coefficient of average contact shear force anisotropy
$E(\theta)$	Density distribution function of contact normal
$\bar{f}_n^c$, $\bar{f}_t^c$	Contact normal force and shear force
θ_a	Second-order principal direction of contact normal anisotropy
θ_n	Second-order principal direction of average contact normal force anisotropy
θ_s	Second-order principal direction of average contact shear force anisotropy
E_k , E_p , E_e	Kinetic, potential, elastic energies
E_{dn}	Normal dissipation energy
E_{kt}	Kinetic energy of translation
E_{kr}	Kinetic energy of rotation
E_f	Friction energy
E_{fd}	Dissipation energy in tangential direction
E_{Md}	Work of dissipation moment
$\Delta\theta$	Non-coaxial angle
$d\nu$, $d\gamma$	Invariants of volumetric and shear strain increments
F_{33}, F_{11}	Fabric tensor components in the axial and radial directions (Wan and Gue 2000)
X , a	Material constants (Wan and Gue 2000)
CN	Coordination number

LISTE DES ACRONYMES

Abbreviation	**Definition**
DSA	Direct Shear Apparatus
DEM	Discrete Element Method
SEM	Scanning Electron Microscope

CHAPITRE 1. Introduction

1.1. Introduction (Français)

1.1.1 Contexte général du projet

Depuis des temps immémoriaux, le sol a été employé à des fins technologiques telles que les structures porteuses au moyen des fondations, la construction de remblais, les trottoirs et les structures de conservation. Avant le développement de la mécanique du sol, tout ceci se faisait sur base de connaissances acquises par l'approche par essai-erreur et par l'expérience. La percée principale dans l'étude scientifique du comportement de sol est attribuée à Coulomb (1773), qui fut le premier à présenter le concept de résistance au cisaillement d'un sol. Selon sa théorie, la résistance au cisaillement du sol peut être divisée en deux composantes, à savoir la cohésion et le frottement interne. L'on dut attendre jusqu' 1920 pour que Terzaghi précise la limitation de la loi de Coulomb, accomplisse un progrès réel dans la connaissance des propriétés fondamentales de la résistance au cisaillement et invente le terme mécanique du sol. La question de la résistance au cisaillement fut aussitôt reprise par d'autres chercheurs et les premiers appareillages de cisaillement direct semblables à leur forme actuelle furent construits (Bolton 1986; Casagrande 1936; Krey 1926; Lee et Seed 1967; Roscoe 1970; Rowe 1962; Skinner 1969). Le premier appareil de compression triaxiale fut également construit par Casagrande et Albert (1930) au Massachusetts Institute of Technology. Le noyau de ces dernières recherches reposait principalement sur des expérimentations en laboratoire sur des échantillons drainés ou non drainés de sol dans des appareils géotechniques standards développés au cours de cette période (tableau 1.1).

De par cette longue histoire d'expériences, les chercheurs ont conclu que la résistance au cisaillement d'un matériau non cohésif peut être représentée par un paramètre simple, l'angle de frottement mobilisé. Il a été suggéré que ce paramètre comporte trois composantes principales: le frottement coulissant intrinsèque (contrôlé par ϕ_μ l'angle du glissement interparticulaire), la résistance mobilisée par la dilatation et la résistance mobilisée par la remise en ordre et le blocage des particules (Figure 1.1). Le paramètre ϕ_μ a été défini différemment par différents

Tableau 1.1 Développement des appareils de laboratoire en mécanique du sol (Tan et al. 2006).

Developed apparatus	Key references
Direct shear test	Collin (1846), Krey (1926), Casagrande (1936) and Terzaghi (1948)
Oedometer apparatus	Terzaghi (1943), Casagrande (1936), Bishop (1982)
Compaction test	Proctor (1933)
Ring shear apparatus	Cooling and smith (1936), Bishop et al. (1971), Bromhead (1979)
Triaxial cell	Casagrande (1930), Taylor (1948)
Cyclic triaxial cell	Grainger and Lister (1962)
Plane strain cell	Cornforth (1964)
Biaxial apparatus	Hambly (1969a)
True triaxial apparatus	Hambly (1969b), Ko and Scott (1967), Sture and Desai (1979)
Hollow cylinder apparatus	Kirkpatrick (1957), Saada and Baah (1967), Hight et al. (1983)
Resonant column apparatus	Hardin and Drnevich (1972), Drnevich et al. (1978)
Undrained triaxial test	Bishop and Eldin (1951)
Effective stress triaxial testing	Bishop and Henkel (1957)

chercheurs en mécanique du sol, mais est généralement pris pour le coefficient moyen de frottement cinétique produit quand une particule typique de sol est amenée à glisser lentement au-dessus d'autres par un déplacement significatif (Procter et Barton 1974).

La dilatation d'un matériau granulaire a été discutée pour la première fois par Reynolds (1885), se trouvant décrite comme un changement du volume associé à la déformation de cisaillement d'un élément dans un matériau que l'on suppose macroscopique et assez grand pour contenir beaucoup de particules comme micro-éléments. Rowe (1962), qui proposa la théorie de la contrainte de cisaillement–la dilatance de cisaillement, prouva que même lorsque les termes de Taylor-Bishop sont appliqués aux essais de cisaillement, l'angle résultant du frottement dépasse toujours l'angle de frottement interparticulaire ϕ_μ des particules comportant un matériau granulaire. Il en conclut que dans la plupart de la gamme d'indices des vides, se retrouve une troisième composante de la résistance au cisaillement autre que la résistance de friction et que la dilatation, qui est développée par l'énergie nécessaire pour réarranger et réorienter des particules de sols.

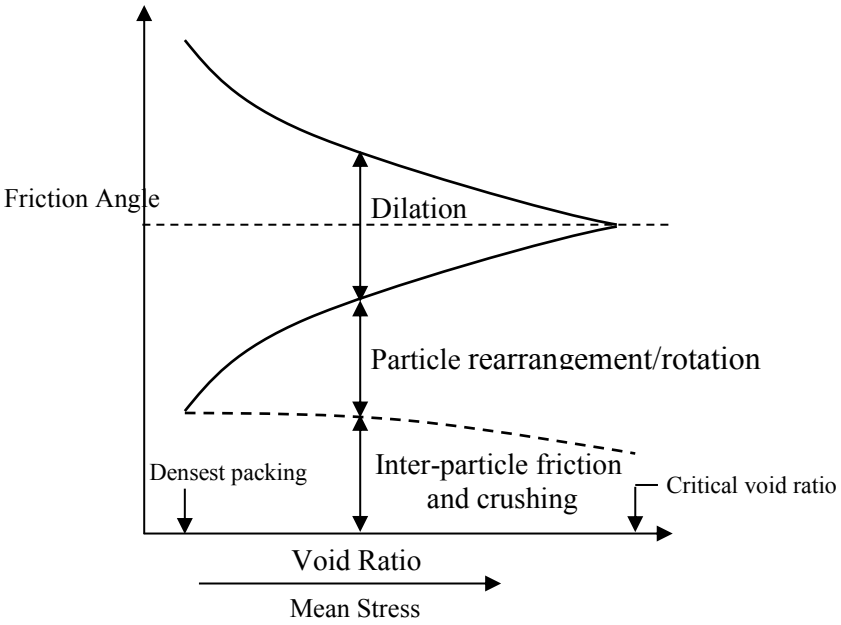

Figure 1.1 résistance au cisaillement des matériaux granulaires

Des progrès significatifs ont été accomplis afin d'indiquer que l'effet des conditions de chargement et de macrostructure ainsi que des caractéristiques des particules sur l'angle de frottement interparticulaire (Cavarretta et al. 2010; Lee et Seed 1967; Liu et Matsuoka 2003; Procter et Barton 1974; Rowe 1962; Skinner 1969; Thornton 2000), l'emballage des particules et leur réarrangement (Guo et Su 2007 ; Lee et Seed 1967 ; Rowe 1962), la dilatation (Bishop 1954; Bolton 1986; Collins et al. 1992; Newland et Allely 1957; Rowe 1962; Schanz et Vermeer 1996; Skempton et Bishop 1950; Taylor 1948), et leur corrélation avec l'angle de résistance au cisaillement.

Le comportement mécanique des matériaux granulaires gravite naturellement autour de la dilatation et de son rapport à la résistance au cisaillement, qui est régie par un certain nombre de facteurs tels que l′indice des vides, les pressions de confinement, l'histoire précédente des déformations ainsi que le chemin de contrainte. Les études menées afin d'établir les lois de rupture, expliquant ce rapport, proviennent d'un théorie proposée il y a plusieurs décennies par Casagrande (1936) et développée par d'autres chercheurs (Bolton 1986; Rowe 1962). En employant les critères de rupture, une gamme complète de résistance du sol peut être obtenue suivant les diverses combinaisons de densité et de contrainte, ce qui peut se révéler salutaires à des fins pratiques :

- Pour le contrôle indépendant des interprétations conventionnelles d'essai, ainsi que l'évaluation de l'uniformité des essais (Bolton 1986; Jewell 1989).

- Pour des études de faisabilité et des calculs de conception préliminaire, avant que des mesures in situ ou en laboratoire aient été effectuées.

- Pour des calculs finaux de conception dans des petits projets où les coûts d'un essai approprié de la résistance au cisaillement ne sont pas justifiés.

Nous devons noter que bien que la dilatation soit toujours importante en tant que contrôlant de l'angle approprié du frottement, on retrouve également beaucoup de cas où la dilatation du sol elle-même a une autre influence sur l'analyse géotechnique et qui doivent être prise en compte dans les calculs :

- En introduisant les équations de lois d'écoulement à la théorie de l'expansion de la cavité afin de présenter l'histoire de la déformation de la dépendance à la résistance du sol (l'angle de frottement et la dilatation), tout en interprétant des essais in situ (pénétromètres de cône, et pressiomètre, et en prévoyant le comportement des pieux dans des sols dilatants (Baligh 1976; Hughes et al. 1977; Salgado et Randolph 2001; Vesic 1972; Yu et Houlsby 1991).

- Examiner la dilatation afin de simuler le comportement non linéaire de déformation et la rupture à la frontière de excavations souterraines (Marshall et al. 2012; Yu et Rowe 1999).

- Examiner la dépendance du niveau de contrainte du sol dans le calcul de la capacité portante et du comportement de charge-déplacement des fondations. (Perkins et Madson 2000; Yamaguchi et al. 1976; Zienkiewicz et al. 1975).

- Proposer le taux de dilatation ou le taux d'expansion pour donner une mesure de la résistance à la liquéfaction (Vaid et al. 1981).

Plusieurs théorisations (Bishop 1954; Newland et Allely 1957; Rowe 1962, 1969; Schofield et 1968 Wroth; Skempton et Bishop 1950; Taylor 1948) considèrent que certains principes dans le mécanisme de dissipation de l'énergie expliquent la relation entre l'angle de frottement et la

dilatation. Cependant, les complexités des lois théoriques d'écoulement semblent présenter un obstacle important à l'exécution réussie et durable dans le cadre des modèles de sol.

Cela a motivé plusieurs chercheurs (Bolton 1986; Collins et al. 1992) à établir des équations empiriques complètes, mais simples, comportant relativement peu de paramètres matériels, comme solutions de rechange aux lois théoriques d'écoulement, pour une mise en application tout aussi facile dans les modèles géotechniques. La loi d'écoulement empirique la plus célèbre a été proposée par Bolton (1986). Cette loi rapporte l'angle de dilatation au niveau de contrainte et à la densité relative du sable et a été employée largement dans la littérature. Cette loi d'écoulement est développée comme un ajustement empirique à la relation de contrainte de cisaillement–dilatance de cisaillement de Rowe. Alternativement, Been et Jefferies (1985) ont observé des tendances fortes quand le paramètre d'état ξ a été tracé avec des valeurs correspondantes de résistance et de dilatation au cisaillement, menant au modèle empirique de Collins et al. (1992). Ces deux lois empiriques d'écoulement ont été adoptées de manière interchangeable dans l'analyse géotechnique afin de rendre compte de la dilatation dans des matériaux frictionnels (Salgado et Randolph 2001; Yu et Houlsby 1991).

Après la recherche pionnière de (Rowe 1962), beaucoup de contributions postérieures sur la modélisation du sable (Bolton 1986; Houlsby 1991b; Nemat-Nasser 1980; Vaid et Sasitharan 1992), considèrent la dilatation comme une fonction unique du rapport de contrainte et de l'état initial du sol, de sorte que la notion de dépendance microstructurale n’est pas prise en compte dans leurs formulations.

Cependant, un examen plus approfondi de la dilatation indique que le comportement des matériaux granulaires est plus subtil, et que la dilatation est la manifestation d'une contrainte cinématique interne impliquant certaines caractéristiques des particules (forme, taille), en tant qu'éléments de base participant à la déformation de la masse granulaire, et d’une connectivité du frottement interparticulaire à l’oeuvre contre la contrainte appliquée (Wan et Guo 2000, 2001). Par conséquent, dans tous les cas, la description de la loi d'écoulement comme facteur clé décrivant le comportement du matériau granulaire, influencera de manière significative l'exécution d'un modèle constitutif et la description insatisfaisante des lois d'écoulement sans

considérer que les caractéristiques micros de la structure puisse affecter la prédicabilité du modèle quant au changement du volume et à la déformation.

1.1.2 Problématique

En dépit de progrès significatifs indiquant l'effet du frottement interparticulaire (Cavarretta et al. 2010; Liu et Matsuoka 2003; Procter et Barton 1974; Rowe 1962; Skinner 1969; Thornton 2000), la forme des particules (Guo et Su 2007; Peña et al. 2007; Santamarina et Cho 2004) ou les caractéristiques de la texture (Cavarretta et al. 2010; Haruyama 1969; Procter et Barton 1974) sur la résistance au cisaillement et la dilatation du matériau granulaire:

- Jusqu'ici, il n'y a eu aucun consensus quant à l'effet de la taille des particules sur la dilatation et sur résistance au cisaillement du matériau granulaire.

- Peu d'études isolent l'effet de la distribution de la taille des particules d'autres facteurs tels que l'angularité du grain. Cependant, aucune évaluation systématique n'a été faite pour évaluer l'importance de la résistance au cisaillement et de la variation de dilatation pour des distributions différentes de taille de particules en ce qui concerne l'angularité des particules (les particules arrondies, sub-angulaires, ou angulaires) d'un type donné de sable.

- Les équations théoriques et empiriques existantes exprimant la relation entre la résistance au cisaillement et la dilatation, ont été traditionnellement développées sans considération explicite des microstructures fortement affectées par des propriétés de particules (taille des particules, forme des particules et aspérité). Un examen rigoureux des données rapportées dans la littérature amène une remise en cause de la précision des formulations empiriques reconnues, telles que les équations de Bolton et de Collins et autres pour prévoir la force - relation de dilatation des matériaux granulaires. Ces rapports empiriques, en fait, ne contiennent aucune fonction tenant compte des caractéristiques constitutives des particules (par exemple, la dimension particulaire, la forme de particules et la gradation des particules) et aucune limite de dimension des particules n'est imposée à leurs validités.

- Malgré l'application étendue des lois empiriques d'écoulement dans des analyses géotechniques, les équations empiriques proposées avec les constantes données ont été

présentées en employant un nombre extrêmement limité de données sans considération explicite des caractéristiques de grain telles que la forme des particules, et la distribution de la dimension particulaire.

Étant donné le rôle notable des lois d'écoulement dans l'analyse géotechnique et leurs points faibles susmentionnés, contribuer à un meilleur arrangement fondamental de l'effet de la distribution de la taille des particules sur des dilatations et le comportement de cisaillement du matériau granulaire semble salutaire. Le résultat de ces recherches peut également éclaircir la question de l'influence de la courbe de distribution de la taille des particules sur le lien direct entre les maximaux de la résistance au cisaillement et de la dilatation du sol granulaire.

1.1.3 Objectifs

L'objectif principal de la thèse est d'évaluer l'influence des caractéristiques des particules (la taille des particules, la forme des particules et la gradation des particules) sur le comportement de dilatation des matériaux granulaires et de sa contribution à la résistance au cisaillement par des études expérimentales. À cette fin, seize courbes différentes de distribution de la taille des particules de trois matériaux différents (billes en basalte, sable de Péribonka, et sable d'Eastmain) dans une gamme allant de 63 μm à 2000 μm ont été examinés dans des essais de cisaillements symétriques directs et de compression triaxiales à différentes contraintes normales et densités relatives initiales.

Des simulations numériques des essais de cisaillements symétriques directs modifiés ont été également effectuées afin d'examiner et d'évaluer la justesse de l'appareil de cisaillement direct (DSA). L'objectif était aussi de d'examiner les ambiguïtés résultant de la complexité des distributions de la contrainte et de la déformation impliquées. Les objectifs principaux de cette thèse peuvent être sous-catégorisés comme suit:

- **Proposer un cadre fournissant un premier aperçu de l'influence des paramètres correspondant à la nature des particules de sable (taille des particules, gradation et forme) qui affecteraient la dilatation et la résistance au cisaillement des matériaux granulaires.** À cette fin, les relations de contraintes de cisaillement–dilatance de cisaillement existantes sont étudiées en détail, et les disparités parmi les estimations de dilatation des relations de contraintes de cisaillement–dilatance de cisaillement existantes pour différents

matériaux sont discutées. Après examen de la sensibilité de la résistance de dilatation et de cisaillement du matériau granulaire aux caractéristiques des particules, les corrélations théoriques et empiriques reconnues de résistance au cisaillement–dilatation de cisaillement ont été élaborées dans des conditions de déformation plane triaxiale en impliquant les facteurs les plus importants.

- **Évaluer la précision des formulations empiriques connues, telles que les équations de Bolton et de Collins et autres par l'examen rigoureux des données rapportées dans la littérature.** Ces relations ne contiennent aucune fonction tenant compte des caractéristiques constitutives des particules, et aucune limite de dimension des particules quant à leurs validités.

- **Ajuster les coefficients des équations de Bolton et de Collins et autres pour expliquer les caractéristiques des particules (par exemple, D_{50} et la taille des particules) en état de condition de déformation plane.** À cette fin, 276 essais de cisaillements symétriques directs ont été effectués sur des échantillons composés de billes de basalte (particules arrondies), et de sables composés de particules angulaires (sable de Péribonka et sable d'Eastmain) dans la gamme de µm 63 au µm 2000 pour obtenir les valeurs de frottement maximal ϕ'_{max} et de dilatation d'angle ψ_{max} sur un éventail de tensions normales et de densités relatives initiales.

- **Présenter les résultats numériques obtenus à partir du code informatique de la DEM SiGran (Roubtsova et al. 2011) pour justifier la fiabilité et l'applicabilité des limites de mesure dans le test de cisaillement symétrique direct.** Un accent particulier est mis sur la validation du modèle de la DEM en comparant les résultats des simulations de la DEM à leurs contreparties physiques à la macro-échelle.

- **Évaluer les impacts potentiels de la taille des particules sur les contraintes de cisaillement–dilatance de cisaillement du matériau granulaire pendant les essais de compression triaxiale** drainée**.** La corrélation de la constante matérielle α de Wan et l'équation de contrainte de cisaillement-dilatance de cisaillement de Guo modifiée avec D_{50} ont été mises au point. En outre, les coefficients d'équation de Vaid et de Sasitharan comme

ajustement expérimental de l'équation de contrainte de cisaillement–dilatance de cisaillement de Rowe pour la compression triaxiale ont été ajustés pour tenir compte du D_{50}.

1.1.4 Contribution et originalité

Afin d'atteindre l'objectif de ce projet de recherche, un grand nombre d'essais en laboratoire ont été exécutés sur des matériaux composés de particules de différentes tailles et angularités. Une évaluation des équations entre la contrainte de cisaillement–dilatance de cisaillement expliquant la taille des particules, la gradation et la forme a été faite en comparant les résultats prévus aux données de la littérature. Des simulations numériques sont présentées dans cette étude afin de soutenir la fiabilité et l'applicabilité des limites de mesure à l'aide de tests physiques de cisaillements symétriques directs. Les formules de résistance au cisaillement -dilatation ajustées peuvent se révéler avantageuses pour évaluer indépendamment la cohérence des forces de cisaillement déterminées expérimentalement et pour introduire des lois d'écoulement plus précises dans les analyses géotechniques analytiques et numériques.

- **Cette étude a imposé des limites de taille de particules à la validité des rapports de dilatation-résistance au cisaillement les plus reconnues en condition de déformation plane et de compression triaxiale (Bolton 1986; Collins et al. 1992; Rowe 1962; Vaid et Sasitharan 1992; Wan et Guo 1999)**. Cette étude prouve que la considération explicite des caractéristiques du grain de sol (par exemple, la condition de déformation plane, la forme des particules et la gradation des particules) peut fortement affecter des valeurs de dilatation et de résistance au cisaillement du matériau granulaire.

- **Une analyse respective des données de résistance au cisaillement et de dilatation rassemblées dans la littérature, ainsi que le grand nombre de résultats de tests en laboratoire sont présentés dans cette étude pour discuter la fiabilité des équations de Bolton.** Bien que l'importance des rapports proposés soit indéniable, il apparaît que leur précision est remise en cause, car ils ont été présentés en recourant à un nombre limité de données et dans des conditions de déformation plane.

- **Dans cette étude, la simulation numérique de la DEM en employant SiGran inclut le vrai nombre de particules, et la taille réelle de l'appareil de cisaillement direct dans la**

simulation à trois dimensions. Les études antérieures au moyen de la DEM sur *l'appareil* de cisaillement direct se limitaient aux simulations à deux dimensions du cisaillement direct (Masson et Martinez 2001; Potts et al. 1987; Wang et al. 2007; Zhang et Thornton 2007) ou tridimensionnelles avec un nombre restreint de particules (Cui et O' Sullivan 2006). En outre, dans l'étude actuelle, une validation quantitative du modèle de la DEM est tentée en rapportant une série d'essais physiques aux simulations équivalentes de la DEM. En comparaison aux études antérieures qui manquent de validation quantitative, ce couplage des simulations numériques aux essais physiques permet aux auteurs de formuler des conclusions plus assurées au sujet de la micromécanique de la réponse de l'échantillon à partir des simulations de la DEM.

Cette thèse reflète le contenu de trois articles soumis, dans le journal de Geotechnical and Geoenvironmental Engineering, de l'ASCE, du journal de Computer and Geotechnics, et de l'International Journal of Geomechanics. Quatre communications évaluées par des pairs (peer-reviewed) ont également résulté de la recherche actuelle.

1.1.5 Structure de la thèse

La structure de la thèse est organisée selon les chapitres suivants:

Chapitre 1, introduction : inclut le rapport, les objectifs et la portée du problème de la recherche.

Chapitre 2, revue de littérature : ce qui inclut la définition des paramètres de résistance au cisaillement, de ses composantes, et de l'analyse des relations de contrainte de cisaillement–dilatance de cisaillement existantes. Ce chapitre illustre également quelques cas où la dilatation du sol et sa contribution à la résistance au cisaillement a une autre influence sur l'analyse géotechnique.

Chapitre 3 : Premier article de journal scientifique soumis : Cet article réexamine les contraintes et les déplacements obtenus aux limites du DSA par des simulations par la méthode des éléments discrets [DEM] (3D) des essais physiques sur des échantillons de particules polydispersées en employant le code informatique SiGran. Basé sur un examen complet des accomplissements progressifs de l'interprétation des données et du développement du DSA

inclus dans ce chapitre, l'exécution de l'appareil physique de cisaillement direct est optimisée en explorant des modifications sur la configuration de test symétrique. L'équilibre entre le changement de micro-échelle de l'énergie des particules et le travail de macro-échelle des forces externes est également présenté. Afin d'atteindre des conclusions assurées au sujet de la réponse de la micromécanique des échantillons de l'appareil de cisaillement direct, les validations quantitatives des modèles de la DEM sont testées en rapportant les essais physiques aux simulations correspondantes de la DEM.

Chapitre 4, deuxième article de journal scientifique soumis : inclut des analyses et l'examen des résultats expérimentaux en employant des cisaillements symétriques directs modifiés. Une analyse respective des données de résistance au cisaillement et de dilatation collectées de la littérature est présentée ce chapitre pour discuter la fiabilité des équations de Bolton. Le chapitre actuel examine alors de manière plus approfondie l'impact potentiel de la taille des particules et de la gradation des corrélations empiriques existantes entre l'angle de frottement et le comportement de dilatation des matériaux granulaires en état de contrainte plate. Après examen de la sensibilité de ces corrélations avec les caractéristiques des particules, les coefficients des équations de Bolton et de Collins et autres ont été ajustés pour rendre compte des caractéristiques des particules.

Chapitre 5, troisième article de journal scientifique soumis : inclut des analyses et l'examen des résultats expérimentaux des essais de compression triaxiale drainée. Ce chapitre examine de manière plus approfondie l'impact potentiel de l'information microstructurale imposée par la géométrie interne des particules (par exemple, la taille des particules, la forme des particules et la gradation des particules) sur la contrainte de cisaillement–dilatance de cisaillement du matériau granulaire pendant l'essai triaxial conventionnel. Dès lors, l'effet microstructural pris en compte dans le calcul de l'équation de la contrainte de cisaillement–dilatance de cisaillement et dans son ajustement empirique en état de condition triaxiale en étant traité en tant que contrainte imposée par la taille des particules et l'obliquité constitutives. En outre, les données expérimentales triaxiales des divers matériaux granulaires sont recueillies à partir de la littérature de manière à élargir les preuves à l'appui des contraintes mises en application dans des relations de la contrainte de cisaillement–dilatance de cisaillement.

Chapitre 6, conclusions et recommandation : inclut les résultats principaux et les découvertes, les contributions potentielles et les applications de la recherche ainsi que les recommandations pour la future recherche découlant de cette thèse.

1.2. Introduction (Anglais)

5.3.4 General context of this research project

From time immemorial, soil has been used for engineering purposes such as supporting structures through foundations, construction of embankments, pavements and retaining structures. Before the development of soil mechanics, this was done purely based on knowledge gained through trial and error approach and experience. The major breakthrough in the scientific study of soil behavior is credited to Coulomb (1773), who was the first to introduce the concept of the shearing resistance of soil. According to his theory, the shearing resistance of soil can be devided into two components, namely cohesion and internal friction. It was as late as 1920 that Terzaghi pointed out the limitation of Coulomb's law, made real progress in the knowledge of fundamental shear strength properties, and coined the term "soil mechanics". The question of shear strength was soon taken up by other researchers and the first direct shear apparatus similar to its present form were constructed (Bolton 1986; Casagrande 1936; Krey 1926; Lee and Seed 1967; Roscoe 1970; Rowe 1962; Skinner 1969). The first triaxial compression machine was also constructed by Casagrande and Albert (1930) at the Massachusetts institute of Technology. The core of these researches relied primarily on laboratory experimentations on drained or undrained soil samples in standard geotechnical apparatuses that were developed during that period (Table 1.1).

Through this long history of experimentation, researchers concluded that the shear resistance of a cohesionless material can be represented by a single parameter, the mobilized angle of friction. It has been suggested that this parameter comprises three main components: intrinsic sliding friction (controlled by ϕ_μ the angle of inter-particle sliding), resistance mobilized by dilation and resistance mobilized by particle rearrangement and interlocking (Figure 1.1). The parameter ϕ_μ has been defined variously by different researchers in soil mechanics, but is generally taken to the average coefficient of kinetic friction generated when one typical soil particle is caused to slide slowly over another through a significant displacement (Procter and Barton 1974).

Table 1.2 Development of mostly used laboratory apparatus (Tan et al. 2006)

Developed apparatus	Key references
Direct shear test	Collin (1846), Krey (1926), Casagrande (1936) and Terzaghi (1948)
Oedometer apparatus	Terzaghi (1943), Casagrande (1936), Bishop (1982)
Compaction test	Proctor (1933)
Ring shear apparatus	Cooling and smith (1936), Bishop et al. (1971), Bromhead (1979)
Triaxial cell	Casagrande (1930), Taylor (1948)
Cyclic triaxial cell	Grainger and Lister (1962)
Plane strain cell	Cornforth (1964)
Biaxial apparatus	Hambly (1969a)
True triaxial apparatus	Hambly (1969b), Ko and Scott (1967), Sture and Desai (1979)
Hollow cylinder apparatus	Kirkpatrick (1957), Saada and Baah (1967), Hight et al. (1983)
Resonant column apparatus	Hardin and Drnevich (1972), Drnevich et al. (1978)
Undrained triaxial test	Bishop and Eldin (1951)
Effective stress triaxial testing	Bishop and Henkel (1957)

The shear dilatancy of a granular material was first discussed by Reynolds (1885), and described as the change in volume that is associated with shear distortion of an element in the material which is assumed to be macroscopic and large enough to contain many particles as micro-elements. Rowe (1962), who proposed stress-dilatancy theory, showed that even when the Taylor-Bishop expressions are applied to shear test data, the resulting angle of friction still exceeds the angle of inter-particle friction ϕ_μ of the particles comprising a granular material. He concluded that throughout most of the range of void ratios there is third component of shear strength other than frictional resistance and dilation, which is developed by energy required to rearrange and reorient soils particles.

Significant progress has been made to indicate the effect of loading and macrostructure conditions as well as the particle level's characteristics on the inter-particle friction angle (Cavarretta et al. 2010; Lee and Seed 1967; Liu and Matsuoka 2003; Procter and Barton 1974; Rowe 1962; Skinner 1969; Thornton 2000), particle packing and rearrangements (Guo and Su 2007; Lee and Seed 1967; Rowe 1962), dilation (Bishop 1954; Bolton 1986; Collins et al. 1992; Newland and Allely 1957; Rowe 1962; Schanz and Vermeer 1996; Skempton and Bishop 1950; Taylor 1948), and their correlation with the shearing resistance.

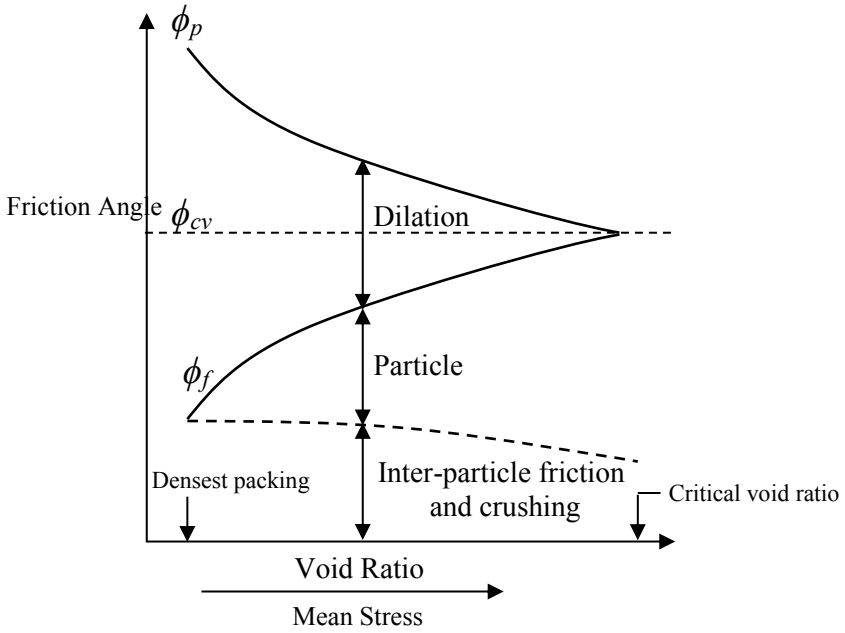

Figure 1.2 Contributions to shearing resistance of granular materials

The mechanical behavior of granular materials significantly influenced by dilatancy and its relationship with the shearing resistance, which is governed by a number of factors such as void ratio, confining stresses, previous deformation history as well as the stress path. Investigations to establish flow rules, explaining this relationship, originate from a theory proposed several decades ago by Casagrande (1936) and further developed by other researchers (Bolton 1986; Rowe 1962). By using the flow rules, a full range of the soil strength can be obtained at various density and stress combinations, which can be beneficial for practical purposes:

- For independent check on the conventional shear test interpretations, as well as assessing the consistency of the test data (Bolton 1986; Jewell 1989).
- For feasibility studies and preliminary design calculations, before any in situ or laboratory measurements have been performed.
- For final design calculations in small projects where the costs of a proper testing of the shearing resistance are not justified.

We should note that although dilation is always important controlling the appropriate angle of friction, there are also many cases where the dilation of soil itself has a further influence on the geotechnical analysis, which have to be considered in the calculations by:

- Using flow rule equations to the cavity expansion theory to introduce the deformation history dependence of soil strength (i.e. angle of friction and dilation), while interpreting in situ tests (e.g. cone penetrometers, and pressuremeter), and predicting the behavior of piles in dilatant soils (Baligh 1976; Hughes et al. 1977; Salgado and Randolph 2001; Vesic 1972; Yu and Houlsby 1991).
- Considering dilation to simulate the nonlinear deformation behavior and failure near an underground excavation boundary (Marshall et al. 2012; Yu and Rowe 1999).
- Considering the stress level dependency of soil strength in bearing capacity computations and the load–displacement behavior of foundations. (Perkins and Madson 2000; Yamaguchi et al. 1976; Zienkiewicz et al. 1975).
- Proposing the dilation angle or expansion rate to give a measure of liquefaction resistance (Vaid et al. 1981).

Some theoretical abstractions (Bishop 1954; Newland and Allely 1957; Rowe 1962, 1969; Schofield and Wroth 1968; Skempton and Bishop 1950; Taylor 1948) consider certain principals of energy dissipation to explain the relationship between friction angle and dilation. However, the complexities of theoretical flow rules seem to present a major obstacle towards successful and robust implementation of these theories into soil models. That motivated researchers (Bolton 1986; Collins et al. 1992) to define comprehensive, but simple empirical equations with relatively few material parameters, as alternatives to theoretical flow rules, that could be easily implemented into geotechnical models. The most famous empirical flow rule was proposed by Bolton (1986) which relates the angle of dilation to the stress level and the relative density of sand, and has been widely used in the literature. This flow rule was developed as an empirical fit to the Rowe's stress- dilatancy relation. Alternatively, Been and Jefferies (1985) observed strong trends when the state parameter ξ was plotted with corresponding values of shearing resistance and dilation, leading to the empirical model by Collins et al. (1992). These two empirical flow rules were adopted interchangeably in geotechnical analysis to account for dilation in frictional material (Salgado and Randolph 2001; Yu and Houlsby 1991).

Following the pioneering work of (Rowe 1962), many later contributions on sand modelling (Bolton 1986; Houlsby 1991b; Nemat-Nasser 1980; Vaid and Sasitharan 1992), assumed

dilatancy as a unique function of the stress ratio and initial state of the soil, so that the notion of microstructural dependence was not considered in their formulations. However, closer examination of dilatancy reveals that the behavior of granular materials is more subtle, and the dilatancy is inarguably the manifestation of an internal kinematic constraint involving particle characteristics (shape, size), as basic elements participating in the deformation of the granular mass, and connectivity with operative inter-particle friction against applied stress (Wan and Guo 2000, 2001). Therefore at any rate, the description of flow rule as a key factor describing granular material behavior, will significantly influence the performance of a constitutive model and inadequate description of flow rules without considering the micro structure characteristics may affect the model's prediction of volume change and deformation.

5.3.4 Problem statement

Despite significant progress indicating the effect of the inter-particle friction (Cavarretta et al. 2010; Liu and Matsuoka 2003; Procter and Barton 1974; Rowe 1962; Skinner 1969; Thornton 2000), particle shape (Guo and Su 2007; Peña et al. 2007; Santamarina and Cho 2004) or texture characteristics (Cavarretta et al. 2010; Haruyama 1969; Procter and Barton 1974) on the shearing resistance and dilation of granular material:

- Until now, there has been no consensus as to the effect of particle size on the dilation and shearing response of granular material.
- A few studies have isolated the effect of particle size distribution from other factors such as grain angularity. However, no systematic assessment have been conducted to evaluate the amount of shearing resistance and dilatancy variation for different particle size distribution with respect to the particle angularity (rounded, sub-angular, or angular particles) of a given type of sand.
- The existing theoretical and empirical equations express the relationship between the shearing resistance and dilatancy have been developed without explicit consideration of microstructures which strongly are affected by particle properties (size, shape, and surface roughness). A close scrutiny of data reported in the literature calls into question the precision of well-known empirical formulations, such as Bolton's (1986) and Collins et al.'s (1992)

equations for predicting the strength-dilation relation of granular materials. These empirical relationships, in fact, contain no function that takes into account the constituent particle characteristics (e.g. size, shape, and particle gradation), and no particle-size limits are imposed with respect o their applicability.

- In spite of extensive application of empirical flow rules in geotechnical analyses, the proposed empirical equations with the given constants were introduced by using extremely limited data without the explicit consideration of the grain characteristics.

Considering the notable role of the flow rules in geotechnical analysis and their shortcomings as mentioned above, contribute to a better fundamental understanding of the effect of grain-size distribution on the dilations and the shearing behavior of granular material seems beneficial. The result of these investigations could also cast some light on the influence of the grain-size distribution curve on the relationship between the peak shearing resistance and the dilatancy of granular soil.

5.3.4 Objectives of the research

The main objective of this thesis is to evaluate the potential influence of particle characteristics (e.g. size, shape and gradation) on the dilation behavior of granular materials and its contribution to the shear resistance through experimental studies. For this purpose, sixteen different grain-size distribution curves of three different materials (basalt beads, Péribonka sand, and Eastmain sand) in the range of 63 μm to 2000 μm were tested in symmetrical direct shear and triaxial compression conditions at different normal pressures and initial relative densities.

Numerical simulations of a modified symmetrical direct shear tests are also presented in this study to evaluate the performance of the direct shear apparatus (DSA) to overcome the ambiguities arise from the complexity of stress and strain distributions during testing. The main objectives of this thesis can be sub-categorized as:

- **Proposing a framework providing an initial insight into the parameters corresponding to the nature of the sand particles (e.g. size, shape and gradation) that affect the dilatation and shear strength of granular materials.** For this purpose, the existing stress-dilatancy relationships are addressed in detail, and the disparities among dilatancy

estimations of the existing stress-dilatancy relationships for different materials are discussed. After evaluating the sensitivity of dilation and shear resistance of granular material to the particle characteristics, the well-known theoretical and empirical shear strength-dilation correlations have been developed in plain strain and triaxial conditions accounting for important factors.

- **Evaluating the precision of well-known empirical formulations, such as Bolton's (1986) and Collins et al.'s (1992) equations by close scrutiny of data reported in the literature.** These relationships contain no functions that takes into account the constituent particles characteristics, and no particle-size limits are imposed.

- **Adjusting the coefficients of Bolton's a(1986) nd Collins et al.'s (1992) equations to account for particle characteristics (e.g. D_{50} and particle angularity) in plane strain conditions**. For this purpose, 276 symmetrical direct shear tests were carried out on samples made up of basalt beads (rounded particles) and sands consisting of angular particles (Péribonka sand and Eastmain sand) in the range of 63 μm to 2000 μm to obtain the values of peak friction ϕ'_{max} and dilation ψ_{max} angles over a wide range of normal pressures and initial relative densities.

- **Presenting the numerical results obtained from DEM computer code SiGran (Roubtsova et al. 2011) to justify the reliability and applicability of boundary measurements in physical symmetrical direct shear test.** Particular emphasis was placed on the validation of the DEM model by comparing the results of DEM simulations with their physical counterparts at the macro-scale.

- **Evacuating the potential impacts of particle geometry on the stress-dilatancy of granular material during drained triaxial compression tests.** The correlation of the material constant α of Wan and Guo's (1999) modified stress-dilattancy equation with D_{50} have been developed. In addition, the coefficients of Vaid and Sasitharan's (1992) equations as an experimental adjustment of Rowe's stress-dilatancy equation for triaxial condition have been adjusted to account for D_{50}.

5.3.4 Statement of originality

To reach the objective of this research project, a large number of different laboratory tests were performed on materials made up of particles with different size and angularities. An evaluation of adjusted stress-dilatation equations accounting for particle size, gradation and shape has been accomplished by comparing the predicted results with data from the literature. Numerical simulations are presented in this study to support the reliability and applicability of boundary measurements in physical symmetrical direct shear tests. The adjusted strength-dilation formulas in this thesis may be beneficial for independently assessing the consistency of the experimentally-determined shear strengths, and introducing more refined flow rules into analytical and numerical geotechnical analyses.

- **This study imposed particle-size limits on well-known dilation-strength relationships validities under plane strain and triaxial compression conditions (Bolton 1986; Collins et al. 1992; Rowe 1962; Vaid and Sasitharan 1992; Wan and Guo 1999)** . This study shows that the explicit consideration of the soil grain characteristics (e.g. size, shape and gradation) can strongly affect dilation and strength values of granular material.

- **A respective analysis of strength and dilation data collected from the literature, together with a large number of laboratory test results are presented in this study to evaluate the reliability of Bolton's equations.** Although the importance of the proposed relationships is undeniable, it is recognized that their validity has been questioned, as they were introduced using very limited of plane strain data.

- **In this study numerical DEM simulations using SiGran included the actual number of particles, and actual size of the direct shear apparatus in 3-Dimensions simulation**. The earlier DEM studies of the direct shear test were limited to 2-dimensional simulations of direct shear (Masson and Martinez 2001; Potts et al. 1987; Wang et al. 2007; Zhang and Thornton 2007) or 3-Dimentional simulation with limited number of particles (Cui and O'Sullivan 2006). In addition, in the current study, a quantitative validation of the DEM model was attempted by relating a series of physical tests to equivalent DEM simulations. In comparison with the earlier studies that lack quantitative validation, this coupling of

numerical simulations with physical tests allows the authors to make more confident conclusions about the micromechanics of the specimen response from the DEM simulations.

This thesis includes three papers, submitted to the Journal of Geotechnical and Geoenvironmental Engineering, ASCE, the Journal of Computer and Geotechnics, and the International Journal of Geomechanics. Four peer-reviewed conference papers also resulted from the present research.

5.3.4 Thesis outline

This thesis is organized into the following chapters:

Chapter 1, Introduction: includes problem statement, objectives and scope of research.

Chapter 2, Literature Review: includes a definition of shear strength parameters, its components, and discussions of existing stress-dilatancy relationships. This chapter also illustrates some cases where the dilation of soil and its contribution to shear resistance has significanr influence on the geotechnical analysis.

Chapter 3: First scientific journal article submitted: This chapter re-examines the stresses and displacements obtained at the DSA boundaries through the three-dimensional (3D) discrete element method (DEM) simulations of physical tests on samples of polydisperse particles using the computer code SiGran. Based on the comprehensive reviews on the gradual achievements of data interpretation and DSA development in this chapter, the performance of the physical direct shear apparatus was optimized by exploring modifications to the symmetrical test configuration. The balance between the micro-scale change in particle energy and the macro-scale work of external forces is also presented. In order to achieve confidential conclusions about the micromechanic response of samples in direct shear testing quantitative validations of the DEM models were made by relating the physical tests to the corresponding DEM simulations.

Chapter 4, Second scientific journal article submitted: includes analyses and discussion of the experimental results using the modified symmetrical direct shear apparatus. A respective analysis of strength and dilation data collected from the literature is presented in this chapter to

discuss the reliability of Bolton's equations. The chapter then examines more closely the potential impacts of particle size and grading on the existing empirical correlations between the friction angle and the dilative behavior of granular materials in plane strain conditions. After examining the sensitivity of of these correlations to the particle characteristics, the coefficients of Bolton's and Collins et al.'s equations were adjusted to account for particle characteristics.

Chapter 5, Third scientific journal article submitted: includes analyses and discussion of the experimental results of drained triaxial compression tests. This chapter examines closely the potential impact of microstructural information imposed by internal particle geometry (e.g. size, shape and gradation) on the stress-dilatancy of granular material during conventional triaxial test. Thereafter, the microstructural effect accounted for into calculation of stress-dilatancy equation and its empirical adjustment in triaxial condition by treating it as a constraints imposed by constituent particle-size and angularity. In addition, experimental triaxial data of various granular materials were taken form the literature to provide evidences in support of the implemented constraints into existing stress-dilatancy relations.

Chapter 6, Conclusions and recommendation: includes the key results and findings, potential contributions and applications of the research, and recommendations for future research stemming from this dissertation.

CHAPITRE 2. Revue de littérature

2.1. Introduction

La résistance au cisaillement du matériau granulaire peut être représentée par un paramètre simple, l'angle du frottement mobilisé qui comporte trois composantes principales de la résistance au cisaillement : le frottement coulissant intrinsèque (contrôlé par ϕ_μ, l'angle de frottement interparticulaire), la résistance mobilisée par la dilatation ou l'élévation des particules et la résistance mobilisée par la remise en ordre et le blocage des particules.

Le paramètre ϕ_μ a été diversement défini par différents chercheurs en mécanique du sol, mais est généralement ramené au coefficient moyen de frottement cinétique produit quand une particule typique de sol est poussée à glisser lentement au-dessus des autres par un déplacement significatif (Procter et Barton 1974). Ce paramètre est considéré conceptuellement comme une constante matérielle, dépend principalement de l'aspérité des particules, et est essentiellement indépendant de la contrainte et de la densité de conditionnement (Lee et Seed 1967; Rowe 1962). Diverses techniques expérimentales ont été développées afin de mesurer ϕ_μ pour un matériau donné, que ce soit en partant du glissement d'un matériau lisse à travers d'autres, selon Horne et Deere (1962), ou de plusieurs particules fixes à travers un bloc lisse, suivant Bowden et al. (1943), pour aller au glissement d'une masse des particules libres à travers un bloc lisse selon Rowe (1962) ou d'une particule fixe au-dessus d'autres suivant Skinner (1969), Procter et Barton (1974), et Cavarretta et al. (2010).

La dilatation peut être décrite comme le volume de changement qui est associé à la déformation de cisaillement d'un élément quand le matériau est considéré suffisamment macroscopique et assez grand pour contenir beaucoup de particules comme microéléments. Le paramètre approprié pour caractériser un matériau de dilatation est l'angle de dilatance ψ introduit par Hansen (1958) et représente le rapport de changement volumétrique plastique $d\varepsilon_v^p$ sur la contrainte de cisaillement plastique $d\varepsilon_s^p$. En déduisant les composants de dilatation de la

résistance au cisaillement de l'ensemble des contraintes, la résistance au cisaillement due à d'autres facteurs mobilisateurs de résistance peut être de ce fait déterminée. Rowe (1962) a proposé une théorie de la contrainte de cisaillement–dilatance de cisaillement, dans laquelle un critère de contenu énergétique est employé pour dériver l'angle critique du glissement entre les particules dans un ensemble aléatoire, qui tient compte des changements de volume qui se produisent dans la déformation des sables. En conséquence, il a prouvé que même lorsque les expressions de Taylor-Bishop sont appliquées aux essais de cisaillement, l'angle résultant du frottement dépasse toujours l'angle du frottement interparticulaire, ϕ_μ, des particules comportant un matériau granulaire. Il a conclu que dans la majeure partie de la gamme d'indices de vides se retrouve une troisième composante de la résistance au cisaillement autre que la résistance de friction et que la dilatation, qui est développée par l'énergie exigée pour réarranger et réorienter des particules de sol.

2.2. Effet des caractéristiques des particules sur la résistance au cisaillement et sur la dilatation de matériau granulaire

Pendant les dernières décennies, un bon nombre de travaux numériques et expérimentaux justifiaient la dépendance de la réaction mécanique vis-à-vis des caractéristiques des particules (par exemple la rugosité, la forme, la taille et la gradation des particules). Généralement, le frottement interparticulaire varie avec la texture des particules (ou la rugosité), qui se rapporte aux petites aspérités présentes sur la surface de la particule. La forme des particules, qui domine l'arrangement spatial des particules et du blocage interparticulaire, est caractérisée par la sphéricité ainsi que l'angularité se rapportant au caractère tranchant ou arrondi des coins à la limite des particules. La dimension particulaire est principalement caractérisée par deux facteurs principaux D_{50} et C_u. Ces facteurs influenceraient le comportement structurel et mécanique du matériau granulaire pendant le cisaillement suivant le déplacement des particules discrètes dans le système. Les effets de ces caractéristiques particulaires sur la résistance au cisaillement du matériau granulaire, recueillie dans la littérature la plus récente, sont présentés dans les paragraphes suivants.

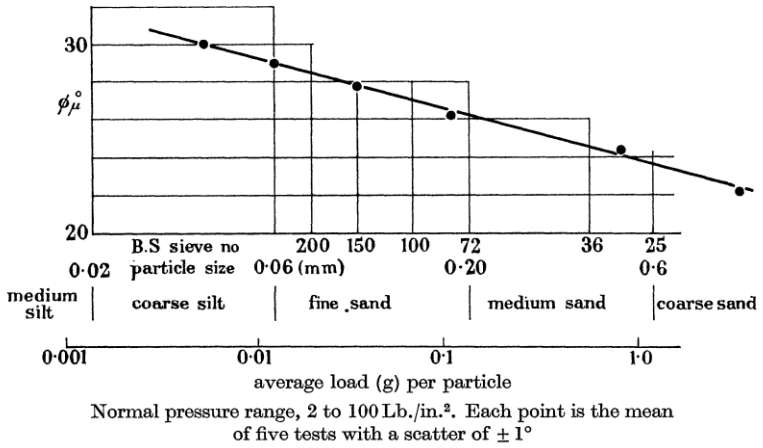

Figure 2.1 ϕ_μ diminue avec l'augmentation de la valeur de la charge par particule, si l'écrasement ne se produit pas (Rowe, 1962)

2.2.1 Angle interparticulaire de frottement ϕ_μ, et son effet sur la résistance au cisaillement

L'étude de Rowe (1962) a montré que la valeur de ϕ_μ pour n'importe quel assemblage d'articles donné diminue avec l'augmentation de la valeur de la charge par particule et si l'écrasement ne se produit pas, une diminution dans ϕ_μ d'environ 5° sur la gamme de pression 1 à 140 kg/cm^2 peut être envisagée (Figure 2.1). Cependant, comme montré par les expériences de Lee et Seed (1967), quand la pression augmente, le nombre de particules augmente également en raison de l'écrasement, de sorte que la charge par particule et ainsi la valeur de ϕ_μ n'est pas susceptible de changer de manière appréciable avec l'augmentation de la pression de confinement. Horne et Deere (1962), et Bromwell (1966) avaient souligné l'effet essentiel que les conditions chimiques extérieures ont sur ϕ_μ. Ils ont également indiqué une croissance significative dans ϕ_μ par l'introduction d'eau sur la surface sèche du matériau testé. On a également remarqué que cet effet diminue avec l'augmentation de l'aspérité de particules. Sur la gamme de force normale utilisée (0.1-0.6 N), ces auteurs n'ont observé aucune variation apparente dans ϕ_μ. Cependant, ceci est en désaccord avec Skinner (1969) qui a observé une diminution significative dans ϕ_μ avec l'augmentation de la force normale sur les particules examinées. Procter et Barton (1974) ont signalé plus précisément que le frottement

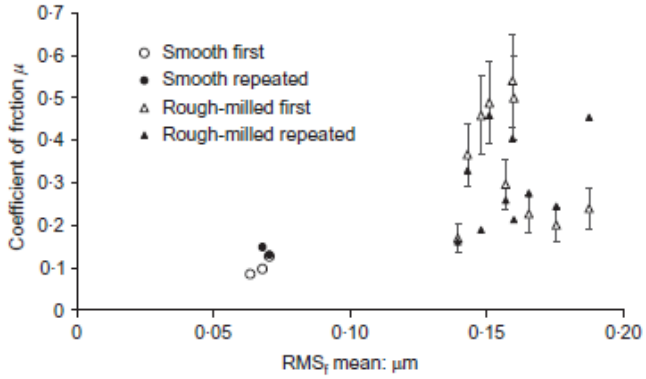

Figure2.2 a mesuré des coefficients interparticulaires de frottement pour le petit ballotini sec, (Cavarretta et al. 2010)

interparticulaire est non seulement une fonction de la composition minérale, mais également de la chimie extérieure prévalante au point de contact. Cette chimie et la capacité de la contrôler, se révèle comme fonction de l'aspérité de la forme et de la surface, aussi bien que de l'état expérimental ambiant. Cavarretta et al. (2010) ont mesuré le frottement interparticulaire à l'aide d'un nouvel appareil et a découvert un rapport clair entre le frottement interparticulaire et l'aspérité des particules (Figure 2.2). Cependant, leurs expériences de macro-échelle ont indiqué que tandis que la réaction matérielle peut dépendre légèrement de l'aspérité, l'influence de la forme des particules est beaucoup plus significative (Figure 2.3).

Skinner (1969) a suggéré que le frottement interparticulaire ne change pas de manière significative l'angle de la résistance au volume constant ϕ_{cv} et au pic ϕ_{max} pour une porosité initiale donnée dans des conditions de déformation plane. Plus récemment, par l'intermédiaire de la simulation tridimensionnelle de la DEM (méthode d'éléments discrets) d'ensemble de sphères soumises à des conditions de de contrainte triaxiale, Thornton (2000) démontre qu'à la fois ϕ_{cv} et ϕ_{max} tendent à augmenter avec ϕ_{μ}. Cependant, l'effet du coefficient interparticulaire ($\tan\phi_{\mu}$) était limité, en particulier quand il était plus grand qu'approximativement 0.5. La conclusion a été encore confirmée par Liu et Matsuoka (2003) sur base de la DEM modélisée pour simuler des séries d'essais en laboratoire de cisaillement direct sur des tiges en aluminium et des essais de cisaillement direct sur des sables. Ils ont observé que l'augmentation de résistance au cisaillement n'est pas proportionnelle à l'augmentation de ϕ_{μ}.

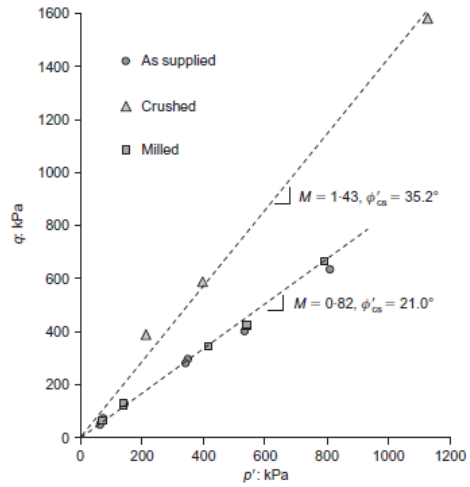

Figure2.3 effet de la rugosité et de la forme des particules sur la fin des états testés du plan q-p' , (Cavarretta et al. 2010)

Leurs résultats sont compatibles avec les résultats de Thornton dans lesquels le coefficient de frottement interparticulaire est moins important quand il est plus grand que 0.5.

2.2.2 Effet de l'angularité des particules sur la dilatation et la résistance au cisaillement

Chan et Page (1997) et Koerner (1970) ont signalé la diminution de ϕ_{cv} avec l'augmentation de l'arrondi des particules. Ils ont montré que l'angularité de la particule peut disposer d'une fibre vérrouillée en plus de fournir des contraintes supplémentaires à la rotation des particules et par conséquent d'augmenter la dilatation. Les données expérimentales de Sukumaran et Ashmawy (2001) ont également prouvé que l'angle de frottement du matériau granulaire croît de manière significative avec l'augmentation de l'angularité des particules (Figure 2.4).

Guo et Su (2007) ont étudié l'effet de l'angularité des particules sur la résistance et la dilatation des matériaux granulaires par une série d'essais triaxiaux sur deux matériaux composés de particules arrondies et angulaires. Ils ont conclu que selon l'indice de vides initial et la pression de confinement, l'angle de frottement au début de la dilatation varie entre ϕ_{μ} et ϕ_{cv} pour des sables se composant de particules arrondies et subarrondies et qu'il pourrait dépasser ϕ_{cv} pour le sable comportant des particules à angularité élevée (Figure 2.5). Leurs résultats

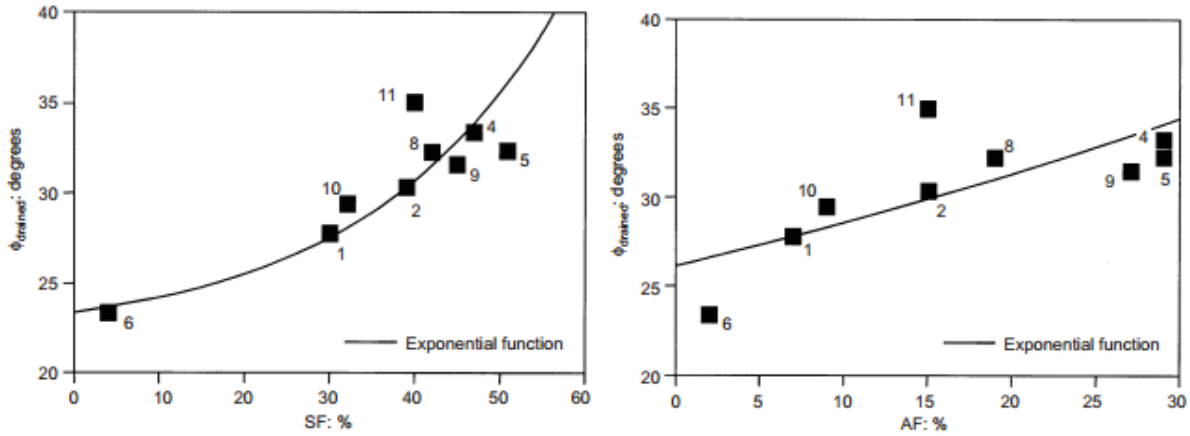

Figure 2.4 rapport entre l'angle de frottement drainé et les facteurs de forme et d'angularité normalisés (Sukumaran et Ashmawy 2001)

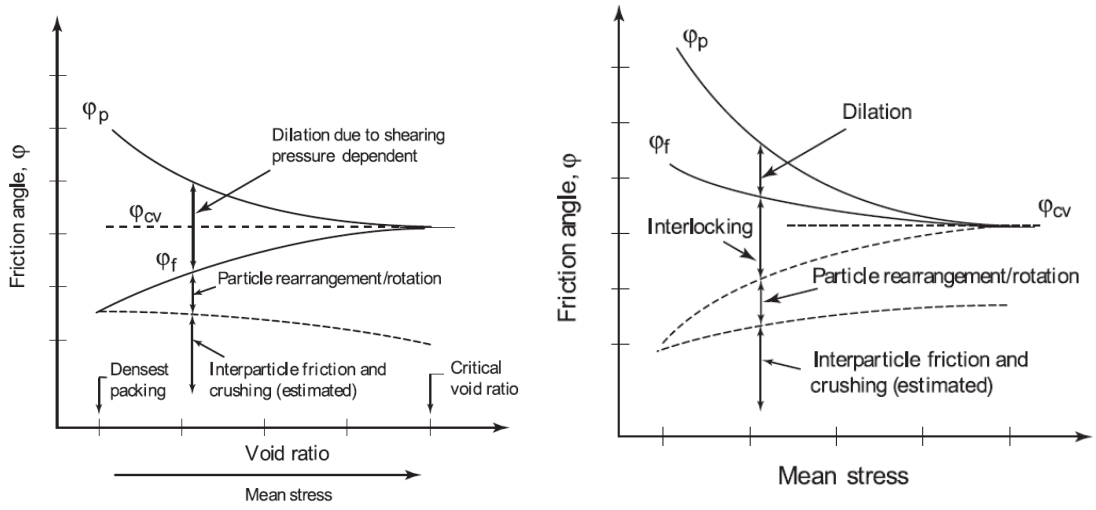

Figure 2.5 un modèle conceptuel alternatif pour la résistance au cisaillement du matériau angulaire (a) angle de frottement vs. l'indice de vides, et (b) angle de frottement vs. pression réelle moyenne (Guo et Su 2007)

expérimentaux ont clairement montré que la dilatation et le verrouillage dus à l'angularité contribuent à la résistance au cisaillement du matériau granulaire. Haruyama (1969) a prouvé que la résistance au cisaillement et la dilatation ont augmenté avec l'augmentation de l'aspérité des particules granulaires dans les essais de compression triaxiale. Cependant, des essais expérimentaux de macro-échelle (Cavarretta et al. 2010; Guo et Su 2007) ont indiqué que l'influence de la forme des particules est beaucoup plus apparente que celle de l'aspérité sur les caractéristiques de dilatation du matériau granulaire.

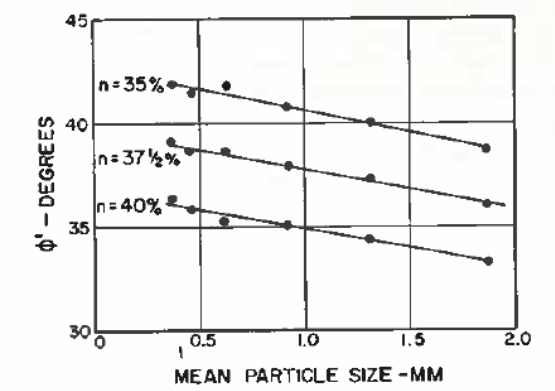

Figure 2.6 relation entre la résistance au cisaillement et la taille des particules pour le sable Leighton Buzzard (Kirkpatrick, 1965)

2.2.3 Effet de distribution de la taille des particules sur la résistance au cisaillement

Durant les dernières décennies un progrès significatif a été accompli afin d'indiquer une corrélation forte entre l'angle de macro-échelle de la résistance au cisaillement pour les matériaux granulaires et le frottement, la forme des particules ou les caractéristiques interparticulaires de texture. Mais jusqu'ici, il n'y a eu aucun consensus quant à l'effet de la taille des particules sur la réaction au cisaillement du matériau granulaire. Peu de recommandations ont été faites sur la façon de considérer l'influence de la courbe de distribution de la taille des particules tout en estimant les composantes de la résistance au cisaillement dans les matériaux angulaires. Bishop (1948) a proposé une première tentative de mettre en relation les propriétés mécaniques du sol avec les caractéristiques de la gradation du matériau granulaire. Il a effectué des essais de cisaillement direct sur une gamme complète de sols non cohésifs et a montré qu'un matériau disposant d'une taille de grain uniforme, que ce soit un sable moyen ou des cailloux d'environ 1 pouce de diamètre, donne des résultats similaires une fois tracé sous la forme d'un angle de frottement au pic (ϕ_{max}) contre la porosité. Kirkpatrick (1965) a étudié l'influence de la taille des particules de la gamme s'étendent de 0.3 millimètres à 2 millimètres pendant des essais triaxiaux drainés. Là où les effets de gradation n'étaient pas présents et les autres propriétés des particules étaient uniformes, on avait constaté que la résistance au cisaillement diminuait à mesure que la taille des particules augmentait (Figure 2.6). Mais les résultats n'apportaient aucune conclusion claire quant à l'influence de la

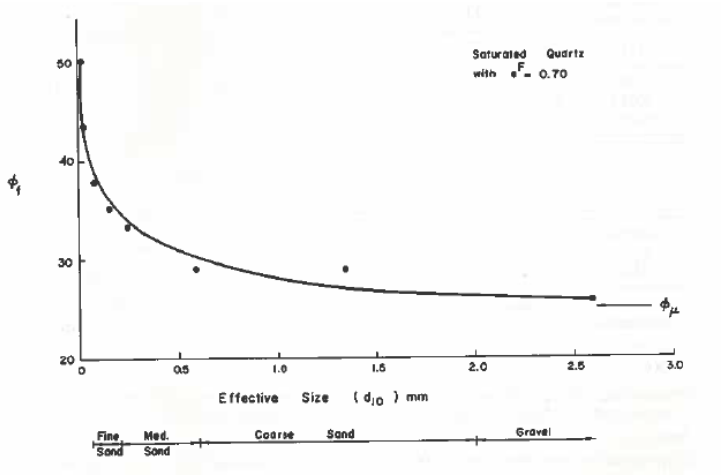

Figure 2.7 effet de la taille des particules sur l'angle drainé de la résistance au cisaillement à dilatation nulle, (Koerner, 1970)

gradation sur la résistance au cisaillement. Koerner (1970) a montré une augmentation de l'angle drainé de la résistance au cisaillement lors d'une dilatation nulle ϕ_f ainsi qu'une diminution avec la taille des particules pour le sol de quartz (Figure 2.7). Cette augmentation était significative avec des tailles de particules inférieures à 0.06 millimètre (sable moyen voire plus fin). L'effet de la variation du coefficient d'uniformité de 1.25 à 5 était négligeable sur ϕ_{max} et ϕ_f dans les sols de quartz, mais dans d'autres sols (feldspath et calcite), C_u a donne des valeurs ϕ_p et ϕ_f plus élevées. Dans ces deux derniers sols minéraux, une sévère dégradation a été notée; ceci a eu pour effet l'abaissement de D_{10} dans les échantillons, qui ont à leur tour augmenté ϕ_f . Par conséquent, Koerner (1970) s'est fortement basé sur les résultats des sol de quartz et a conclu que, à une densité relative donnée, la gradation a un effet relativement mineur sur ϕ_f .

Zelasko et al. (1975) ont également effectué des essais semblables à ceux de Koerner (1970) sur des sables secs - premièrement sur une grande quantité de taille uniforme et ensuite sur une quantité limitée avec la gradation améliorée $C_u = 1.55\text{-}2$. Sur la base des résultats de ses essais, il a souligné que l'arrondi des particules et la densité relative exercent l'influence la plus forte sur la résistance au cisaillement. L'effet du diamètre des particules est apparu insignifiant, et l'influence de la dégradation de la taille de particule améliorée à une densité relative donnée se révélait mineure comparée à l'effet de l'arrondi.

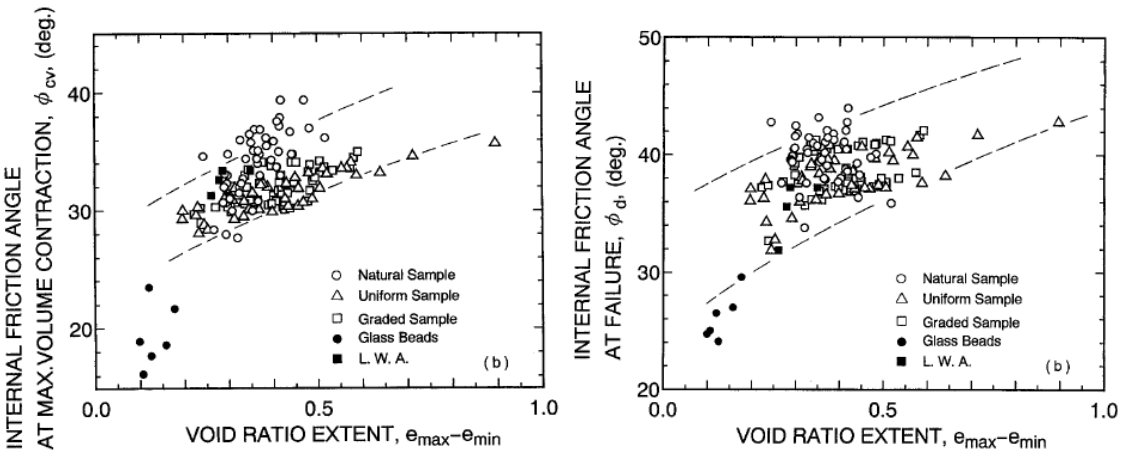

Figure 2.8 rapports de l'angle de frottement à la contraction maximale du volume avec $(e_{max}-e_{min})$, (Miura et al. 1998)

Ici, il est important de se rappeler que la densité de conditionnement ou de volume des vides dans le squelette du sol est liée à la distribution de la taille des particules (Cubrinovski et Ishihara 1999; Miura et al. 1997; Youd 1973) et du contenu subtil du sol (Cubrinovski et Ishihara 2002; Charger et al. 1998). Youd (1973) a montré l'évolution à la baisse de e_{max}et e_{min} en fonction d'un C_u accru, indépendamment de l'angularité des particules, tandis que Cubrinovski et Ishihara 1999, 2002, utilisant une base de données très grande, ont développé un rapport unique entre $(e_{max}-e_{min})$ et la taille du grain médian D_{50}. Cette équation implique que $(e_{max}-e_{min})$ augmente quand D_{50} diminue, ce qui est compatible avec les résultats obtenus par Miura et al. (1997). La prise en considération de la variation de l'ampleur de l'indice de vides peut être utile pour interpréter l'influence de la gradation sur la résistance au cisaillement, et permet de surmonter la complexité observée par Kirkpatrick (1965). Par exemple, Miura et al. (1998) ont également effectué une série d'essais de compression triaxiale considérant l'influence de l'ampleur de l'indice de vides, qui détermine, pour différentes valeurs de D_{50} et C_u, le comportement mécanique global des sols avec une distribution de taille de particules donnée (Figure 2.8). Cette étude a prouvé que l'angle du frottement interne mobilisé à la contraction de volume maximale, ϕ_{cv}, est dépendant de $(e_{max}-e_{min})$, et que l'angle interne de frottement au pic ϕ_{max} croît légèrement avec l'augmentation de $(e_{max}-e_{min})$, et que l'angle interne de frottement à l'échec au pic ϕ_{max} croît légèrement avec l'augmentation de $(e_{max}-e_{min})$.

2.3. Rapports de résistance au cisaillement-dilatation et leurs applications aux problèmes géotechniques réels

Le comportement mécanique des matériaux granulaires tournent naturellement autour de la dilatation et de son rapport avec la résistance au cisaillement, qui est régie par un certain nombre de facteurs tels que le de l'indice de vides, les pressions de confinement, l'histoire antérieure de déformation tout autant que le chemin de contrainte. Par exemple, un spécimen granulaire meuble se contractera sans interruption à l'application de la contrainte deviateur. D'une part, un spécimen dense peut seulement se contracter au commencement, et ensuite, se dilate en raison d'une tendance des particules à glisser et à s'empiler les unes sur les autres au point que la déformation se produise. Ce phénomène bien connu dénommé contrainte de cisaillement–dilatance de cisaillement a été identifié pour la première fois par Reynolds (1885). Par la suite, un certain nombre de tentatives théoriques (Bishop 1954; De Josselin de Jong 1976; Newland et Allely 1957; Rowe 1962, 1969; Schofield et Wroth 1968; Skempton et Bishop 1950; Taylor 1948) et expérimentales (Bolton 1986; Collins et al. 1992; Lee et Seed 1967; Negussey et al. 1988; Roscoe 1970) ont été faites afin d'expliquer la déformation volumétrique de l'ensemble granulaire lors du cisaillement sur la base d'observations macroscopiques. Il convient de noter que ces rapports peuvent être appliqués dans deux sens distincts. D'abord, ils peuvent être employés pour exprimer le rapport entre l'angle de frottement mobilisé et le taux de dilatation courant au cours de l'expérimentation (Bishop 1954; Rowe 1962, 1969; Schofield et Wroth 1968; Skempton et Bishop 1950). Deuxièmement, ils peuvent être employés pour exprimer le rapport entre l'angle de frottement maximal et le taux maximal de dilatation lors de plusieurs essais sur le même matériau (Newland et Allely 1957; Taylor 1948; Bolton 1986; Collins et al. 1992).

Les rapports proposés de contrainte de cisaillement–dilatance de cisaillement ont été traditionnellement développés sans considération explicite des microstructures. Cependant, comme présenté dans la section 2.2, un réexamen plus étroit du matériau granulaire pendant le cisaillement indique que son comportement de résistance et de dilatation au cisaillement est plus subtil et fortement affecté par les propriétés des particules (par exemple, la taille de la particule, la forme de la particule et son aspérité) participant à la déformation de la masse granulaire. De façon générale, l'arrangement des particules et le réseau de forces induites, alors que les

particules tournent et glissent, peut uniquement déterminer la structure interne et la résistance au cisaillement de la masse granulaire pendant la déformation. Évidemment, à la fois l'arrangement des particules, leurs mouvements relatifs et le réseau de forces sont affectés par les caractéristiques des particules en tant qu'éléments constitutifs de base (Goddard et Didwania 1998; Oda et Kazama 1998; Wan et Guo 2001). Ceci résulte par la suite en la dépendance de la contrainte de cisaillement– dilatance de cisaillement vis-à-vis de la structure interne du matériau granulaire. L'information microstructurale peut être expliquée dans le calcul de la dilatation en la traitant comme une contrainte imposée par la géométrie interne du grain aux déformations macroscopiques (Goddard et Bashir 1990; Matsuoka 1974; Tokue 1979).

Puisque la contrainte de cisaillement–dilatance de cisaillement est un tel facteur clé dans la description des matériaux granulaires, ce sera inévitablement une partie intégrante du modèle constitutif jouant habituellement le rôle de potentiel plastique (Bardet 1990; Guo 2000; Nova et Wood 1979; Vermeer 1982). En tout cas la description de la contrainte de cisaillement–dilatance de cisaillement influencera de manière significative l'exécution d'un modèle constitutif. On a constaté qu'une description insatisfaisante de la contrainte de cisaillement–dilatance de cisaillement, qui ne prend pas suffisamment en considération la microstructure, ne peut pas correctement prévoir des changements de volume du sol dans les cas où la dilatation du sol elle-même a une autre influence sur l'analyse géotechnique. Le manque de considération de la microstructure lors de l'étude de la relation contrainte de cisaillement–dilatance de cisaillement et de ses ajustements expérimentaux simplifiés indique la condition requise à l'amélioration concrète des lois d'écoulement de par l'inclusion des propriétés des particules afin de prévoir la résistance au cisaillement et sa contribution en terme de dilatation (Guo 2000). Cette section fournit des exemples d'analyses géotechniques, où la dilatation du sol elle-même a des influences sur le comportement de déformation et de rupture du sol. La dépendance de la résistance du sol vis-à-vis de la dilatation et du niveau de contrainte est insérée dans ces calculs par l'introduction d'équations de lois d'écoulement à ces analyses géotechniques. L'examen minutieux de ces cas géotechniques peut fournir des perspectives intéressantes quant à l'importance d'adopter des lois précises d'écoulement dans l'analyse théorique afin d'accorder les résultats aux pratiques géotechniques.

2.3.1 Comportement de pieux axialement chargés dans un sol non cohésif

La prévision de la capacité en pointe et de la capacité en friction de pieux enfoncés dans les sols demeure un problème difficile pour la technologie géotechnique, car l'analyse de l'installation de pieux dans le sol pose un grand problème de déformation, impliquant un matériau fort et des non-linéarités géométriques. Pendant les dernières décennies, beaucoup de méthodes semi-analytiques ou empiriques ont été employées couramment dans l'analyse et la conception de la fondation de pieux. La théorie de l'expansion de la cavité s'est avérée être un outil théorique très utile dans l'élaboration des méthodes semi-analytiques pour estimer la capacité des pieux. Les processus d'expansion de la cavité sont opérationnels dans un certain nombre de problèmes importants pour la mécanique de sol; y compris le contrôle des pressiomètre, le battage de pieux, le pieux chargé jusqu'à rupture, le test de pénétration de cône et la détonation de dispositifs explosifs dans des dépôts de sol.

2.3.1.1 La capacité en pointe de pieux enfoncés (théorie modifiée de l'expansion de la cavité pour expliquer la dilatation)

Dans des problèmes géotechniques tels que le comportement de pieux lorsqu' une forte contrainte est exercée sur le mouvement du sol, le fait que le sol se dilate devient beaucoup plus important dans les calculs. La théorie de l'expansion de la cavité présentée par Yu et Houlsby (1991) et Yu (1990) démontre que la dilatation peut être prise en compte dans les calculs de capacité en pointe et de capacité en friction des pieux. L'application de la théorie de l'expansion de la cavité aux problèmes géotechniques a été présentée par Gibson et Anderson (1961), et modifiée par Yu et Houlsby (1991) et Yu (1990) pour expliquer la dilatation dans des matériaux en friction. La pression exercée sur le bout des pieux enfoncés peut être estimée en employant la théorie sphérique de l'expansion de la cavité. L'analogie est exposée dans la Figure 2.9. L'analyse implique un traitement détaillé de la contrainte et de la déformation dans la zone d'un sol près du pieu se déformant plastiquement, et une zone externe qui demeure

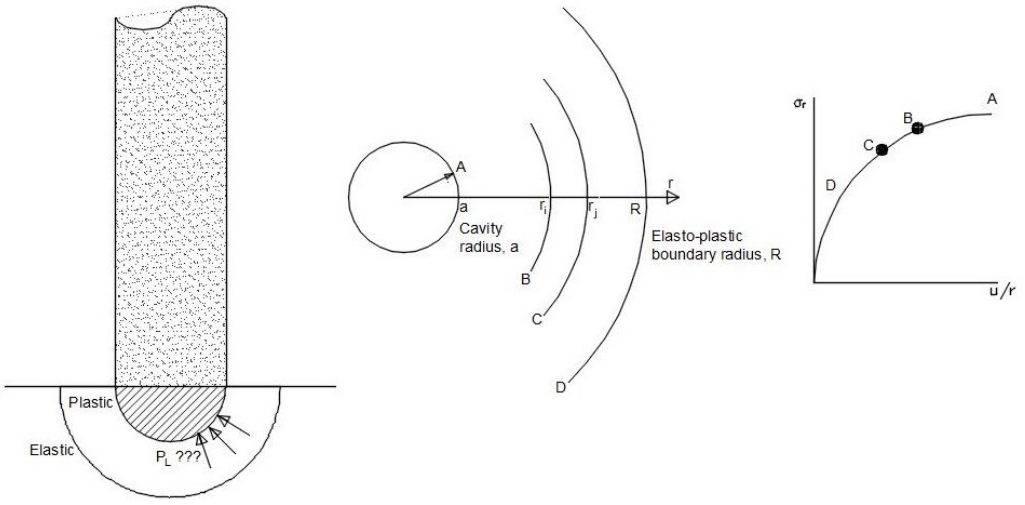

Figure 2.9 Réaction de la nomenclature et de la pression pour l'expansion de la cavité (Houlsby 1991a)

élastique. Les pressions calculées de l''expansion de la cavité peuvent être employées en tant qu'évaluations de la capacité en pointe des pieux.

Dans les théories modifiées de l'expansion de la cavité (Collins et al. 1992; Yu et Houlsby 1991; Yu 1990), l'angle du frottement et de la dilatation est considéré comme variant selon l'un des deux modèles : le modèle du paramètre d'état (Been et Jefferies 1985) ou le modèle de Bolton (1986). Selon le modèle du paramètre d'état :

$$(\phi'_{max} - \phi'_{cv}) \equiv f(\xi) = A[exp(-\xi) - 1] \tag{2.1}$$

$$\psi_{max} \equiv g(\xi) = B[exp(-\xi) - 1] \tag{2.2}$$

là où ϕ_{cv} est l'angle de frottement critique; A et B est la constante empirique qui dépend des caractéristiques du sable et du type de chargement; ξ est le paramètre d'état dans la mince coquille ij.

Selon les modèles de Bolton (1986):

$$\phi'_{max} - \phi'_{cv} = f(D_R, p') = cI_R \tag{2.3}$$

$$I_R = D_R(Q - \ln p') - R \tag{2.4}$$

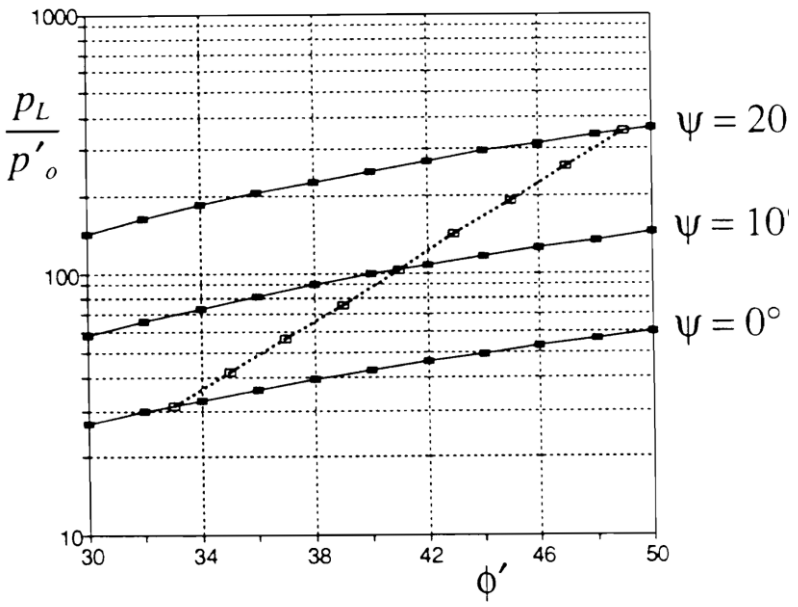

Figure 2.10 variation de la pression sphérique maximale avec l'angle du frottement pour des angles de dilatation différents (Houlsby 1991a)

là où $c = 3$ pour les essais de compression triaxiale, et $c = 5$ pour des essais de déformation plane; D_R est la densité relative en tant que nombre entre 0 et 1 à l'intérieur de la coquille mince ij; Q et R sont les paramètres appropriées qui dépendent des caractéristiques du sable. Dans les modèles cylindriques et sphériques, le rapport :

$$\phi'_{max} - \phi'_{cv} = 0.8\psi_{max} \tag{2.5}$$

proposé par Bolton (1986) entre le frottement et l'angle de dilatation est supposé tenir.

Quelques exemples de l'analyse, montrant la variation de l'expansion de la cavité avec l'angle du frottement pour différentes valeurs d'angle de dilatation, sont présentés dans la Figure 2.10. L'expansion de la cavité de la pression a été divisée par l'effort p_0 à une grande distance du pieu. Les trois courbes principales indiquent les pressions calculées pour des angles de dilatation de 0°, 10°, et 20°. Les autres paramètres exigés (constants dans toutes ces analyses) sont le module de cisaillement $G = 500p_0$ et le coefficient de Poisson $\nu = 0.2$. L'augmentation de la capacité en pointe calculée croit de plus de cinq fois alors que l'angle de dilatation se voit augmenté de 0° à 20°.

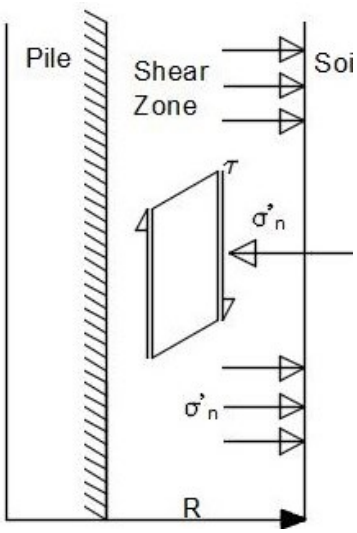

Figure 2.11 Théorisation de la zone de cisaillement à côté d'un pieux (Houlsby 1991a)

2.3.1.2 Capacité de friction de pieux (évaluant le rôle de la dilatation)

Comme mentionné ci-avant, la dilatation est toujours importante en tant qu'elle contrôle l'angle approprié de frottement. Cependant, il existe quelques cas où la dilatation du sol exerce une influence supplémentaire sur les résultats de cisaillement comme, par exemple, en affectant la capacité de friction des pieux. Quand un pieu est chargé verticalement le comportement du sol entourant le pieux pourrait être théorisé de la manière représentée dans la Figure 2.11. Cependant, le comportement réel sera plus complexe. Une bande relativement mince du sol près du pieux se déforme en cas de cisaillement simple, mais, dans ce cas-ci, c'est la déformation verticale qui est nulle : cela ressemble à un test conventionnel simple de cisaillement tourné à 90°. Tout comme les cisaillements de sol qu'il dilate, ainsi le sol en dehors de cette zone est poussé vers l'extérieur. Le résultat est que la contrainte normale exercée sur l'élément du sol dans le cisaillement simple ne demeure pas constante. L'expansion du sol environnant peut être modelée comme analogue à un test de pression-mètre, ainsi il existe un rapport entre le mouvement extérieur et le changement de la contrainte normale. Par simplicité, ce rapport peut être considéré comme élastique, et le résultat est :

$$\Delta\sigma'_n = 2G\frac{\Delta R}{R} \tag{2.6}$$

Cependant, dans la pratique la distinction entre la zone de cisaillement mince (dans laquelle le sol se déforme plastiquement) et la zone externe (dans laquelle il est supposé que le sol reste élastique) ne sera pas aussi claire que dans ce modèle simple. Un modèle plus complexe a pu être créé en employant l'analyse numérique. L'approche adoptée ici a été employée avec succès par Johnson et al. (1988) au sein de laquelle la contrainte normale dans un test de cisaillement simple a été mise en relation avec le mouvement vertical, afin de modeler le comportement du sol autour des pieux en sable de carbonate. Dans ce modèle de comportement du pieux la dilatation devient très importante, puisque plus le se sol dilate, plus la contrainte normale devient grande. L'influence de la dilatation prévue en augmentant la contrainte horizontale sur des pieux a été étudiée par Carnek et al. (1973) et Jardine et Christoulas (1991). Ces chercheurs ont passé en revue des signes de l'augmentation de la contrainte normale sur l'axe de pieux due à la dilatation et discutent certains des facteurs qui influencent cette augmentation. L'importance de cette augmentation peut varier considérablement suivant les états du sol (Frank et Tadjbakhsh 1986).

2.3.2 Effet du niveau de contrainte sur la capacité de portance et sur le comportement de charges-déplacement fondations peu profondes

La détermination de la capacité de portance et la prévision du comportement de charges-déplacement des fondations ont constitué une préoccupation importante dans la conception des fondations. Plusieurs méthodes classiques ont été développées pour prévoir la capacité de portance des fondations au siècle dernier. Terzaghi et Peck (1948), Taylor (1948), Meyerhof (1963), et Vesic (1973) peuvent être mentionnés ici pour leurs travaux sur la détermination de la capacité de portance du sol. La formule célèbre triple-n, énoncée à l'origine par Terzaghi (1943) peut être considérée comme le bénéfice le plus valable de leurs travaux présentés comme suivant :

$$q_{ult} = cN_c + qN_q + 0.5\gamma BN_\gamma \tag{2.7}$$

là où, q_{ult} est la capacité de portance finale, c'est la cohésion, q est la pression de surtaxe, B est la largeur des fondations, γ est la densité du sol et N les coefficients, qui sont des fonctions d'angle de frottement du sol, sont les facteurs de la capacité de portance.

Un certain nombre de tests de charge complets avaient été réalisés pour vérifier la formule de capacité de portance ou pour prévoir la capacité de portance des fondations dans différents types de sol (Briaud et Gibbens 1999; Fellenius et Altaee 1994; Ismael 1985). Les recherches prouvent que pour des fondations sur des sols relativement denses, la valeur mesurée de la capacité de portance est souvent plus haute que les valeurs obtenues à partir de l'équation théorique basée sur un angle de frottement à l'état critique; entre-temps, l'utilisation de l'angle de frottement maximal a comme conséquence des capacités de portance plus élevées que les valeurs mesurées (Clark 1998; Eslami et al. 2004). En outre, le troisième facteur de capacité de portance N_γ augmente de manière illogique avec l'angle de frottement qui mène à des valeurs de capacités de portance très élevées pour de grandes fondations. De telles observations ont résulté d'un effet important appelé l'effet d'échelle, qui peut être lié au niveau de contrainte éprouvé par le sol. Eslami et al. (2004) ont présenté un aperçu des erreurs dans la capacité de portance des fondations peu profondes et de la contradiction entre les résultats des approches théoriques et ont conclu que la capacité de portance obtenue à partir des méthodes théoriques est souvent exagérément conservatrice pour les petites fondations mais irrationnellement hautes pour de grandes fondations.

Les effets d'un certain nombre de paramètres importants ont été étudiés pour ajuster les données expérimentales avec les résultats de l'analyse théorique. Parmi eux, la profondeur, l'échelle et la rugosité de base des fondations se sont avéré des facteurs importants pour l'intensité d'une charge potentiellement limitée sur des fondations. Les résultats d'Ismael (1985) ont indiqué que l'influence de la profondeur des fondations est très faible. Cependant, sur base de ces résultats, Fellenius et Altaee (1994) ont prouvé que la largeur de la fondation joue un rôle très important dans la capacité de portance. Ceci peut être lié au comportement du sol sous différents états de contrainte imposée. Les paramètres de résistance au cisaillement du sol ont été considéré comme dépendants du niveau de contrainte expérimentée, également connu sous le nom de niveau de contrainte (Bolton 1986; Budhu 2007; Clark 1998; Holtz et Kovacs 1981; Maeda et Miura 1999). Cette dépendance peut être envisagée comme la raison des différences entre les approches expérimentales et théoriques dans la détermination de la capacité de portance des fondations. Depuis, les deux premiers facteurs dans la formule de capacité de portance N_c et N_q ont été bien déterminés par des solutions de forme close d'un

Tableau 2.1 Facteur de capacité de portance N_γ, obtenu à partir d'essais expérimentaux et de méthodes théoriques.

$B(m)$	N_γ (experiment)	ZEL		Meyerhof (1950)		
		N_γ	$\phi_{Eq.}(^\circ)$*	N_γ for ϕ_{cs}	N_γ for ϕ_{peak}	$\phi_{Eq.}(^\circ)$
0.03	580	-	-	33**	211-873	48.5
0.3	450	510	47.5	33	211-873	48
0.6	350	410	46.5	33	211-873	47
0.8	300	370	46	33	211-873	46
1.2	270	320	45.5	33	211-873	45.5
1.6	250	300	45	33	211-873	45

*By suggested equation based on ZEL method

** Corresponding value obtained from ZEL method is 53 for ϕ_{cs} and 246-956 for ϕ_{peak}

problème de plasticité dans la mécanique du sol, le problème majeur dans la capacité portance est souvent le troisième facteur N_γ. La capacité portante des fondations peu profondes sur des sols non cohésifs dépend fortement - du troisième facteur de portance N_γ. Théoriquement, le troisième facteur, varie de manière significative avec une augmentation de l'angle de frottement du sol (Bowles 1996; Eslami et al. 2004; Michalowski 1997).

Jahanandish et al. (2010) et Veiskarami et al. (2011) se sont concentrés sur l'effet du niveau de contrainte sur la capacité de portante des fondations au moyen d'une étude numérique. Les résultats sont également comparés aux données expérimentales existantes. Selon cette étude, l'effet du niveau de contrainte a été évalué sur base de la capacité de portance de fondations peu profondes sur des sols à friction dense avec des angles de frottement interne relativement élevés. Sur base de la méthode de ZEL présentée par Roscoe (1970) un code informatique a été développé par Veiskarami et al. (2011) pour étudier l'effet du niveau de contrainte sur N_γ, et pour fournir des valeurs modifiées de N_γ pour des usages pratiques. Puisque la méthode de ZEL est capable de considérer des variations des paramètres de résistance au cisaillement du sol afin de prévoir la capacité de portance réelle de fondations peu profondes, tout en prenant en compte la nature dépendante du niveau de contrainte des éléments du sous-sol. Pour tenir compte de l'effet du niveau de contrainte, il est nécessaire de définir un rapport entre l'angle maximum de frottement du sol et la pression de confinement. La dépendance du niveau de contrainte de l'angle de frottement du sol a été exprimée par le rapport suggéré par Bolton (Eqs. 2.3 et 2.4). Il rapporte l'état de sable dense (sa densité relative) à son angle de frottement

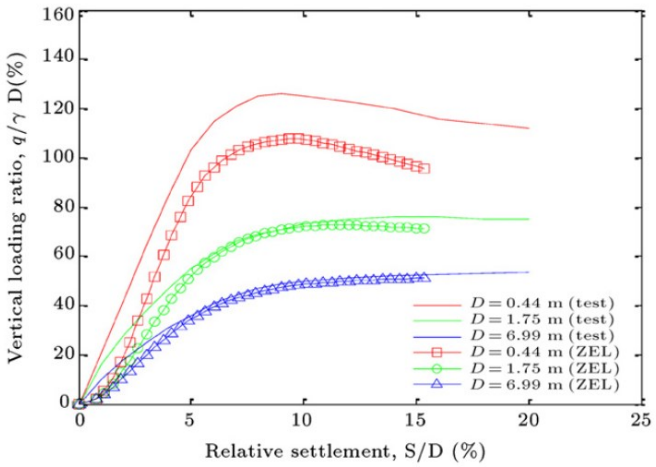

Figure 2.12 Résultats des analyses de charges-déplacement en comparaison avec les données expérimentales de Clark (1998)

mobilisé maximum en fonction du niveau de contrainte dans différents tests de cisaillement en laboratoire.

$$\phi'_{max} - \phi'_{cv} = f(D_R, p') = cI_R$$

$$I_R = D_R(Q - \ln p') - R$$

La comparaison entre les résultats obtenus à partir de la méthode de ZEL et ceux obtenus expérimentalement par Jahanandish et al. (2010) et Veiskarami et al. (2011) a indiqué que tandis que l'effet du niveau d'effort est considéré, la méthode de ZEL fournit des prévisions raisonnables sur la capactié de portance (tableau 2.1) et sur les comportements de charges-déplacement de fondations peu profondes (Figure 2.12).

Figure 2.12 montre la transition entre l'échec général de cisaillement et les modes de défaillance de cisaillement locales quand la taille de la fondation augmente. Ce phénomène peut être considéré comme le résultat direct de la dépendance du niveau de contrainte des paramètres de résistance au cisaillement du sol, qui sont prévus par la méthode basée sur le niveau de contrainte ZEL et le code informatique développé. De telles observations suggèrent d'employer une courbe de charges-déplacement pour trouver la charge finale réelle sur les fondations, plutôt qu'une évaluation relativement grossière de la formule conventionnelle de capacité de portance. L'approche de charges-déplacement, basée sur la méthode de ZEL présentée, en considérant

l'effet du niveau de contrainte, évite deux problèmes communs impliqués dans les équations de capacité de portance : d'abord, en prenant une valeur constante de l'angle de frottement du sol sans l'effet de la taille de la fondation, largement observée par les chercheurs au moyen d'essais expérimentaux, et en second lieu, en ne donnant aucune considération au tassement relatif de la fondation en rupture, ce qui est important pour l'exécution de la structure. La méthode basée sur le niveau de contrainte présentée dans cette section peut également capturer le mécanisme possible de rupture pour différentes tailles de fondation sur le même type de sol.

CHAPITRE 3. Évaluation micromécanique de la fiabilité et de l'applicabilité des mesures aux frontières dans l'essai de cisaillement direct symétrique.

Avant-propos

Auteurs et affiliation :

Samaneh Amirpour Harehdasht: Étudiante au doctorat, Université de Sherbrooke, Sherbrooke, Faculté de génie, Département de génie civil.

Varvara Roubtsova: Chercheuse, Institut de Recherche d'Hydro-Québec, Varennes (Québec).

Mohamed Chekired: Chercheur, Institut de Recherche d'Hydro-Québec, Varennes (Québec).

Mahmoud N. Hussien: Chercheur postdoctoral, Université de Sherbrooke, Sherbrooke, Faculté de génie, Département de génie civil.

Mourad Karray: Professeur, Université de Sherbrooke, Faculté de génie, Département de génie civil.

Date de soumission : juillet 2016
État de la soumission : en évaluation par le comité de lecture de la revue.

Revue : Computer and Geotechnics

Titre français : Évaluation micromécanique de la fiabilité et de l'applicabilité des mesures aux frontières dans l'essai de cisaillement direct symétrique.

Contribution au document

Ce chapitre réexamine les contraintes et les déplacements obtenus aux limites du DSA par des simulations par la méthode des éléments discrets [DEM] (3D) des essais physiques sur des

échantillons de particules polydispersées en employant le code informatique SiGran. Basé sur un examen complet des accomplissements progressifs de l'interprétation des données et du développement du DSA inclus dans ce chapitre, l'exécution de l'appareil physique de cisaillement direct est optimisée en explorant des modifications sur la configuration de test symétrique. L'équilibre entre le changement de micro-échelle de l'énergie des particules et le travail de macro-échelle des forces externes est également présenté. Afin d'atteindre des conclusions assurées au sujet de la réponse de la micromécanique des échantillons de l'appareil de cisaillement direct, les validations quantitatives des modèles de la DEM sont testées en rapportant les essais physiques aux simulations correspondantes de la DEM

Résumé français

Cet article présente les analyses DEM des réactions à la fois micro- et macro-mécaniques des échantillons tridimensionnels (3D) denses des 102248 sphères de verre testées dans le DSA symétrique virtuel employant le code informatique SiGran. L'accent a été particulièrement mis sur la validation du modèle DEM par la mise en comparaison des résultats des simulations DEM avec leurs équivalents physiques à une échelle macro. La performance du dispositif physique de cisaillement direct est optimisée au moyen de l'exploration des modifications apportées à la configuration du test symétrique. Les résultats numériques fournissent des données quantitatives au sujet des différentes formes d'énergie consommées durant le cisaillement, confirmant d'autres résultats physiques et numériques publiés que nous avons consultés. Les résultats à l'échelle micro révèlent que les paramètres maximaux obtenus à partir de l'arrangement symétrique - adopté dans cette étude - sont très proches de ceux d'un cisaillement simple idéal, soit parce qu'ils permettent une déformation uniforme le long de la bande de cisaillement définie, une orientation horizontale de l'extension linéaire nulle ainsi qu'une coaxialité des contraintes principales et des déformations graduelles à l'état limite. En d'autres mots, les résultats à l'échelle micro, présentés dans cette étude, fournissent de nouvelles preuves qui corroborent l'utilisation ultérieure des mesures à l'état limite dans des tests physiques de cisaillement direct symétrique.

Mots-clés: Essais en laboratoire, analyse numérique, la force de cisaillement

Abstarct

This paper presents DEM analyses of both the macro and micromechanics responses of three-dimensional (3D) dense samples of 102248 glass spheres tested in virtual symmetrical DSA using the computer code SiGran. Particular emphasis is placed on the validation of the DEM model by comparing the results of DEM simulations with their physical counterparts at the macro-scale. The performance of the physical direct shear apparatus is optimized by exploring modifications to the symmetrical test configuration. The numerical results provide quantitative data on different forms of energy consumed during shearing confirming other published physical and numerical results found in the literature. The micro-scale results showed that peak state parameters obtained from the symmetrical arrangement, adopted in this study, are very close to those of an ideal simple shear test, as it permits a uniform deformation within the developed shear band, a horizontal orientation of the zero linear extension, and a coaxiality of principal stresses and incremental strains at the peak state. In other words, the micro-scale results, presented in this study, provide new evidences that corroborate the further use of the boundary measurements in physical symmetrical direct shear tests.

Keywords: Laboratory tests, Numerical analysis, Shear strength

3.1 Introduction

Knowledge of the main factors dominating the strength characteristics of geomaterials has attracted the attention of many researchers and geotechnical engineers since the early 1920s and the relevant literature is abundant among others (Bolton 1986; Lee and Seed 1967; Roscoe 1970; Rowe 1962; Skinner 1969; Terzaghi 1920). The core of these researches relied primarily on laboratory experimentations on drained or undrained soil samples in standard geotechnical apparatuses that has been also developed during that period. Through this long history of research, a common understanding has been gradually formed among the geotechnical community on the inter-particle friction angle, particle rearrangement, and dilation. In the recent decades, the research effort has been more directed towards understanding the fundamental micro-mechanism underlying the strength response and deformation properties of soil as it is, in fact, essential to better interpret important geotechnical phenomena such as sand boils and soil liquefaction (Ishihara 1993; Seed and Idriss 1971; Seed and Lee 1966).

Today's understanding of the micro-scale response of soil is chiefly based on numerical simulations of traditional soil tests, such as triaxial and the direct shear tests. The direct shear apparatus (DSA) is, in particular, one of the oldest and most commonly used laboratory devices, which was constructed by Collin as early as 1846 for slope stability analysis (Skempton 1949). Developing the DSA in its present form dates back to Krey (Krey 1926), which later modified by Casagrande (1936) and Terzaghi (Terzaghi and Peck 1948) to account for the vertical expansion and contraction measurements. However, since the exact state of stress within the shear band was unknown the reliability of traditional direct shear interpretation was questionable (Morgenstern and Tchalenko 1967; Saada and Townsend 1981).

Different boundary constraints or developments have been implemented, through the years, on the direct shear apparatus to ameliorate its results and to obtain peak shear strength very close to that of an ideal simple shear. For example, Jewell (1989) proposed the symmetrical arrangement where the top loading platen was secured to the upper half of the shear box. In this arrangement, the out-of-balance moment that tends to rotate the upper frame and the load pad is prevented allowing the loading platen and the upper half of the box to move as a unit throughout the entire test. In the same context, Shibuya et al. (1997) developed another arrangement in which the load pad can be either fixed or point-contacted to the loading piston resulting in a non-tilting mode of motion during the test. Moreover, the opening between the two halves of the box can be maintained at any prescribed value. Lings and Dietz (2004) applied some modifications to the symmetrical arrangement of Jewell (1989) to improve its performance by transmitting the shear load through ball races bearing on wings attached to the sides of the shear box, resulting in what so-called winged DSA (WDSA). In fact, numerous numerical and experimental endeavors have been utilized to examine, in detail, the soil stress and strain development within a shear box. Some of these attempts are listed in Table 3.1 (Cui and O'Sullivan 2006; Jewell and Wroth 1987; Jewell 1989; Lings and Dietz 2004; Masson and Martinez 2001; Ni, Q et al. 2000; Potts et al. 1987; Shibuya et al. 1997; Wang et al. 2007; Zhang and Thornton 2007). The influences of some factors such as the non-uniform deformation and non-coaxiality of principal axes of stress and incremental strain on the interpretation of direct shear test results, discussed by many authors (Jewell 1989; Wang et al. 2007) are also summarized in Table 3.1.

Table 3.1 Examples of DSA experimental and numerical previous investigations.

Author(s)	Type of work	Main findings
Jewell & Wroth (1987)	Experimental study Symmetrical arrangement 'induced' rotational restraint	• Uniform band of deforming sand is generated across the sample center. • The deviation of the zero linear extension direction at peak from the horizontal is negligible.
Potts et al. (1987)	Numerical simulation 2D FEM	• The strains and stresses within the failure zone at the peak are uniform. • Progressive failure effect is found to be minor within the final failure zone.
Jewell (1989)	Experimental study Symmetrical arrangement	• Symmetrical DSA results correspond closely to those in the simple shear for both φ_{ps} and Ψ. • Non-uniform deformation and non-coaxiality behavior can be considered to interpret DSA results.
Shibuya et al. (1997)	Experimental study 'enforced' rotational restraint	• Nonrotating loading platen is needed to optimize the results. • Effect of wall friction and membrane are not pronounced in a symmetrical arrangement.
Ni et al. (2000)	Numerical simulation 3D DEM (PFC^{3D})	• The major deformation of each sample is located within a narrow shear zone at its mid-height.
Masson & Martinez (2001)	Numerical simulation 2D DEM	• The shear process induces a clear change in contact and contact force orientations. • There is a correlation between the induced anisotropy of the microstructure and macroscopic loading.
Lings & Dietz (2004)	Experimental study The Winged DSA (WDSA)	• Symmetrical arrangement (Jewell 1989) is recommended to adopt in routine direct shear tests. • Upper-frame rotation has an almost negligible effect on the measured parameters in symmetrical tests.
Cui & O'Sullivan (2006)	Numerical simulation 3D DEM	• Significant stress and strain non-uniformities exist within specimens undergoing direct shear tests. • Shear stresses calculated along the boundary are lower than that calculated close to the mid-height.
Wang et al. (2007)	Numerical simulation 2D DEM (PFC^{2D})	• The effect of non-coaxiality is minor for granular material at peak state. • Deviation of zero linear extension direction from the horizontal at peak state is small. • The strength and volume change behavior evaluated at the boundaries of the DSA are valid.
Zhang & Thornton (2007)	Numerical simulation 2D DEM	• The principal directions of stress and strain-rate are coaxial under steady-state conditions. • Evolution of stress ratio inside the shear band is similar to that inferred from boundary forces. • The dilation in the shear band is much greater than that obtained from the boundary observations.

Based on the brief review of literature on the gradual achievements of data interpretation and DSA development presented in Table. 3.1, as well as other comprehensive reviews on the subject that have been published elsewhere (Arthur et al. 1997; Cerato and Lutenegger 2006; Gutierrez and Wang 2010), the performance of the physical direct shear apparatus in this study was optimized by exploring modifications to the symmetrical test configuration. This paper re-examines the stresses and displacements obtained at the DSA boundaries through the three-dimensional (3D) discrete element method (DEM) simulations of physical tests on samples of polydisperse particles using the computer code SiGran (Roubtsova et al. 2011). The balance between the micro-scale change in particle energy and the macro-scale work of external forces is also presented. In order to achieve confident conclusions about the micromechanics response of samples in direct shear tests, the quantitative validations of the DEM models were attempted by relating the physical tests to the corresponding DEM simulations. Experimental direct shear tests were mainly carried out using the symmetrical arrangement suggested by (Jewell 1989) and its underlying features described in detail in Appendix A.

3.2 Laboratory test procedure

3.2.1 Material

The experimental part of this study was performed using the polydisperse particle standard. microspheres produced by Whitehouse Scientific Ltd, England, having the range size of 500 to 2000 μm each with good sphericity. The particle size distribution, determined by electroformed sieve analysis and the microscopy method, mechanical, and physical properties of selected polydisperse spherical particles are shown in Table. 3.2.

3.2.2 Shear box testing device, and physical testing procedure

In the current study, the performance of the symmetrical direct shear apparatus has been optimized by exploring different test configurations (e.g., fix load pad to the upper frame, modified collar attachment, initial gap between the shear-box frames, and the use of a thin membrane). A section and plan of the modified symmetrical direct shear apparatus are shown

Table 3.2 Properties of polydisperse spherical particles.

500-2000 (μm)	Size at Fixed Percentiles (μm)							
	1	5	10	25	50	75	90	95
Final Mean Size (μm)	524	623	691	853	1011	1248	1534	1687
(+/-) 95% confidence	3.2	4.9	5.7	7.8	11	24	48	38
Mechanical/ Physical Properties	Young Modulus (N/mm^2)				6.89×10^4			
	Rigidity Modulus (N/mm^2)				2.96×10^4			
	Poisson ratio				0.21			
	Specific Gravity (gr/cm^3)				2.43-2.49			

in Figure. 3.15 of Appendix A. These modifications were suggested by a number of researchers (Jewell and Wroth 1987; Jewell 1989; Lings and Dietz 2004; Shibuya et al. 1997) to ensure the accuracy of results obtained during shearing. The characteristic most commonly addressed in these studies is the tendency for the load pad and upper frame to rotate during conventional testing.

In the tests conducted here, the polydisperse samples were prepared and sheared in dry conditions. Three direct shear tests were performed at three different normal pressures (50, 200, and 400 kPa) and at a constant relative density of approximate 90%. The maximum and minimum densities of each sample were measured in the dry state, using the method specified by Muszynski (2006).

3.2.3 Theoretical background

The DEM program SiGran used in this study is based on the discrete element method pioneered by Cundall and Strack (1979). An explicit time-stepping numerical scheme is implemented in the DEM method to describe the behavior of the assembly of particles interacting via contact logic, and offer a thorough perspective of the response at the particulate level as well as the overall behavior. The DEM keeps track of the motion of individual particles and updates any contact with neighboring elements according to the Newton's second law. The detailed description of the motion of the particle (i^{th} particle) used in this study is given below (Figure. 3.1). Note that, the subscript j refers to the j^{th} neighboring particle, and k is the number of neighboring particles.

$$m_i \frac{d\vec{V}_i}{dt} = m_i\vec{g} + \sum_{j=1}^{k}\left(\vec{F}_{cn,ij} + \vec{F}_{dn,ij} + \vec{F}_{ct,ij} + \vec{F}_{dt,ij}\right) + \vec{F}_{ft} \qquad (3.1)$$

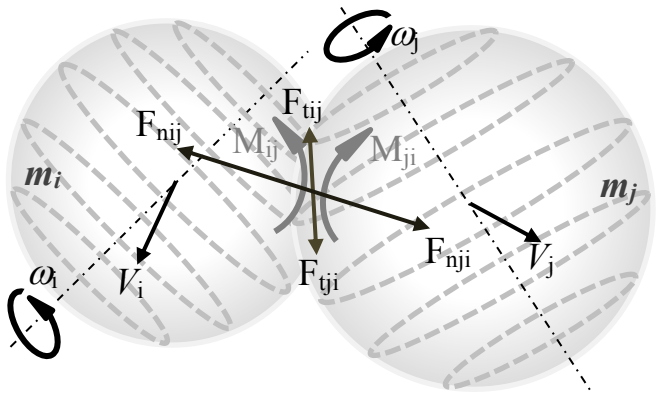

Figure 3.1 Interactive forces between two particles.

$$I_i \frac{d\vec{\omega}_i}{dt} = \sum_{j=1}^{k} \left(\vec{T}_{ij} + \vec{M}_{ij}\right) + \vec{M}_{ft} \tag{3.2}$$

m_i, and I_i are the mass (kg) and moment of inertia (kg.m^2) of particle i, respectively. $\vec{v}_i$ and $\vec{\omega}_i$ are the transitional and rotational velocities of particle i.

$F_{cn,ij} = -K_n \delta_n^{\frac{3}{2}} \vec{n}$ (N) is the normal force of contact.

$\frac{d\vec{F}_{ct,ij}}{d\vec{\delta}_t} = -K_t$ (N) is the tangential contact force, which is limited by Coulomb's law $\left|F_{ct,ij}\right| \le \mu_s F_{cn,ij}$.

$F_{dn,ij} = -C_n \vec{V}_{n,ij}$ (N), and $F_{dt,ij} = -C_t \vec{V}_{t,ij}$ (N) are the normal and tangential damping forces, respectively.

In these equations $K_n = \frac{4}{3} E^* \sqrt{R^*}$, $C_n = 2\sqrt{m^* K_n}$, $K_t = 2\sqrt{R\delta_n}\left(\frac{G_i}{2-\nu_i} + \frac{G_j}{2-\nu_j}\right)$, and $C_t = K_n \sqrt{\frac{K_t}{K_n}}$.

$$\frac{1}{E^*} = \frac{1-\nu_i^2}{E_i} + \frac{1-\nu_j^2}{E_j} \tag{3.3}$$

$$\frac{1}{R^*} = \frac{1}{|R_i|} + \frac{1}{|R_j|} \tag{3.4}$$

where E is Young's modulus (Pa), ν is Poisson ratio, R_i is the particle radius (m), and μ_s, μ_r are the sliding and rolling (m) friction coefficient. δ_n, and δ_t are the normal and tangential contact displacement.

$\vec{T}_{ij} = R_i\left(\vec{F}_{ct,ij} + \vec{F}_{dt,ij}\right)\ (N.m)$, and $\vec{M}_{ij} = -\mu_r\left|\vec{F}_{cn,ij}\right|\frac{\omega_i}{|\vec{\omega}_i|}\ (N.m)$ are the rolling torque, and the friction torque, respectively.

3.2.4 Input data and simulation process

The simulation were conducted on a polydisperse system of 102248 glass spheres. The same particle size distribution as experimental tests were used for simulations. In DEM models the assigned micro-parameters in the models other than those directly measured were chosen as to produce the desired macro-properties of the material being tested in the laboratory (Table 3.3).

Sample preparation was simulated by placing the particles randomly into the shear box and considering their interaction under the force of gravity. Once the sample was generated, the virtual specimen were subjected to 50, 200 or 400 kPa normal stress. Normal stress was applied as a small displacement at the top boundary. This displacement must be sufficient to stabilize a vertical force after a perturbation of particles at each time step, and small enough to preserve the stability of the numerical solution. In each step, the displacement was calculated using the practical Eq. 3.5, which takes into account the required normal stress and the diameter of the smallest particle:

$$\delta_v = -1.10^{-3} d_{min}\left(S_r - S_t\right)/S_r \qquad (3.5)$$

δ_v is the displacement of the top wall (mm), S_r and S_t are respectively the required and current normal stresses (Pa), d_{min} is the diameter of the smallest particle (mm).

Table 3.3 Input Micro-Parameters for DEM simulations.

Parameter	Value
Young's Modulus	68.9 GPa
Poisson Ratio	0.21
e_{max} - e_{min}	0.69- 0.51
Density	1603 kg/m^3
Coefficient of sliding friction particle-particle	0.2
Coefficient of sliding friction wall-particle	0.3
Coefficient of rolling friction	5.10^{-3} mm

Shearing was imposed by displacing the upper half of the shear box horizontally at a constant velocity equal to that the experimental tests while the lower half was restrained from moving.

The top and bottom boundaries were free to move vertically, but not to rotate. During all simulations, no out-of-plane motion was permitted. The test arrangement adopted for these simulations is schematically illustrated in Figure. 3.2.

3.3 Macroscopic shear test results

In the analysis, virtual and physical samples were all sheared at the same initial relative density and under the three normal stresses of 50, 200, and 400 kPa. The computed and measured ratios of shear stress to normal stress (τ/σ_n) evaluated at the boundaries at different normal stresses are plotted against the corresponding horizontal displacements in Figure. 3.3a. It can be seen from Figure. 3.3a that the peak stress ratio occurs earlier at a relatively low stress level (50 kPa), and the maximum stress ratios decreases with increasing the applied normal stress from 0.65 to 0.57 and from 0.63 to 0.53 for both measured and computed curves, respectively. This reduction in the stress ratio with increasing normal stress is in agreement with earlier results reported by

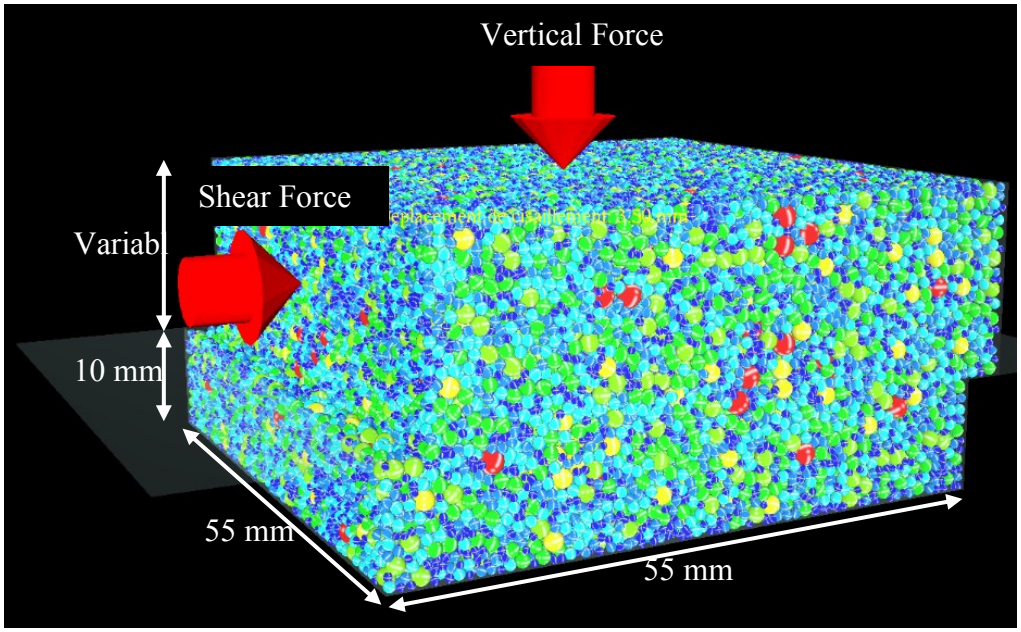

Figure 3.2 Schematic representation of the shear box test simulation

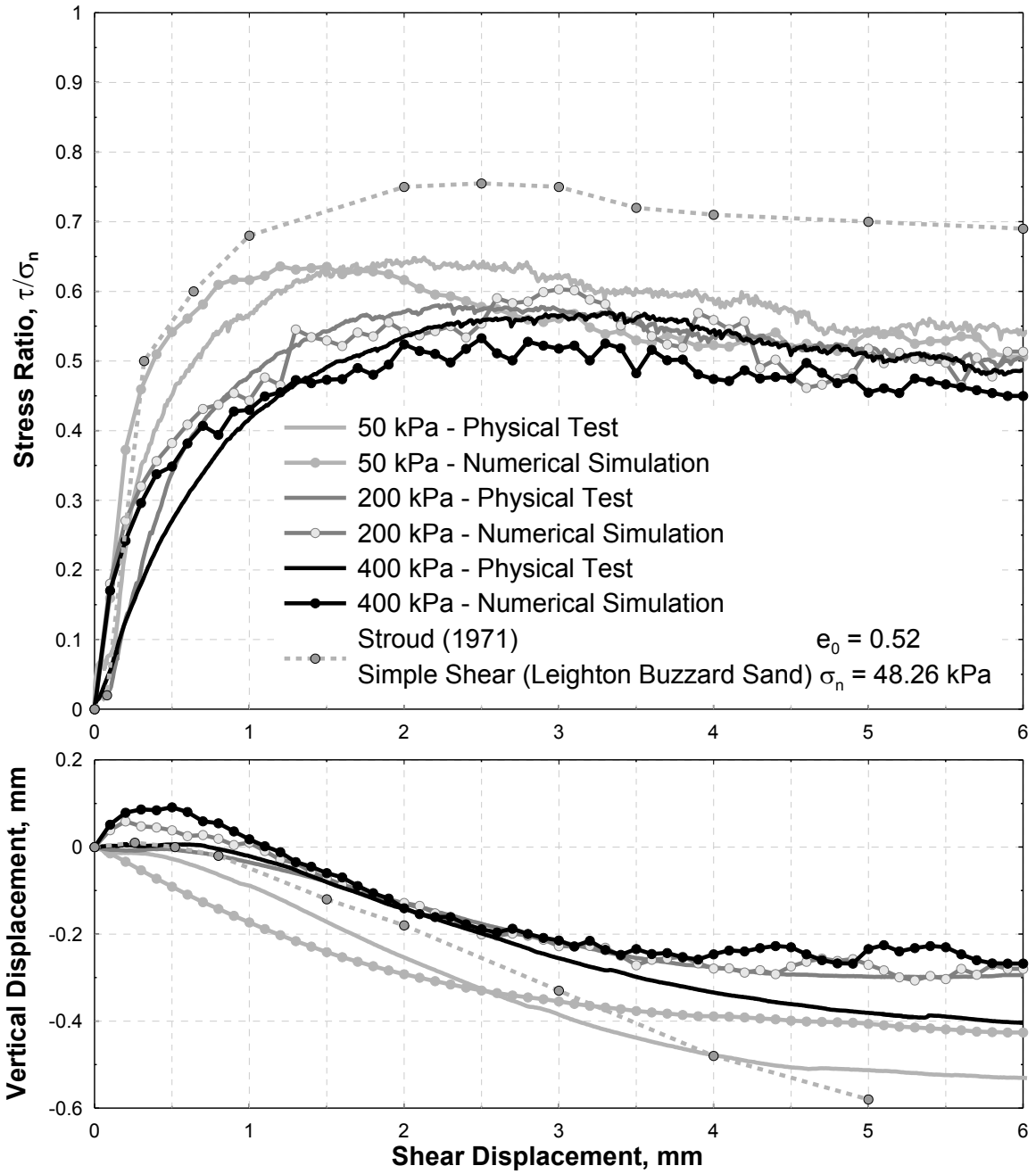

Figure 3.3 Computed and measured strength and deformation responses: (a) stress ratio-shear displacement curves; (b) vertical displacement-shear displacement curves.

Cui and O'Sullivan (2006), Ni, Q et al. (2000), and Zhang and Thornton (2007) also based on DEM simulations. For all cases examined, Figure 3.3a shows also that when the horizontal displacement exceeds a certain limit of 4.5 mm, the stress ratio (τ/σ_n) decreases toward a residual value of about 0.5 at the critical state, irrespective of the initial stress applied.

Table 3.4 Peak and critical state strength ratios and dilation angles evaluated by experimental

Parameter	$\sigma_n = 50kPa$	$\sigma_n = 200kPa$	$\sigma_n = 400kPa$
Experimental Tests			
Peak $(\tau/\sigma)_{ds}$ [1]	0.65	0.58	0.57
Peak ϕ_{ds} (°)[2]	32.96	30.14	29.66
Peak ϕ_{ps} (°)-Eq. (13)[3]	34.19	31.50	31.08
Critical State ϕ_{ds} (°)	28.23	26.56	25.96
Peak ψ (°)[4]	18.50	14.13	13.10
Numerical Simulations			
Peak $(\tau/\sigma)_{ds}$	0.63	0.60	0.53
Peak ϕ_{ds} (°)	32.45	31.09	28.05
Peak ϕ_{ps} (°)-Eq. 13	33.48	32.34	29.06
Peak ϕ_{ps} (°)-Eq. 14	33.61	31.36	29.29
Critical State ϕ_{ds} (°)	27.06	25.54	24.21
Peak ψ (°)	19.07	14.30	13.50
Peak $\Delta\theta$ (°)[5]	-1.28	-3.00	0.00
Peak $\Delta\psi$ (°)[6]	0.85	2.30	1.50
Orientation of Shear band			
Mohr-Coulomb (°)	7.74	7.32	8.53
Roscoe (°)	0.53	1.15	0.75

Note:

[1] τ is the average horizontal shear stress; σ is the average vertical normal stress

[2] $\phi_{ds} = \tau/\sigma$ is the direct shear friction angle

[3] ϕ_{ps} is the plane strain friction angle

[4] $\psi = d\upsilon_y / d\upsilon_x$ is the dilation angle measured in boundaries, where $d\upsilon_y$ and $d\upsilon_x$ are the rate of change of vertical and horizontal displacement, respectively.

[5] $\Delta\theta$ is the angle between principal stress and principal strain incremental directions

[6] $\Delta\psi$ is the difference in the computed dilation angle in boundaries to that inside the shear band

The computed and measured relative vertical displacements of the bottom and top boundaries versus shear displacement are portrayed in Figure. 3.3b for all cases considered. A positive vertical deflection refers to a decrease in volume, whereas a negative deflection indicates a volume increase. At relatively low normal stress of 50 kPa, dilation of the sample takes place at a very early stage of testing. However, when higher normal stress was applied, the virtual samples undergo contractive behavior at the beginning of the test, followed by less significant dilation than that of the lower stress level (50 kPa). For the three numerical cases, the highest dilatancy rate occurs at the peak state, thereafter the rate of dilation decreased with continuous

shearing while the critical state was reached. This observation is in agreement with the dilation behavior observed in the experiments. It can be seen that the measured and the calculated peak dilatancy angles deducted from the boundaries measurements underestimate slightly by $\Delta\psi$ less than 2.5° than that inside the shear zone due to averaging effects. The other macro-scale test results are summarized in Table. 3.4.

The simple shear test results of Stroud (1971) on dense sample made up of Leighton buzzard sand (rounded particles, $D_{50}=780\mu m$, $e_0=0.52$, $\sigma_n=48.26kPa$, $\phi_\mu=15°-20°$) are also shown in Figure. 3.3 to verify the macro-scale results of physical tests. As can be seen in this figure, there is a marked similarity between the two set of simple shear and improved arrangement of symmetrical direct shear for glass beads ($D_{50}=1000\mu m$, $e_0=0.53$, $\sigma_n=50kPa$) results. In both simple shear and direct shear tests following a negligible initial volumetric compression at small axial strain, significant dilation occurs, until the mobilized stress ratio approaches its maximum value. Further shearing, however, induces significant dilatation but a relatively small change in stress ratio, resulting in a plateau on stress ratio-axial strain curves.

3.4 Micromechanical analysis

3.4.1 Evolution of anisotropy parameters in fabric

Results of numerous numerical investigations (Bathurst 1985; Cui and O'Sullivan 2006; Thornton 2000) have shown that two competing micro-scale processes take place during transition to critical state. The first process is a tendency to disorder, which can be observed as a reduction in the coordination number, and a corresponding increase in void ratio, *e*. Superimposed on this process is a tendency to create the fabric anisotropy and contact forces (Bathurst and Rothenburg 1990). The coordination number (CN) is a scalar parameter defined as the mean contact numbers per particle for a granular assembly, where C is the number of contacts, and N is the number of particles.

$$CN = 2C/N \tag{3.6}$$

Figure. 3.4a shows the evolution of CN versus the shear displacement for three values of normal stresses. Figure. 3.4a illustrates that CN decreases rapidly during the initial 8% of the total shear

displacement, and flatten off to a relatively steady value while the critical value is attained. In the same context, Figure. 3.4b shows that CN does not reflect a significant rearrangement of particles, so that the initial reduction in CN values does not attribute to a rapid reduction in density (increase in Δe). In addition, Figure. 3.4 suggests that higher normal stress value may assist specimen with a larger CN to sustain higher shear stress value in agreement with earlier observations (Bathurst 1985; Cui and O'Sullivan 2006; Oda 1977). However, the coordination number alone is an incomplete description of micro-scale shear deformation, as it carries no information on relative particle orientation and interparticle forces.

Another key parameters controling the degree of deformation and non-coaxility between principal axes in granular materials subjected to monotonic shearing are the ratio between the degrees of fabric anisotropy and that of force anisotropy, and the angle between the principal fabric direction and the applied loading direction (Bathurst 1985; Rothenburg 1981). These parameters can be quantified by using the data registered during the numerical simulations in the micro-scale. In addition referring to the work by Bathurst and Rothenburg (1990), one may use the second-order form of Fourier series expansion to approximate the directional distribution of those micro quantities (Eqs 3.7-3.9):

$$E(\theta)=\frac{1}{2\pi}\{1+a\cos 2(\theta-\theta_a)+b\cos 4(\theta-\theta a)\} \tag{3.7}$$

$$\bar{f}_n^c = f_n^o\{1+a_n\cos 2(\theta-\theta_n)\} \tag{3.8}$$

$$\bar{f}_t^c = f_n^o\{a_w - a_s \sin 2(\theta-\theta_s)\} \tag{3.9}$$

where the non-dimensional a, a_n, a_s, a_w, and b are coefficients of anisotropy which are measures of the intensity of contact normal $E(\theta)$, normal force $\bar{f}_n^c$, and tangential force $\bar{f}_t^c$ distributions in the directions of anisotropy denoted by θ_a, θ_n, and θ_s, respectively.

Rothenburg (1981) developed powerful relationships, which equate the micromechanical parameters identified above to the macro-scale shear capacity of the system. So that, if distributions for contact force components and contact normal are assumed to have coaxial directions of anisotropy then:

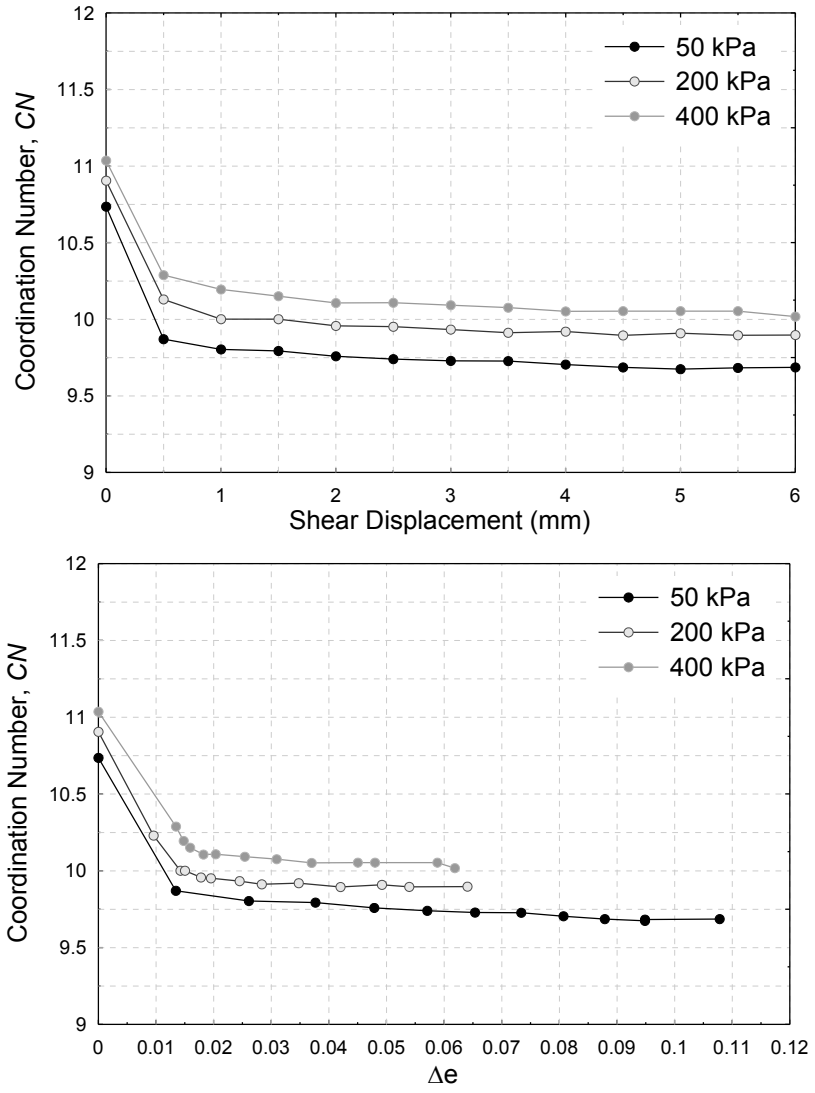

Figure 3.4. Evolution of the coordination number (*CN*) as a function of: (a) shear displacement; and (b) change of void ratio.

$$\frac{\sigma_t}{\sigma_n} = \frac{1}{2}\left(a + a_n + a_s\right) \tag{3.10}$$

The evolution of fabric anisotropy and contact force anisotropy, i.e. initial, peak, and ultimate states, for the three series of virtual tests are plotted in Figures. 3.5-3.7, in terms of the anisotropy magnitudes and directions. After shearing begins, the significant increase in the contact anisotropy is generated primarily by the reduction in the number of contact normal falling within 10 degrees of the minor principal stress direction (Bathurst 1985; Oda and Konishi 1974).

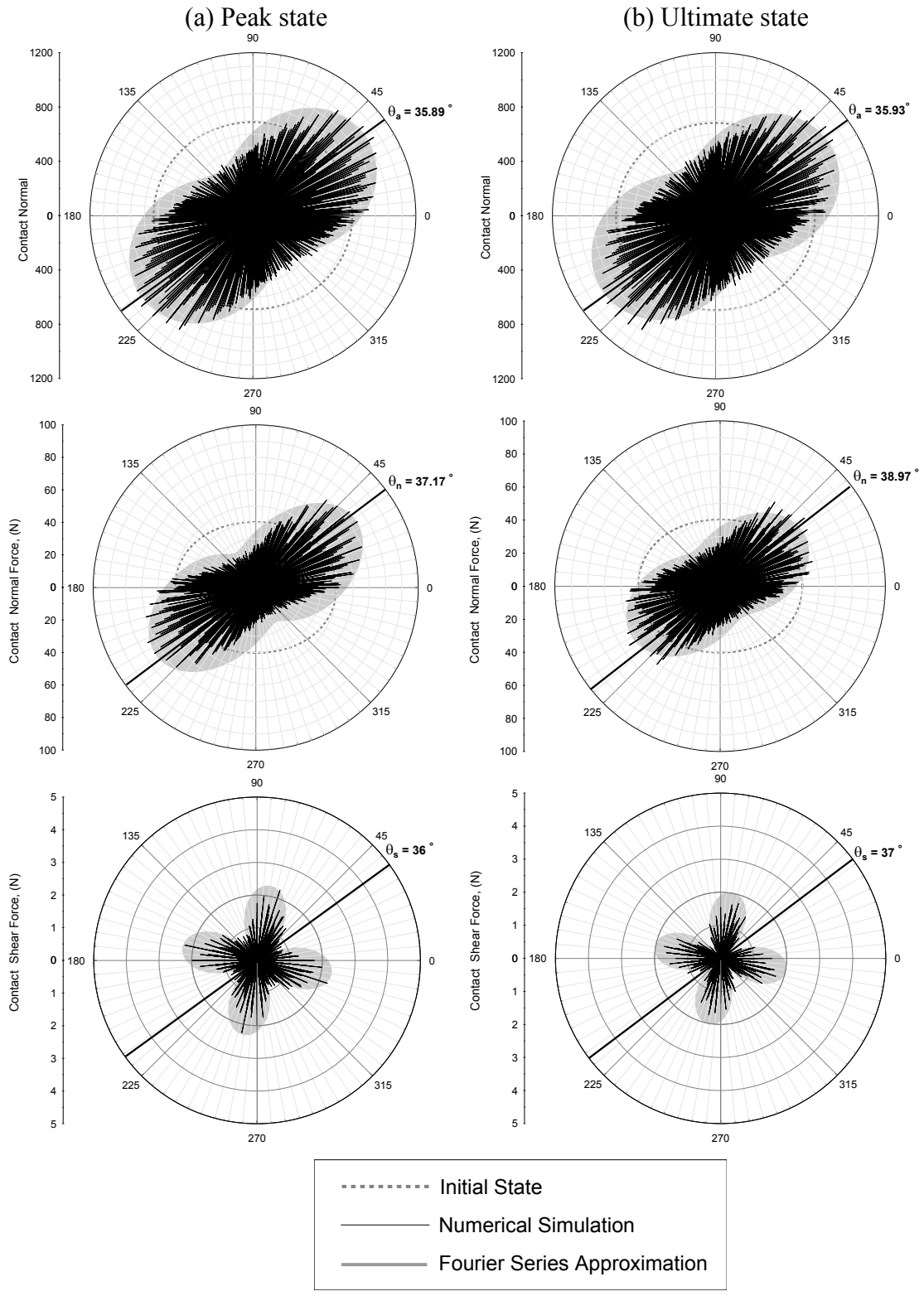

Figure 3.5. Anisotropies of contact normal, contact normal force, and contact shear force inside the sample during shear process (σ_n=50 kPa): (a) at peak state (1 mm displacement) and (b) at steady state (6 mm displacement).

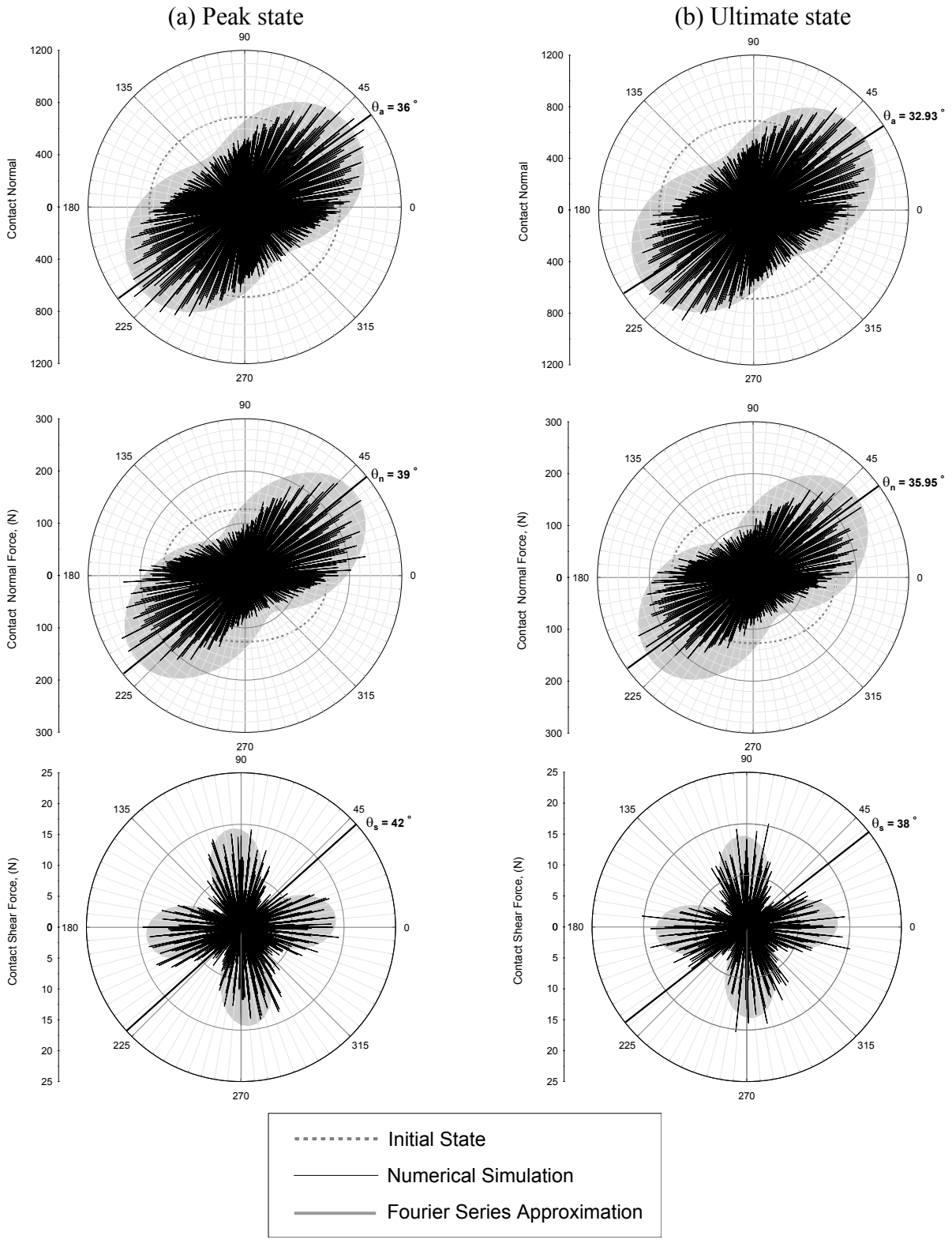

Figure 3.6. Anisotropies of contact normal, contact normal force, and contact shear force inside the sample during shear process (σ_n=200 kPa): (a) at peak state (2.5 mm displacement) and (b) at steady state (6 mm displacement).

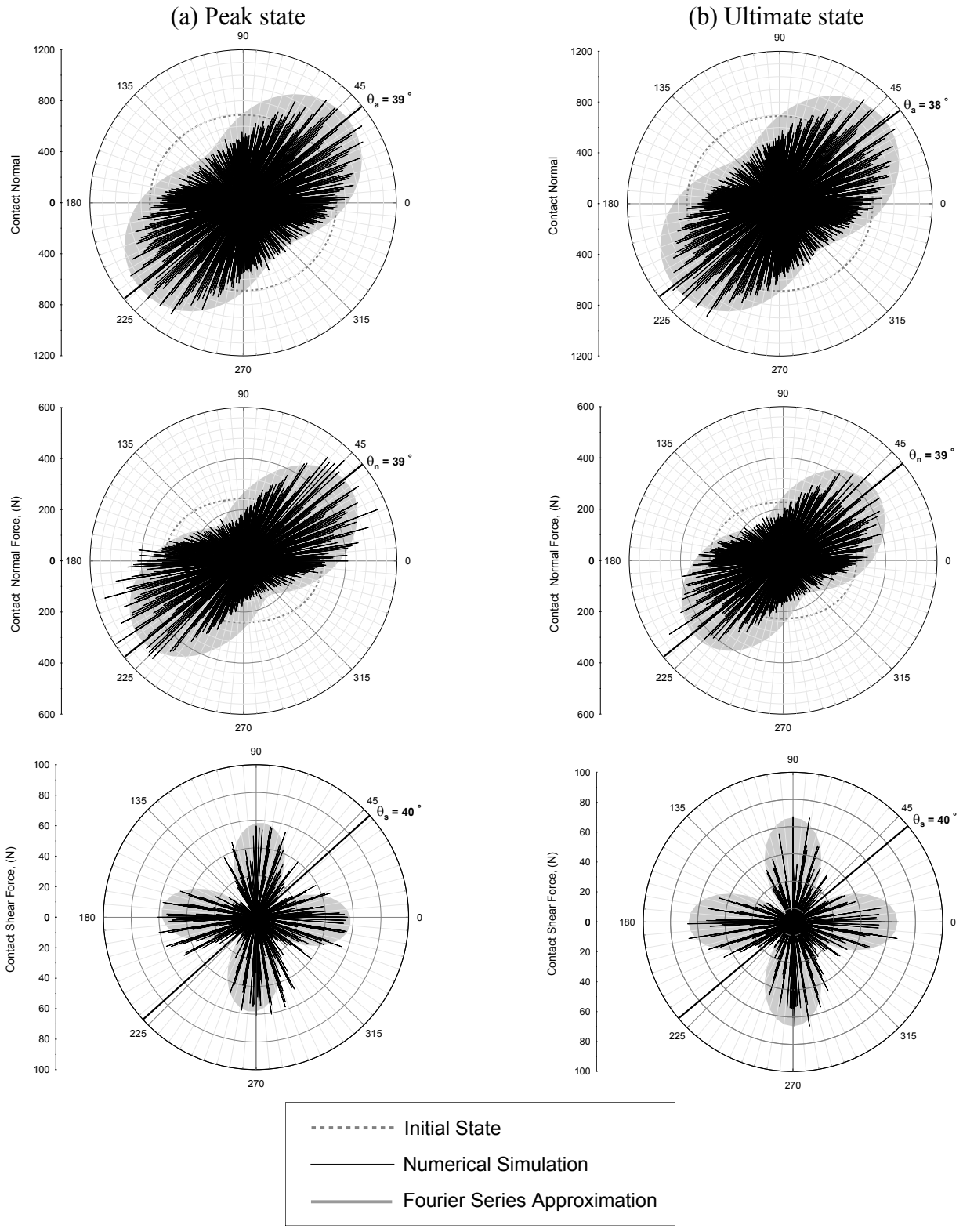

Figure 3.7. Anisotropies of contact normal, contact normal force, and contact shear force inside the sample during shear process (σ_n=400 kPa): (a) at peak state (2 mm displacement) and (b) at steady state (6 mm displacement).

Distinctive peaks of number of contacts in θ_a direction represent the higher order chains of contacts extend through the upper right to the lower left corner.

In Figures 3.5-3.7, the distribution functions $E(\theta)$, $\bar{f}_n(\theta)$ and $\bar{f}_s(\theta)$ (Eqs. 3.7-3.9) appear to well represent the trends of the computed data in all stages. However, unlike approximations using Fourier series, the anisotropies using numerical data do not display full symmetry. This could be interpreted according to (Wang et al. 2007) who attributed the asymmetry of the anisotropies to the asymmetry in external loads applied on the shear box boundaries.

Comparing Figures 3.5 to 3.7 shows that the distribution of contact normal at various states are quite similar at different applied normal stresses in that it increases slightly with the increase of the normal stress. This is consistent with the aforementioned observation in Figure. 3.4 where the larger coordination number achieved at higher normal stress values. On the other hand, it can be seen in Figures 3.5 to 3.7 that although the distribution patterns of normal and tangential contact force are similar, their magnitudes are highly dependent on the applied normal stress.

Normal and tangential contact force distributions during shearing are also shown in Figures. 3.5-3.7, so that the evolution of the coefficients of the contact force anisotropy a ,a_n, a_s, a_w, and the principal contact force directions θ_a, θ_n and θ_s were obtained from similar plots every 0.5 mm of horizontal displacement and presented in Figure. 3.8. This figure shows that the value of a_w is nearly zero and can be eliminated from Eq. 3.9. Figure 3.8 shows also a rapid increase in a_n and a_s values at the initial stage of shearing. In the three normal stresses examined, normal and tangential contact force anisotropies reach their maximum values at the peak state. With further shear distortion, the value of a_n decreases gradually while that of a_s fluctuates around a constant value. The orientation of contact normal θ_a and contact force tensors anisotropies θ_n and θ_s are coincided during all stages of the test as illustrated in the lower parts of Figures 3.8a-c, especially at the peak state. Their minor deviations from coaxiality in other states (stages of shearing) are also negligible, thus Eq. 3.10 is still valid.

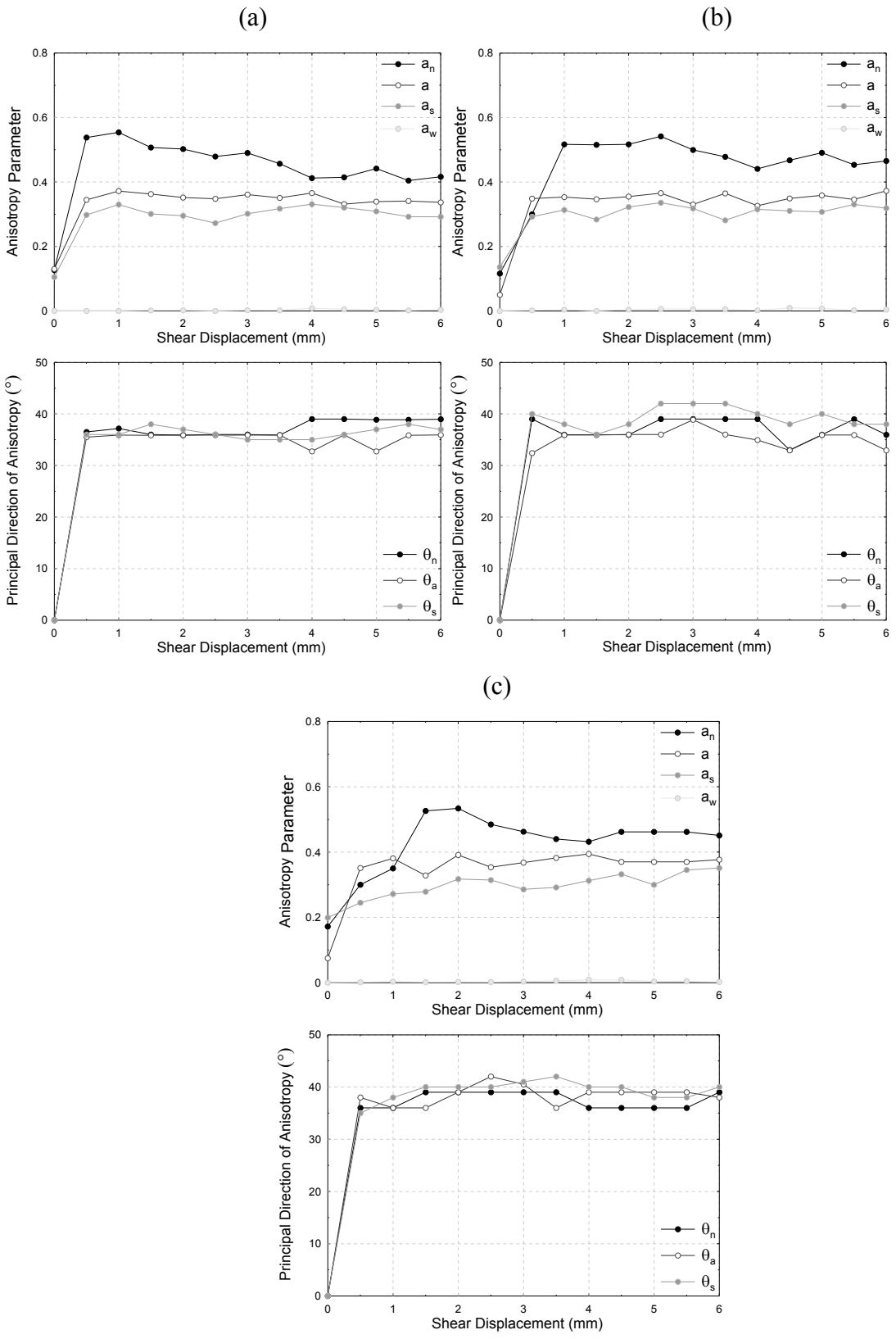

Figure 3.8. Magnitudes and orientations of anisotropies during shear at applied normal stress of: (a) σ_n=50 kPa, (b) σ_n=200 kPa, and (c) σ_n=400 kPa.

(a) 50 kPa

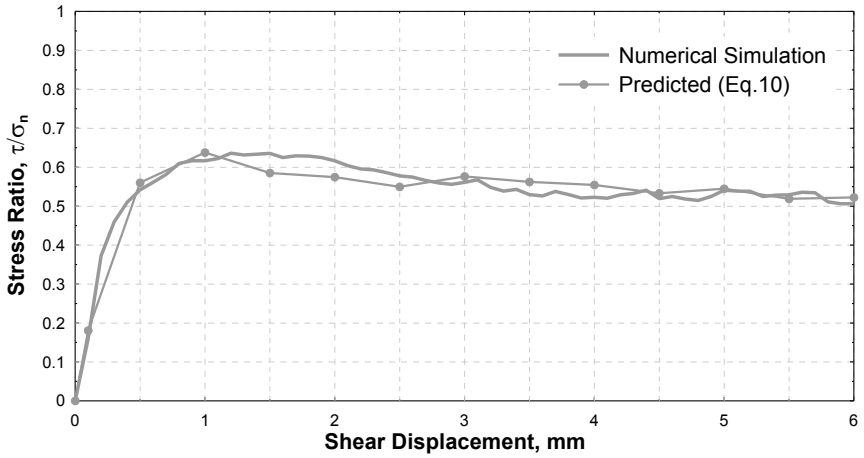

(b) 200 kPa

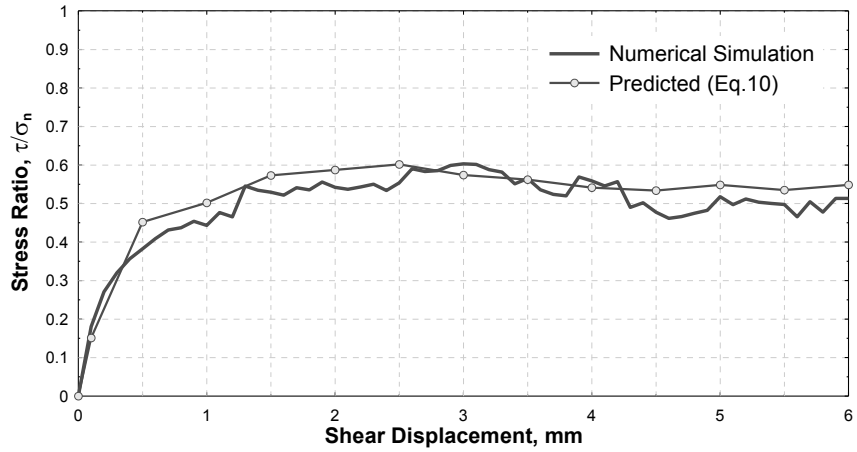

(c) 400 kPa

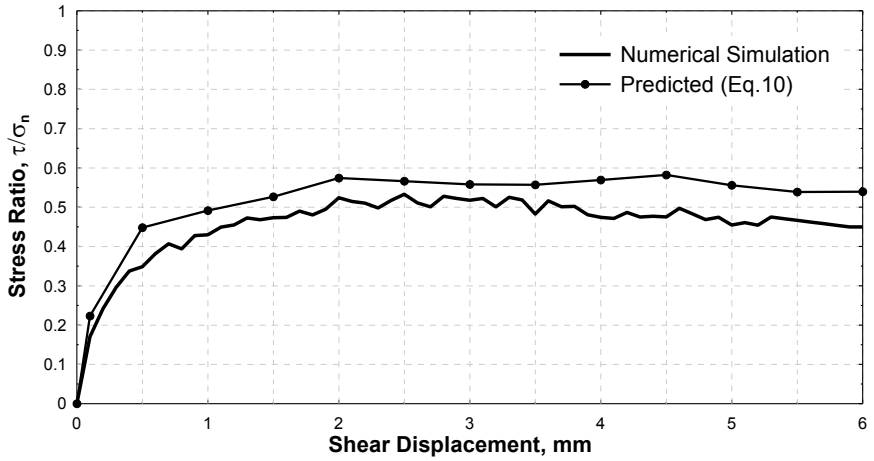

Figure 3.9. Comparison between predicted stress ratios using anisotropy parameters (Eq. 10) and obtained stress ratios from simulations at different normal stresses.

Tracing the anisotropy parameters during the direct shear test, the results of numerical simulations using Eq. 3.10 are shown in Figure. 3.9 for the three applied normal stresses. These predicted curves appear to be reasonable approximations to the obtained invariant stress ratios from simulations, while the discrepancy is less than 8% at peak state, confirms again the coaxiality of the contact force components and contact normals anisotropies during shearing.

3.4.2 Energy dissipation

The work done by external forces must equal the energy consumed internally due to the particle motions, including particle translation, rotation, rolling, and sliding at contacts during an equivalent time step of shearing. This equilibrium is achieved and shown in Figure 3.10 for the tested samples under different normal stresses. As expected, Figure 3.10 shows that the total energy in the samples consumed during shearing increase proportionally with the increase in the applied normal stress.

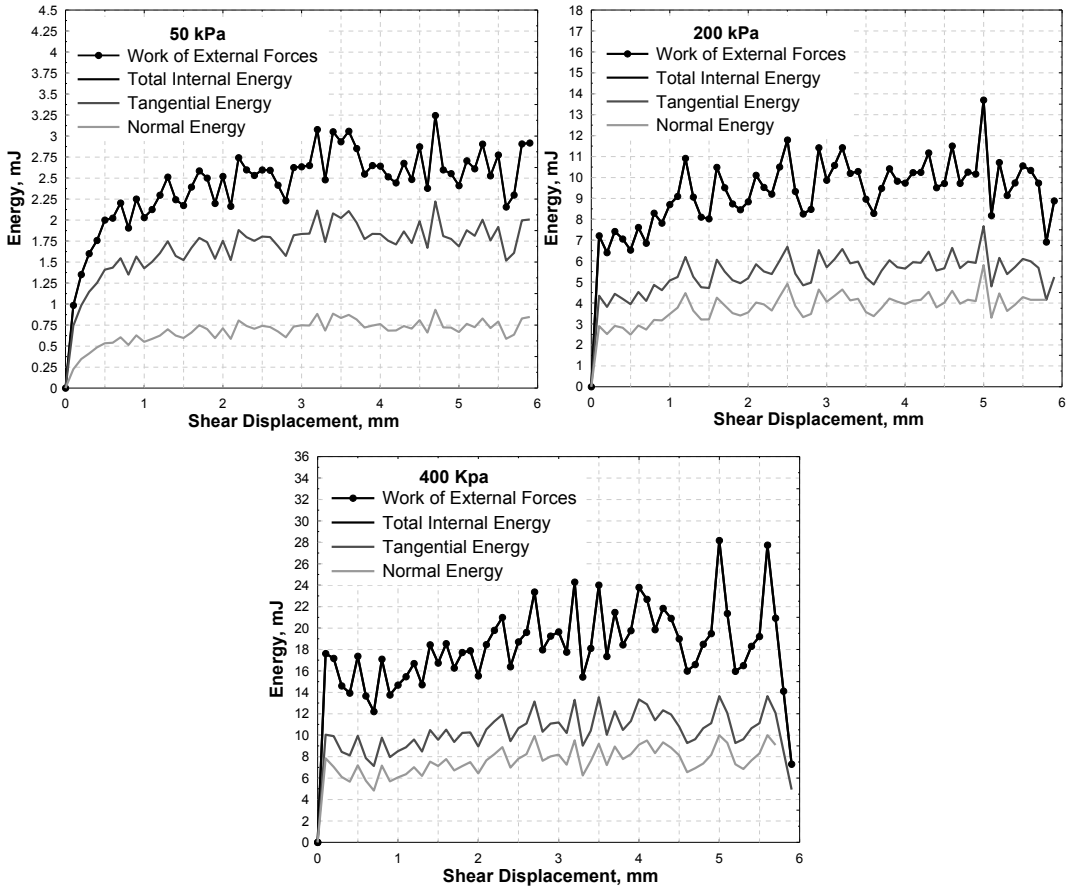

Figure 3.10. The balance of the external work and total internal energy;
and two significant components of total energy (normal and tangential energy).

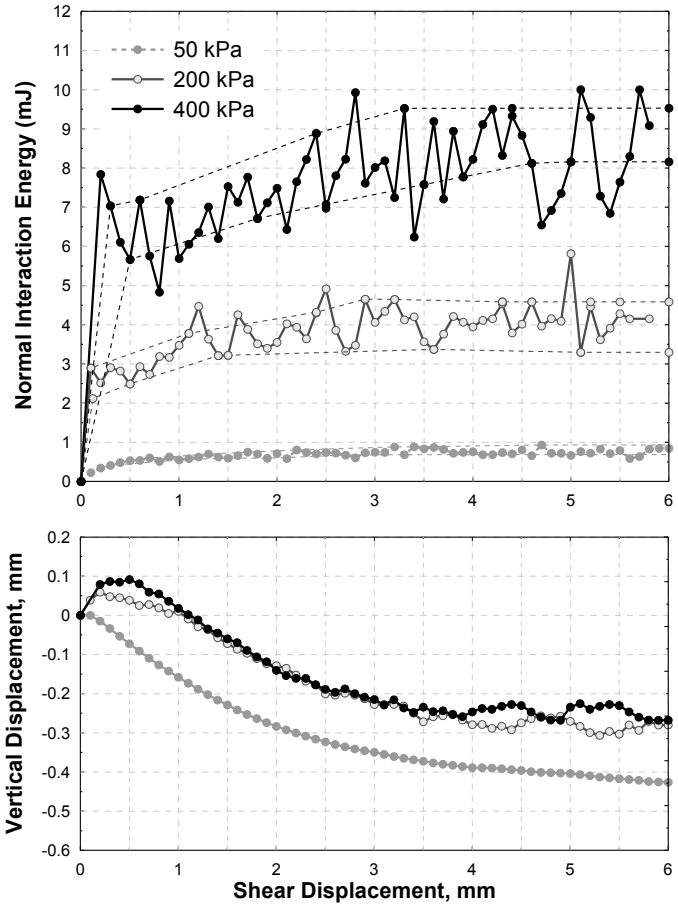

Figure 3.11. Variation of normal energy and its corresponding vertical displacement with shear displacement

According to Roubtsova et al. (2015), part of the internal energy is absorbed by the normal interactions of particles, when a particle falling on the other particles (Figures 3.10-3.11). This part of the internal energy, which can be calculated using Eq. 3.11, is associated with the volume change due to vertical displacement of the particles, irrespective of the tangential forces, and rolling moments.

$$E_k + E_p + E_e + E_{dn} = \sum_{i=1}^{n} \frac{m_i v_i^2}{2} + \sum_{i=1}^{n} m_i h_i g + \sum_{i=1}^{n} \sum_{j=1}^{k} \frac{2}{5} k_{nij} \delta_{nij}^{\frac{5}{2}} + \sum_{i=1}^{n} \sum_{j=1}^{k} \int_0^{\delta_{ij}} F_{dnij} d\delta_n = const \qquad (3.11)$$

where E_k, E_p, E_e, and E_{dn} are the kinetic, potential, elastic, and normal dissipation energies for all n particles. k is the number of contacts for particle i with neighboring particles j.

The variation of normal energies and their corresponding vertical displacements versus shear displacements are portrayed in Figure 3.11 for the three virtual tests. The increase of normal energy, which is required to induce the dilation, with increasing applied normal stress is apparent in this figure. The smooth curves (dashed lines) capturing the trend of data, show the initiation of normal energies at the beginning of shearing and their gradual increase to the point of zero rate of dilation and complete shear band formation.

The second part of the total energy associated with the rotation, rolling and sliding motion of particles can be expressed using Eq. 3.12. Detailed descriptions of the equations used in the energy analyses presented here can be found in (Roubtsova et al. 2015). In the current simulations, the spherical particles were allowed to rotate considering the rolling friction coefficient of $5.10^{-3} mm$.

$$E_{kt} + E_{kr} + E_p + E_f + E_{fd} + E_{Md} = \sum_{i=1}^{n} \frac{m_i v_i^2}{2} + \sum_{i=1}^{n} \frac{I_i \omega_i^2}{2} + \sum_{i=1}^{n} m_i h_i g + \sum_{i=1}^{n} \sum_{j=1}^{k} \int_{0}^{L} F_f d\delta_t + \sum_{i=1}^{n} \sum_{j=1}^{k} \int_{0}^{L} F_{dt} d\delta_t + \sum_{i=1}^{n} \sum_{j=1}^{k} \int_{0}^{\phi} M_d d\phi = const \quad (3.12)$$

where E_{kt} in the kinetic energy of translation, E_{kr} is the kinetic energy of rotation, E_f is the friction energy, E_{fd} is the dissipation energy in tangential direction, and E_{Md} is the work of dissipation moment. ϕ is a relative angle of rotation of particles during interaction (rad).

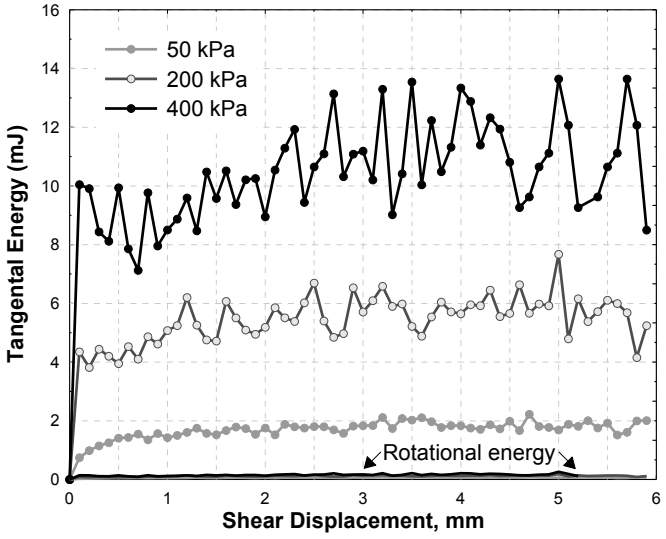

Figure 3.12. The tangential energy as sum of the rotational energy and sliding/rolling energy.

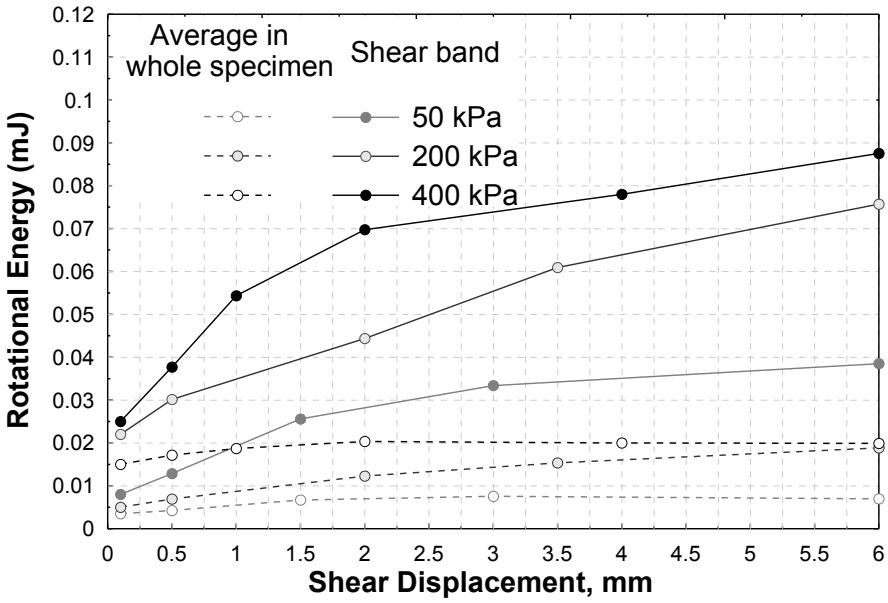

Figure 3.13. Variation of rotational energy versus shear displacement for the whole specimen and particles inside the shear band

In Figure. 3.12, the internal energy due to tangential interaction of the particles is shown as the sum of the energies dissipated through the rotational and sliding/rolling of particles. As shown in this figure for the three normal stresses, the average rotational energy consumed inside the sample is practically small within the whole specimen, whereas it steadily increases with shear displacement inside the shear band (Figure. 3.13). In other words, the tangential interaction energy can be mainly equated to the rolling and sliding of particles. The ratios of the consumed energy associated with the normal to the tangential interaction of particles are 36%, 50% and 74% respectively for normal stresses of 50, 200, and 400 kPa in Figure. 3.10. The ratio of the rotational energy to the tangential energy is less than 3% for the three cases (Figure. 3.12).

Although the amount of rotational energy is small compare to the energies associated with the normal interaction and sliding/rolling of particles, it stated as a good indicator of shear localization leading to the establishment of shear bands (Bardet 1994; Dyer and Milligan 1984; Jewell and Wroth 1987; Oda and Kazama 1998; Potts et al. 1987; Zhang and Thornton 2007). Figure. 3.14 presents the spatial distribution of rotational energy inside the samples together with the rotational energy along their heights during different stages of shear distortion (O-A, A-B, B-C, and B-D). During stage O–A, the rotational energy at the mid-height of the sample

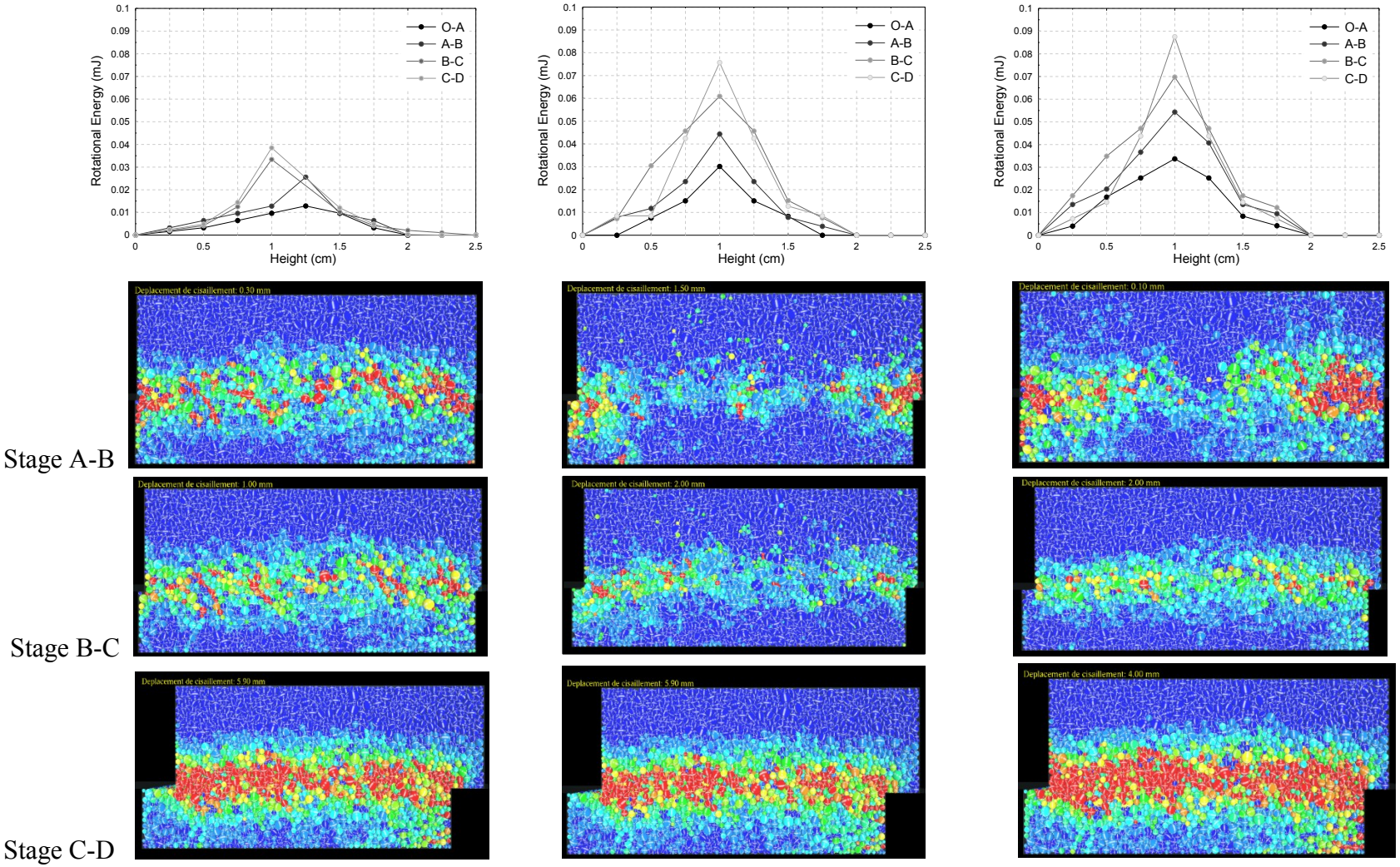

Figure 3.14. Variation of rotational energy along height of specimen and spatial distribution of rotational energy at different stages (a) O–A start of shearing; (b) A–B start of dilation; (c) B–C, peak state (d) C-D steady state

starts to increase. However, the energy is relatively small when compared with those of later stages. It should be noted that in stage A-B, the resolution of rotational enerigies are two times greater than those of other stages, in order to visualize the formation of shear band clearly at all stages. Stage A-B corresponds to the strain localization at the two lateral boundaries, owing to the boundary constraint. As shearing proceeds, the shear zone extends slowly toward the middle of the box from the boundaries. At the peak state (stage B-C), a distinct shear band has been formed over the length of the middle plane, where the rotational energy becomes more pronounced. As more shear deformation is applied, the rotational energy becomes more significant for the particles inside the central shear zone than the particles outside. This is the stage where the upper half of the shear box and particles are subjected to the uniform block-like

motion (Stage C-D). The spatial distributions of rotational energy during shearing is consistent with the dispersion of individual particles rotation find in other studies (Bardet 1994; Ni, Q et al. 2000; Zhang and Thornton 2007), describing the extent of uniform shear zone located at the mid-height of the specimen.

3.4.3 Verification of the peak plane strain friction angle

The two possible orientations suggested for the shear band at peak state are along planes of maximum mobilized strength based on the Mohr-Coulomb failure criterion or along the direction of the zero linear extension (Roscoe 1970). According to (Arthur et al. 1988; Dyer 1985) owing to the degree of constraints imposed on the sample in direct shear test, soil may have no choice but to develop along the zero-extension direction and satisfy Roscoe's solution. However, the Mohr–Coulomb solution yields the upper-bound value of orientations measured from the horizontal (Table. 3.4). The shear band orientation predicted from the Roscoe equation justifies the assumption of horizontal zero linear extension direction made at peak state, where the deviation of the zero linear extension direction from the horizontal at the peak state is less than 1.15° for the three numerical cases examined.

Assuming uniform deformation inside the shear band, coincidence between principal axes, and horizontal zero linear extension direction, the plane strain frictional shearing resistance of the sand can be derived from the geometry of Mohr's circle (Davis 1968):

$$\sin\phi_{ps} = \frac{\tan\phi_{ds}}{\cos\psi\left(1+\tan\psi\tan\phi_{ds}\right)} \tag{3.13}$$

Nevertheless, the plane strain angle of friction interpreted from this equation would be in error due to the underestimated angle of dilation evaluated at the boundaries, deviation of the zero linear extension from horizontal, or non-coaxiality between the principal axes of stress and incremental strain. (Jewell 1989; Wang et al. 2007) extended Davis's relation to take full account of these conditions. An extended relationship based on (Wang et al. 2007) is used herein to account for the non-coaxiality of principal axes and the deviation of the zero linear extension direction from horizontal:

$$\sin\phi_{ps} = \frac{\tan\phi_{ds}}{\cos(a-2\Delta\theta)+\sin(a-2\Delta\theta)\tan\phi_{ds}} \tag{3.14}$$

where $\Delta\theta$ is the non-coaxial angle and a is a geometrical angle derived from the Mohr's circle of incremental strain as , $d\nu$ and $d\gamma$ are invariants of volumetric and shear strain increment:

$$\sin a = \frac{d\nu/2 - d\varepsilon_{yy}}{d\gamma/2} \tag{3.15}$$

A slight difference, less than 1°, between the plane strain angle of frictions using Eq. 3.13 and Eq. 3.14 presented in Table 3.4 reveals the minor effect of non-coaxiality in the three numerical cases at peak states. These observations, in full agreement with Jewell and Wroth (1987) and Wang et al. (2007), verify the precision of the stresses and displacements evaluated at the boundaries of direct shear apparatus where the symmetrical arrangement (Jewell 1989) is implemented.

3.5 Conclusion

The prime objective of this study was to analyze the macro and micromechanics behavior of granular material (polydisperse particles) tested in symmetrical direct shearing as suggested by Jewell (1989) by means of three-dimensional (3D) discrete element method (DEM). The numerical results were compared to their experimental counterparts at the macro-scale under different applied normal stresses. The balance between the micro-scale change in particle energy

and the macro-scale work of external forces as well as the coaxiality between the principal stresses and the principal strains increments directions are discussed. Of the findings of this study, the following conclusions can be drawn:

1. The evolution of the shear stress to normal stress ratio (τ/σ_n) and the boundary dilation angles obtained from DEM simulations are almost similar to those inferred from the boundary calculations of the physical tests. However, the values of the dilation angles inside the shear zone of the virtual samples are slightly greater than the boundary dilation angles of the physical tests.

2. The distribution of the contact normal and the contact forces exhibits the same evolution patterns of anisotropy under different applied normal stresses. However, significant discrepancies are noted in the distributions of the magnitude of the normal and the tangential contact forces.

3. There is a good agreement between the approximated (τ/σ_n) curves obtained from the anisotropy parameters and the stress ratio from the boundaries of the virtual samples, which confirms the coaxiality of the contact force components and contact normal anisotropies during shearing.

4. The numerical results show that the energy transmitted by the external forces to the sample is consumed primarily by the normal interaction of particles as well as their relative movements through rolling and sliding. Although the ratio of the rotational energy to the tangential energy is less than 3%, it is still an indicator of the strain localization.

5. The micro-scale results show that the strain localization initiates from the boundaries and extends towards the middle of the shear box while developing a continuous and uniform shear band along the middle plane of the box. Correspondingly, rotational energy localizes within the shear zone whereas it steadily increases with the shear deformation.

6. The slight difference between the plane strain friction angles calculated from the conventional Dave's equation (Davis, 1968) and those obtained from the extended equation of Wang et al. (2007) accounting for the non-coaxiality behavior as well as the deviation of

zero linear extension direction, confirms again the minor effect of the non-coaxiality at the peak state.

The results presented in this paper suggest that the measurements at the boundaries of the symmetrical direct shear test are quite appropriate for determining strength and volume change behavior of granular soils.

APPENDIX A: Mechanical details of the symmetrical direct shear apparatus adopted for this study

The mechanical details of the shear apparatus developed for this study are shown in Figure 3.15. The sample is contained within a shear box, and confined between a retaining plate and load pad. The steel shear box, square in plan, is split horizontally at mid height, forming an upper and lower frame. The underlying features of the apparatus are as follows:

a) *Sample geometry:* The specimen is square in plan, with a length and width of 55 mm.

b) *Symmetrical arrangement:* The modifications and suggestions proposed by (Jewell and Wroth 1987; Jewell 1989) were implemented in the direct shear apparatus to achieve the so-called symmetrical arrangement. They proposed the load pad to be fixed to the upper frame, where there would be no out-of-balance moments tending to cause rotation. According to (Jewell 1989) the moment created by the lever arm between the horizontal forces is exactly balanced by the moment created by the eccentric vertical force acting on top of the sample in a symmetrical arrangement. Using radiography technique and dial gouges to measure lateral tipping and horizontal rotation, (Jewell 1989) proved there is no tendency for either to occur in a symmetrical arrangement.

c) *Shear Load:* Shear load is applied to the apparatus in the displacement-controlled fashion at a constant velocity of 0.0051 mm/s, driven by an electric motor. The shear load applied at the level of the mid-plane of the sample and is transmitted to shear box by a rigid connector **A**.

d) *Roller bearings:* The direct shear carriage mounted on freshly cleaned and lubricated two track rollers **F**, which allow free movement in the direction of shear and prevent any lateral

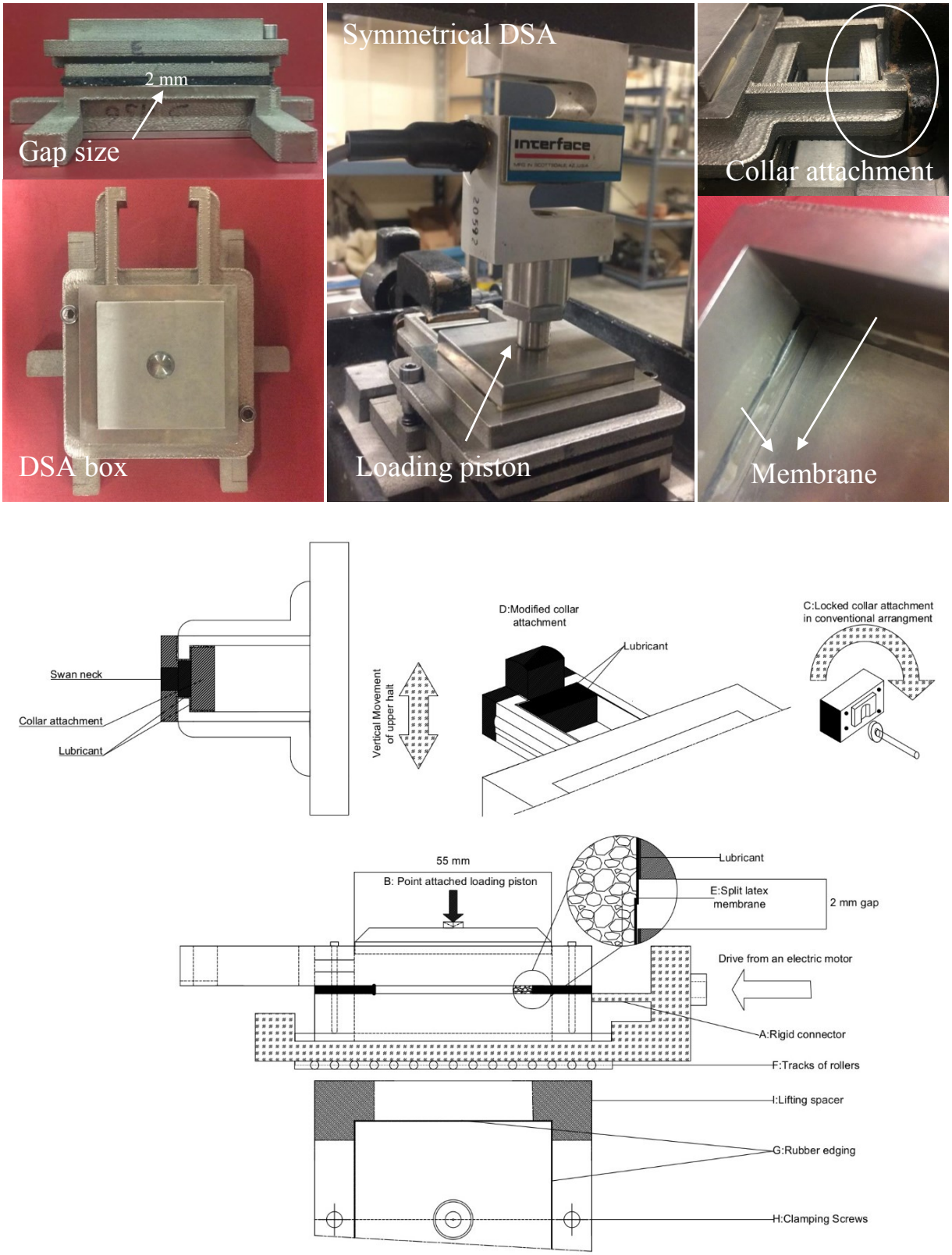

Figure 3.15. General arrangement of symmetrical shear box.

movement. The lower half of the box fit firmly into the shear box against the spacer blocks at the driving end of the carriage.

e) *Normal load:* The loading piston **B** is point contacted to the load pad, which results in not-tilting modes respectively (Jewell and Wroth 1987; Jewell 1989). The vertical load applied directly to the top piston using a system of an air compressor attached to a lever, and is kept constant during testing.

f) *Collar attachment:* Unlike the conventional arrangement, a locked collar attachment **C** prevents vertical displacement and creates clockwise moment on the upper half; the arrangement of the collar attachment **D** in using apparatus ensures freedom of vertical movement with no induced friction and momentum, so that dilation can take place unimpeded.

g) *Gap size:* Researchers suggested the initial gap between the upper and lower halves of the shear box, so that the whole of the horizontal shear force can be transmitted through the specimens itself. Head 1982) suggested a gap lightly more than the diameter of the largest particles. Jewell (1989) recommended 0.5 mm opening between the upper and lower halves to run the direct shear test. Similarly, ASTM (American Society for Testing and Materials) 1990 recommends a standard value of 0.64 mm gap size for tests on fine sands. Lings and Dietz (2004) recommended a gap size of $5D_{50}$ for direct shear tests on Leighton Buzzard sand (Rounded particles, D_{50}=780 μm). However, they also mentioned that there would be a range (between 2 mm to 4 mm), where identical results of both peak friction and peak dilation angles were recorded. In this study, the direct shear test results with different gap sizes of 0.5 mm, 2 mm , 4 mm and 5 mm were compared, and the gap size of 2mm was adopted. Peak friction and peak dilation angles varied by 5° for the range of gap sizes investigated. The small gap of 0.5 mm showed enhanced friction and dilation angles up to 4°, and preventing the probable contraction of samples at the beginning of the test. The peak friction and dilation angles were similar for both gap sizes of 4 mm and 5 mm. Samples with gap size of 2 mm showed the maximum difference just over 1° compare to samples with larger gap size. In additions, compared to samples with larger gap size no unintended jamming of the membrane and escape of material into the gap occurred during sample preparation and shearing for adopted gap size of 2 mm.

h) *Edging*: During the shearing, especially when the sample dilated excessively, the collapse of the material at the edges might occur and assist a progressive failure mechanism. The outflow of the sample would increase the moment during shearing and cause the upper shear box and the top plates to tilt. A supplementary split membrane of thin latex **E** was therefore laid over the interior walls of the frames, to prevent the sample from flowing out. This technique has been used previously (Al-Douri and Poulos 1992; Lings and Dietz 2004; Shibuya et al. 1997), showing the effect of membrane expected to be not the problem for the symmetrical type of shear box used in this study (Shibuya et al. 1997). This is in agreement with our observations for samples with small gap size of 0.5 mm, where outflow was minor and the effect of the membrane on shearing behavior seemed practically negligible. These samples showed nearly constant volume soon after reaching the maximum shear strength, and the failure envelopes nearly coincide for samples with and without the membrane.

i) *Mechanical details:* Further details of the direct shear can be seen in Figure. 3.15, showing using thick rubber **G** secures the load pad in symmetrical tests from rotation. The two halves are temporary fixed together by means of two clamping screws **H**, which have to be removed before proceeding to the shearing stage. The comprehensive arrangement of lifting spacers **I** is used to pre-set the gap between the frames. Lifting spacer has to be removed carefully before applying the normal force.

CHAPITRE 4. Influence de la taille des particules et de la gradation sur la relation de résistance au cisaillement - dilatation des matériaux granulaires

Avant-propos

Auteurs et affiliation :

Samaneh Amirpour Harehdasht: Étudiante au doctorat, Université de Sherbrooke, Sherbrooke, Faculté de génie, Département de génie civil.

Mahmoud N. Hussien: Chercheur postdoctoral, Université de Sherbrooke, Sherbrooke, Faculté de génie, Département de génie civil.

Mourad Karray: Professeur, Université de Sherbrooke, Faculté de génie, Département de génie civil.

Varvara Roubtsova: Chercheuse, Institut de Recherche d'Hydro-Québec, Varennes (Québec).

Mohamed Chekired: Chercheur, Institut de Recherche d'Hydro-Québec, Varennes (Québec).

Date de soumission : juillet 2016
État de la soumission : en évaluation par le comité de lecture de la revue.

Revue : Journal of Geotechnical and Geoenvironmental Engineering, ASCE

Titre français : Influence de la taille des particules et de la gradation sur la relation de résistance au cisaillement - dilatation des matériaux granulaires.

Contribution au document

Ce chapitre inclut des analyses et l'examen des résultats expérimentaux en employant des cisaillements symétriques directs modifiés. Une analyse respective des données de résistance au

cisaillement et de dilatation collectées de la littérature est présentée ce chapitre pour discuter la fiabilité des équations de Bolton. Le chapitre actuel examine alors de manière plus approfondie l'impact potentiel de la taille des particules et de la gradation des corrélations empiriques existantes entre l'angle de frottement et le comportement de dilatation des matériaux granulaires en état de contrainte plate. Après examen de la sensibilité de ces corrélations avec les caractéristiques des particules, les coefficients des équations de Bolton et de Collins et autres ont été ajustés pour rendre compte des caractéristiques de particules.

Résumé français

Un examen minutieux des données rapportées dans la littérature remet en cause la précision des équations empiriques bien connues de Bolton et Collins *et al.* Ces relations empiriques ne reprennent en effet aucune fonction prenant en considération les caractéristiques des particules, et aucune limite à l'égard de la taille des particules. Le présent article examine l'influence potentielle de la taille et de la gradation des particules sur la relation force-dilatation de cisaillement des matériaux granulaires à partir des résultats de 276 tests de cisaillement symétrique direct. Seize courbes de distribution différentes de taille de grain de trois matériaux différents ont été testées à différentes pressions normales et densités relatives initiales. Il a été démontré que la contribution de la dilatance à la force de cisaillement n'est pas influencée par la variation du coefficient d'uniformité C_u. Cependant, il décroît significativement avec l'augmentation de la taille de la particule moyenne D_{50}. Les coefficients des équations de Bolton et de Collins *et al.* ont été dès lors ajustés en tenant compte de D_{50}. Une mise en comparaison des prédictions à partir des formules empiriques proposées avec les données ϕ'_{max} et ψ_{max} issues de la littérature révèle que la prise en compte de la taille des grains amène des résultats plus cohérents.

Mots-clés: la taille de la particule, la forme, la force de cisaillement, le comportement de dilatation

Abstarct

A close scrutiny of data reported in the literature calls into question the precision of well-known empirical Bolton's and Collins et al.'s equations. These empirical relationships, in fact, contain no function taking into account the constituent particles characteristics, and no particle-size limits are imposed on their validities. The present paper examines the potential influence of particle size and grading on the shear strength-dilation relation of granular materials from the results of 276 symmetrical direct shear tests. Sixteen different grain-size distribution curves of three different materials were tested at different normal pressures and initial relative densities. It is demonstrated that while the contribution of dilatancy to the shear strength is not influenced by the variation in the coefficient of uniformity C_u in the investigated range, it significantly decreases with increasing mean particle size D_{50}. The coefficients of Bolton's and Collins et al.'s equations have been, therefore, adjusted to account for D_{50}. A comparison of the predictions by the proposed empirical formulas with ϕ'_{max} and ψ_{max} data from the literature shows that accounting for the grain size yields more authentic results.

Key words: Particle size, Shear strength, Dilation, Coefficients, Shape, Flow rule.

4.1 Introduction

Following the pioneer work of Casagrande (1936), a number of theoretical (Bishop 1954; De Josselin de Jong 1976; Newland and Allely 1957; Rowe 1962, 1969; Schofield and Wroth 1968; Skempton and Bishop 1950; Taylor 1948) and experimental (Bolton 1986; Collins et al. 1992; Lee and Seed 1967; Negussey et al. 1988; Roscoe 1970) attempts have been made to explain the volumetric deformation of a granular assembly upon shearing (i.e. dilatancy). Some of the outcomes of these researches are listed in Table 4.1. In particular, Taylor (1948), based on modifications of the Coulomb concept of shearing resistance, introduced the concept that the strength of dense sand (represented by a peak friction angle ϕ'_{max}) consisted in part of inter-particle rolling and sliding (represented by critical state friction angle ϕ'_{cv}) and in part of particle interlocking (represented by dilation angle ψ_{max}). Rowe (1962) applied the principle of energy minimization and arrived at the first stress-dilatancy relation (Eq. 4.5) that has been later validated by De Josselin de Jong (1976) with an alternative approach based on the laws of

friction. Although the Rowe's theoretical relation has been used as a flow rule in a number of soil plasticity models to simulate the stress–strain behavior of granular materials (Hughes et al. 1977; Molenkamp 1981; Wan and Guo 1998), the complexities of it and the theoretical flow rules in general present a major obstacle towards successful and robust implementation into soil models.

As alternatives to the theoretical stress–dilatancy relations, some researchers defined comprehensive, but simple empirical equations with relatively few material parameters. For example, Bolton (1986) took an experimental approach and proposed the famous empirical flow rule (Eq. 4.8) described as operationally indistinguishable from that of Rowe's Equation. The main advantage of this flow rule is that any angle of shearing in excess of the friction angle of loose earth is seen to be due solely to the geometry of the volumetric expansion, which is necessary before shearing can take place. Bolton (1986) summarized also the previous works performed on strength and dilatancy of sands (Billam 1972; Roscoe 1970; Rowe 1962; Vesic and Clough 1968) and proposed a relative dilatancy index I_R, which is also used to estimate the rate of dilatancy of soil, thereby the plane strain strength parameters, based on correlation with the relative density D_R, and effective stress, p' (Eq. (4.9)).

In the same context, Collins et al. (1992) reviewed the experimental data of Been and Jefferies (1985) on the variation of peak friction angle ϕ'_{max} on with the state parameter ξ, and proposed empirical relationships (Eqs. 4.10 and 4.11) similar to those of Bolton. Using these formulations, the strength of sand can be evaluated based on the actual state of the soil by combining the influence of void ratio and stress state. Eqs. (4.8)-(4.9) and Eqs. (4.10)-(4.11) were adopted interchangeably in geotechnical analyses to account for dilation in frictional material (Salgado and Randolph 2001; Yu and Houlsby 1991).

Although the importance of Bolton's and Collins's relationships is undeniable, it is recognized that their reliabilities have been questioned as they were introduced using an extremely limited number of plane strain data. Moreover, they neglect the explicit consideration of the soil grain characteristics (e.g. particle size, particle shape, and particle gradation) that can strongly affect dilation and strength values. Some researchers called into question the reliability of Bolton's

Table 4.1 Example of theoretical relations and empirical equations between friction angle and dilation.

Authur(s)	Proposed relation		Notes
Taylor (1948)	$\tan\phi'_{max} = \sin\phi'_{cv} + \tan\psi_{max}$ [1]	(4.1)	direct shear condition
Skempton and Bishop (1950)	$\tan\phi_r = \tan\phi_{max} - \frac{\delta V}{\delta \Delta}$ [2]	(4.2)	direct Shear condition
Bishop (1954)	$\tan^2\left(45 + \frac{1}{2}\phi_r\right) = \left(\frac{\sigma'_1}{\sigma'_3}\right) - \sigma_3 \frac{d\varepsilon_v}{d\varepsilon_1}$ [3]	(4.3)	triaxial compression
Newland and Allely (I957)	$\phi'_{max} = \phi_f + \theta$ [4]	(4.4)	direct shear condition $\theta = d\varepsilon_v / d\varepsilon_1$ triaxial compression $\tan\theta = \frac{\left(\sqrt{\sigma'_1/\sigma'_3} \cdot d\varepsilon_v / d\varepsilon_1\right)}{\left(1 + (\sigma'_1/\sigma'_3) + d\varepsilon_v / d\varepsilon_1\right)}$
Rowe (1962)	$\left(\frac{\sigma'_1}{\sigma'_3}\right) = \left(1 - \frac{d\varepsilon_v}{d\varepsilon_1}\right)\left(\tan^2\left(\frac{\pi}{4} + \frac{\phi_f}{2}\right)\right)$ [5]	(4.5)	plane-strain and triaxial compression
Schofield and Wroth (1968)	$\beta\frac{q}{p} = M - \frac{d\varepsilon_v}{d\varepsilon_s}$ [6]	(4.6)	$M = \frac{6\sin\phi'_{cv}}{(3 - \sin\phi'_{cv})}$
Rowe (1969)	$\sin\phi'_{max} = \frac{\sin\phi'_{cv} + \sin\psi_{max}}{1 + \sin\phi'_{cv}\sin\psi_{max}}$	(4.7)	plane-strain
Bolton (1986)	$\phi'_{max} - \phi'_{cv} = b\psi_{max}$	(4.8)	$b = 0.8$ plane-strain and triaxial compression
	$\phi'_{max} - \phi'_{cv} = f(D_R, p') = cI_R$ [7] $I_R = D_R(Q - \ln p') - R$	(4.9)	$Q = 10$, $R = 1$ $c = 3$ triaxial compression $c = 5$ plane strain
Collins et al. (1992)	$(\phi'_{max} - \phi'_{cv}) \equiv f(\xi) = A[\exp(-\xi) - 1]$	(4.10)	$0.6 \le A \le 0.95$, $\xi = (e - e_{cr})$
	$\psi_{max} \equiv g(\xi) = B[\exp(-\xi) - 1]$	(4.11)	$B = (5A/4)$

Note:

[1] ϕ'_{max} maximum friction angle; ϕ'_{cv} critical state friction angle; ψ_{max} maximum dilation angle

[2] ϕ_r residual friction angle; δV expansion of sample per unit area; $\delta\Delta$ relative displacement of the two halves of the box

[3] $\left(\frac{\sigma'_1}{\sigma'_3}\right)$ principal stress ratio; $d\varepsilon_v$ rate of unit volume change; $d\varepsilon_1$ rate of major principal strain change

[4] θ ; ϕ_f reduced value of ϕ corrected for energy due to expansion $\phi_f \prec \phi_r$

[5] ϕ_f Rowe's friction angle $\phi_\mu \le \phi_f \le \phi_{cv}$

[6] $\beta = 1$ under axisymmetric conditions; q deviator stress; p mean effective stress; $d\varepsilon_s$ deviator strain

[7] D_R relative density; p' effective stress

and Collins et al.'s formulations with their commonly used constants. For example, Pedley (1990) pointed out that even when employing the suggested minimum cut off stress of $p' = 150kN/m^2$ to limit the predicted strength, the experimental data are still overestimated by Bolton's equations.

A respective analysis of strength and dilation data collected from the literature is presented in this paper to discuss the reliability of Bolton's equations. It seems that an application of Eqs. (4.8)-(4.9) with the constants proposed by Bolton (1986) to sands with different particle-size distributions may strongly over-predict ϕ'_{max} values. The present paper then examines more closely the potential impact of particle size and grading on the existing empirical correlations between the friction angle and the dilation behavior of granular materials in plane strain conditions (Eqs. (4.8)- (4.11)). For this purpose, 276 symmetrical direct shear tests have been carried out on samples made up of basalt beads (rounded particles), and sands consisting of angular particles (Péribonka sand and Eastmain sand) in the range of 63 μm to 2000 μm to obtain the values of peak friction ϕ'_{max} and dilation ψ_{max} angles over a wide range of normal pressures and initial relative densities. The reliability and applicability of boundary measurements in physical symmetrical direct shear tests used in this study to interpret the plane strain frictional shearing resistance of granular material has been discussed and confirmed using the DEM computer code SiGran (Roubtsova et al. 2011) presented in Chapter 3. After examining the sensitivity of Eqs. (4.8)-(4.11) to the particle characteristics, the coefficients of Bolton's and Collins et al.'s equations have been adjusted to account for particle characteristics, in particular for D_{50}. A comparison of the predictions by the proposed empirical formulas with ϕ'_{max} -data from the literature is also provided in this paper.

4.2 Reliability of Bolton's flow rules to predict ϕ'_{max} based on data reported in the literature

Before describing the experimental testing program and results on the potential influence of particle size and grading on the shear strength-dilation relations of granular materials, a brief review is given in this section to discuss the reliability of Bolton's equations. In other words, a comparison between the peak friction angle ϕ'_{max} predicted by Bolton's Eqs. (4.8) and (4.9) with the ϕ'_{max} data from the literature has been undertaken to investigate if the maximum shear resistance can be accurately expressed without accounting for the particle characteristics. Fig. 4.1 collects approximately 200 values of ϕ'_{max} measured in different laboratories by different researchers on sands with different D_{50}, and C_u values. The data were obtained from symmetrical direct shear and plane strain compression tests. The predicted values were calculated using all required parameters (p' , D_R , ϕ'_{cv} , ψ_{max}) given in respective literature.

When Eq. (4.8) is used to estimate ϕ'_{max}, the scatter of data shown in Fig. 4.1a from the line described by $\phi'^{pred}_{max} = \phi'^{meas}_{max}$ is quite significant, especially for higher ϕ'_{max} values with an over-estimation reaches 8 degrees. A similar plot (Fig. 4.1b) is also given for Eq. (4.9) where the measured ϕ'_{max} versus predicted ϕ'_{max} data shows also a relatively large scatter extending to $\phi'^{pred}_{max} = \phi'^{meas}_{max} + 14^\circ$. In both Figs. 4.1a-b, the majority of the data points are plotted above the bisecting line, showing the over-prediction of ϕ'_{max} values for sands using both equations. In addition, analyzing the data in Fig. 4.1a shows that ϕ'_{max} values of sands with small D_{50} values (< 350 μm) are located at the lower boundary of the group of data points (averaged 1.42 ± 0.78 degrees), while the points laying at the upper boundary (averaged 4.29 ± 2.05 degrees) are attributed to sands with larger D_{50} values (> 700 μm). Moreover, the dispersed data points in Fig. 4.1b shows that the over-prediction of ϕ'_{max} value is still large (averaged 4.15 ± 3.42 degrees) when using Eq. (4.9) instead of Eq. (4.8). This observation is in agreement with the results reported by Pedley (1990), who observed the over-estimation of plane strain data by Eq. (4.9), even when applying the suggested minimum cut off stress of $p' = 150 kN/m^2$.

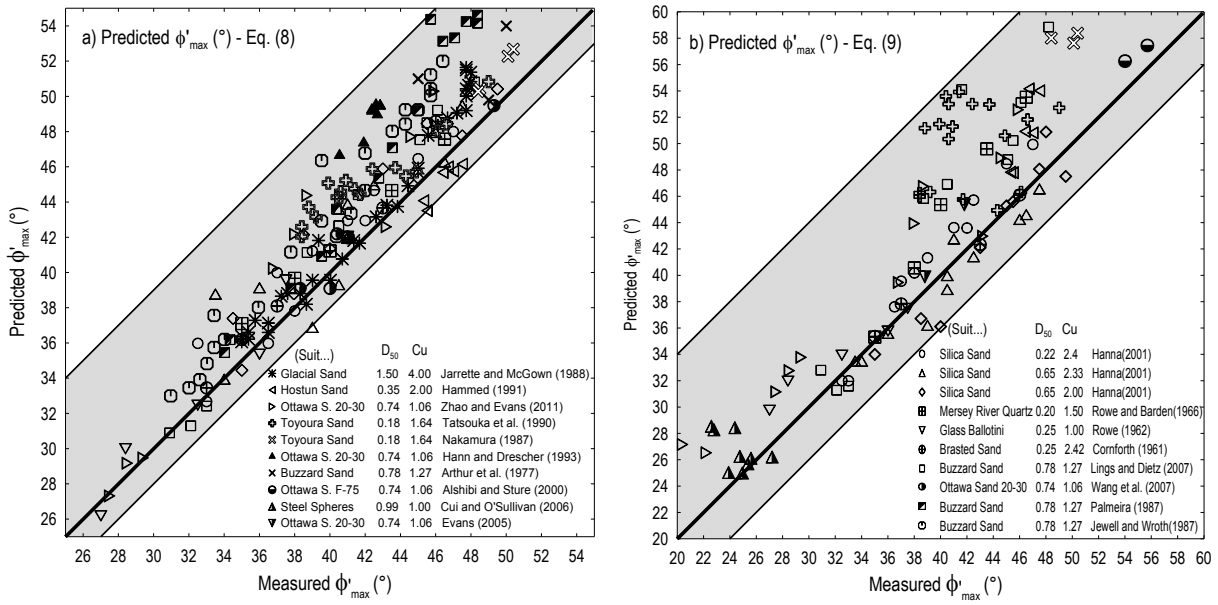

Figure 4.1 Comparison of ϕ'_{max} predictions by: a) Eq. (4.8) and b) Eq. (4.9), respectively with ϕ'_{max} data from the literature.

The results shown in Figs 4.1a-b demonstrates the relative inefficiency of Eqs. (4.8) and (4.9) to accurately predict the soil peak friction angle ϕ'_{max}. However, they do not show a clear tendency concerning the influence of D_{50} and C_u on ϕ'_{max} as the data gathered from the literature are correspond to only a number of D_{50} data of standard sands and materials having a rather uniform particle size distribution. Therefore, more data of granular materials having different particle size distributions would be beneficial to reflect the dependence of ϕ'_{max} values predicted from Eq. (4.8) and Eq. (4.9) on particle size distributions and extend these equations based on D_{50} and C_u values. 276 direct shear tests on 16 different particle-size distributions of different granular materials were performed on this purpose. Descriptions of the tested materials, testing program, test results and analysis are given next.

4.3 Material and testing program

4.3.1 Material

Majority of the present work was performed on basalt microspheres produced by Whitehouse Scientific Ltd, England, in 20 individual narrow distribution grades between 63 and 2000 μm

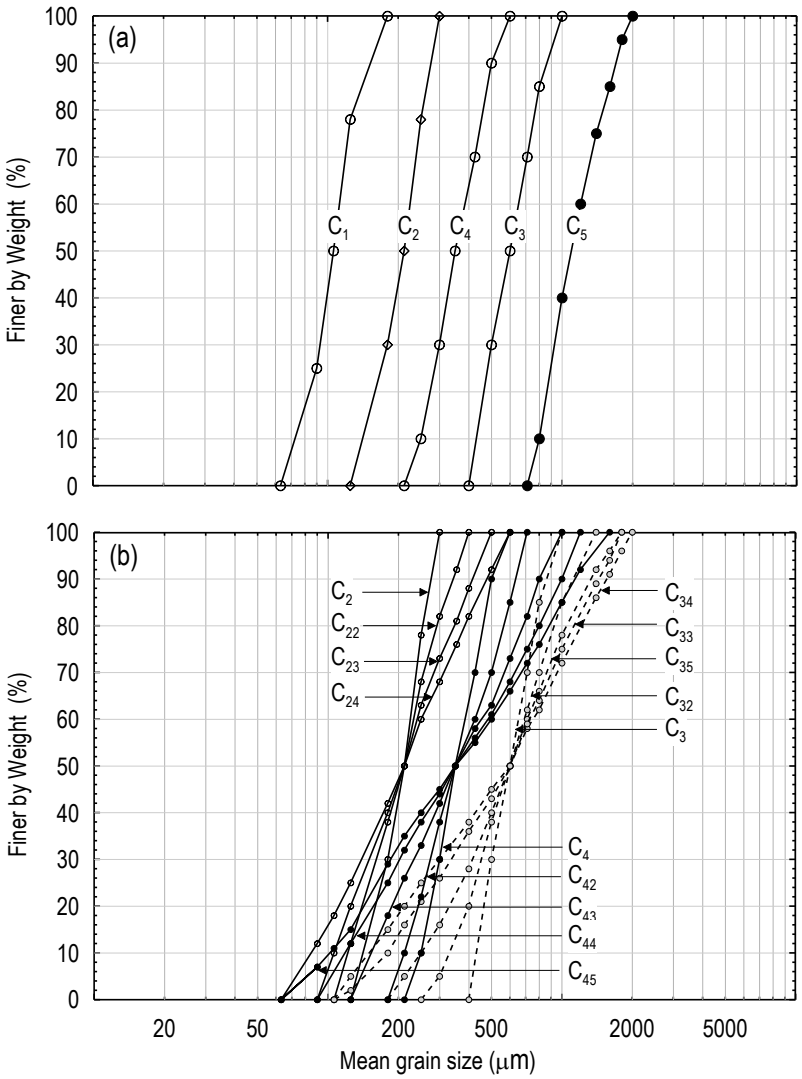

Figure 4.2. Tested grain-size distribution curves: a) C_1 to C_5, $C_u = 1.5$ and b) series 2, 3, and 4, $C_u = 1.5$ to 5.

each with good sphericity. These gradations were mixed to produce the 16 particle-size distribution curves presented in Fig. 4.2. The curves are linear in semi-logarithmic scale. The influence of grain size represented by D_{50} on the shearing behavior of the basalt beads was studied tests on uniform distributions C_1 to C_5 (Fig. 4.2a) with an identical coefficient of uniformity ($C_u = 1.5$) and D_{50} ranging between 106 μm to 1000 μm. An investigation into the effects of gradation was also performed on the same material using three series of tests (i.e., series 2, 3, and 4 with D_{50} of 212, 600, and 350 μm, respectively) (Fig. 4.2b). In each series, C_u varies between 1.5 and 5. Values of D_{50} and C_u of the 16 grading curves considered are summarized in Table 4.2.

Table 4.2. Parameters D_{50}, C_u, e_{max}, and e_{min} of the tested particle-size distribution curves; Summary of constants used in different correlations (4.9)-(4.11), and (4.17)-(4.21).

							Eq. (4.17)			Eqs. (4.9) and (4.18)			Eqs. (4.10) and (4.19)			Eqs. (4.11), (4.20), and (4.21)				
			D_{50}	C_u	e_{max}	e_{min}	c_1	c_2	b	c_3	c_4	c	c_5	c_6	A	c_7	c_8	c_9	c_{10}	B
Basalt Microspheres, G_s= 2.9 (gr/cm^3)	**Series**	1	C_1	106	1.5	0.77	0.57			0.76			4.66			1.26					1.72
			C_2	212	1.5	0.75	0.56														
		2	C_{22}	212	2.0	0.74	0.54			0.68			3.78			0.99					1.44
			C_{23}	212	3.0	0.73	0.53														
			C_{24}	212	4.0	0.70	0.51														
			C_4	350	1.5	0.72	0.54														
			C_{42}	350	2.0	0.70	0.53														
		4	C_{43}	350	3.0	0.66	0.46			0.63			3.25			0.79					1.24
			C_{44}	350	4.0	0.61	0.43	1.60	0.16		18.89	0.30		-0.39	3.08		-0.41	3.64	1.05	0.40	
			C_{45}	350	5.0	0.58	0.41														
			C_3	600	1.5	0.70	0.50														
			C_{32}	600	5.0	0.69	0.49														
		3	C_{35}	600	2.0	0.65	0.46			0.58			2.77			0.58					1.01
			C_{33}	600	3.0	0.61	0.43														
			C_{34}	600	4.0	0.56	0.40														
		5	C_5	1000	1.5	0.69	0.51			0.53			2.38			0.38					0.80
Péribonka G_s= 2.7 (gr/cm^3)	**Series**	1	C_1	106	1.5	0.88	0.55			0.81			5.09			0.68					0.84
		4	C_4	350	1.5	0.82	0.56	1.30	0.10	0.71	13.56	0.21	3.96	-0.14	1.34	0.52	-0.12	1.40	0.86	0.25	0.70
			C_{45}	350	5.0	0.64	0.46														
		5	C_5	1000	1.5	0.85	0.6			0.65			3.17			0.37					0.57
Eastmain G_s= 2.7	**Series**	1	C_1	106	1.5	0.91	0.63			0.84			5.49			0.62					0.76
		4	C_4	350	1.5	0.88	0.62	1.28	0.09	0.74	10.08	0.13	4.70	-0.12	1.18	0.48	-0.10	1.23	0.83	0.24	0.65
		5	C_5	1000	1.5	0.86	0.64			0.68			4.10			0.35					0.54

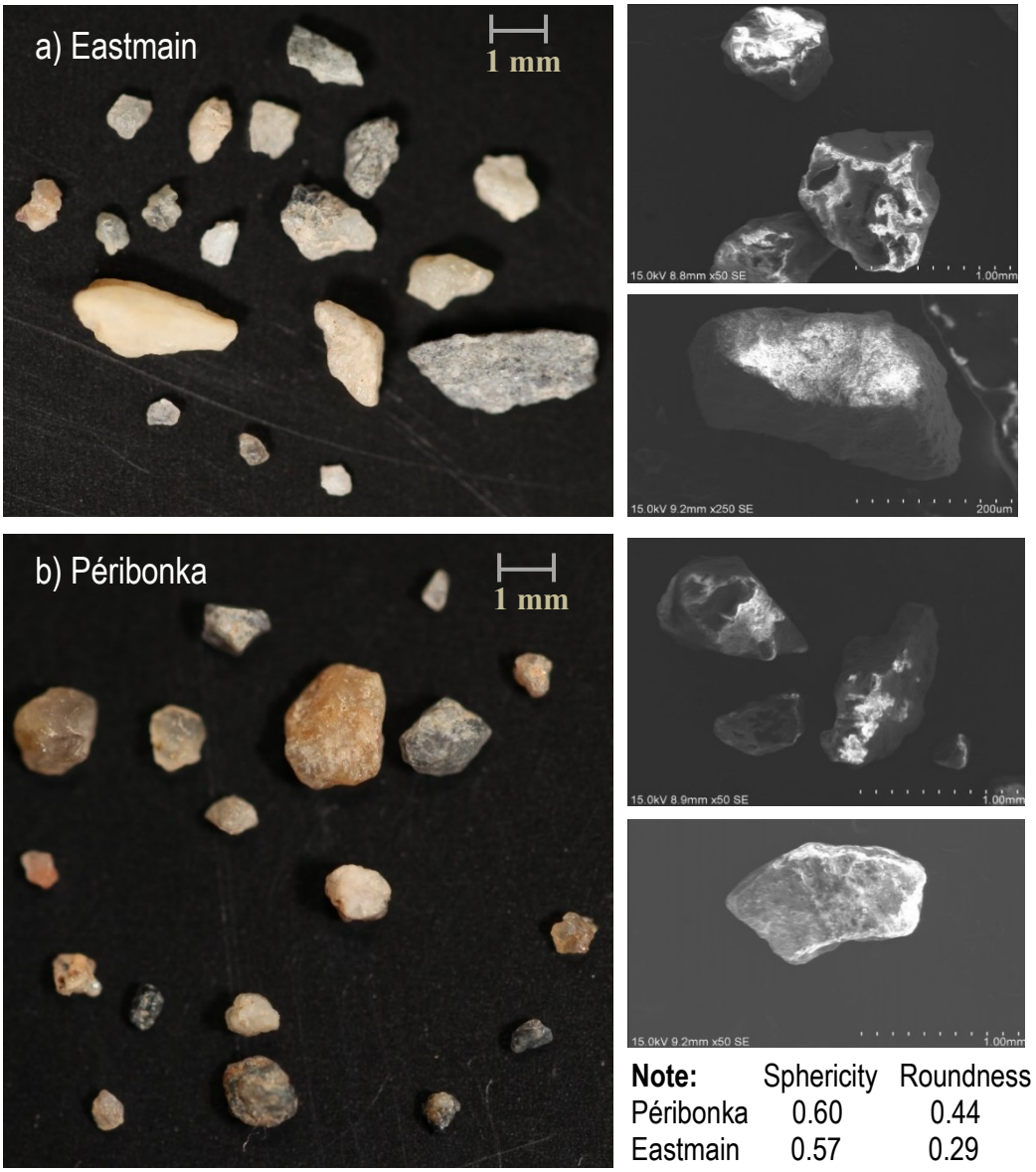

Figure 4.3. Particles of a) Eastmain sand and b) Péribonka sand in the range of 63 μm to 2000 μ.

In order to investigate whether the trend of the results obtained for the uniform basalt beads could also be observed in other materials with different particle shapes, a number of additional tests was performed on two different sands (Péribonka and Eastmain sands) with different particle angularities and deliberately prepared particle-size distribution curves as shown in Table 4.2. Péribonka sand is quartz sand with sub-angular to sub-rounded particles, while Eastmain sand is quartz sand made up of angular to sub-angular particles. The particle shapes of these two materials are shown in Fig. 4.3, where the images for

grains smaller than $250\,\mu m$ were obtained using scanning electron microscope (SEM). The data clearly shows that the particles of Eastmain sand are more angular than those of Péribonka sand, in terms of both particle spericity and roundness. Sieve analyses on the three tested materials were carried out before and after the tests and no obvious evidence of particle crushing was observed.

4.3.2 Shear box testing device, specimen preparation and testing procedure

Experimental direct shear tests were carried out using the symmetrical arrangement suggested by Jewell (1989). In this study, the performance of the symmetrical direct shear apparatus was optimized by exploring different test configurations (e.g., fix load pad to the upper frame, modified collar attachment, initial gap between the shear-box frames, and the use of thin membrane laid over the interior walls of the frames) to the $55mm \times 55mm$ direct shear apparatus. These modifications were suggested by the number of researchers (Jewell and Wroth 1987; Jewell 1989; Lings and Dietz 2004; Shibuya et al. 1997) to ensure the accuracy of results obtained during shearing. The characteristic most commonly addressed in these studies is the tendency for the load pad and upper frame to rotate during conventional testing. The mechanical details of the shear apparatus developed and examined for this study are described in Amirpour Harehdasht et al. (2016). During the test, shear load is applied to the lower section of the box in the displacement-controlled fashion at the level of the mid-plane of the sample with the constant velocity of 0.0051 mm/s, while the upper part was restrained against horizontal movement.

The reliability of boundary measurements in physical symmetrical direct shear tests to interpret the plane strain frictional shearing resistance of granular materials has been discussed and confirmed by Amirpour Harehdasht et al. (2016) using the DEM computer code SiGran (Roubtsova et al. 2011). Provided macro and micro-scale results, Amirpour Harehdasht et al. (2016) showed that the peak state parameters obtained from the symmetrical arrangement are very close to those of ideal simple shear, as it permits a uniform deformation within the developed shear band, a horizontal orientation of the zero linear extension, and a coaxiality of principal stresses and incremental strains at the peak state. This makes the plane strain frictional shearing resistance of the soil precisely derived from the conventional Dave's equation (Eq. (4.13)).

All samples of the granular materials were prepared and sheared in dry conditions. For each grading curve, 12 direct shear box tests were performed at four different normal pressures (50, 100, 200 and 400 kPa) and three relative densities (D_r = 50%, 70%, 90%) giving a total of 276 tests. The maximum and minimum densities of each distribution were measured in the dry state, according to the method specified by Muszynski (2006). Many conventional (ASTM, American Society for Testing and Materials *D 4253-00, D 4253-00, D 1557-00,* 2001a; b; c) and alternative methods (Oda 1976; Yoshimine et al. 1998; Youd 1973) of obtaining limit densities exist, but they generally require a relatively large specimen and were therefore not applicable to the small amount of material available for each distribution (maximum 150 grams). The minimum and maximum void ratios obtained are also summarized in Table 4.2. Each test specimen was prepared in the shear box in three layers of equal thickness. Dry mixtures were carefully laid down in the shear box using a spoon to prevent particle segregation. To obtain the different desired densities, mechanical compaction of each layer was applied. The state of the compactions was monitored by measuring the sample height, until the required density was achieved.

4.4 Test results

4.4.1 Investigating the effect of grading characteristics on the direct shear friction angle and the dilation angle

To efficiently evaluate and improve Eqs. (4.8)-(4.11) to reflect the particle characteristics (e.g. particle size, particle shape, and particle gradation), the peak direct shear friction angle ϕ'_{ds} and the maximum dilation angle ψ_{max} have to be deduced directly from the direct shear tests obtained from boundary measurements through Eqs. (4.12)-(4.14). ϕ'_{ds} was obtained from boundary measurements of the average horizontal shear stress τ_{yx} and the average vertical normal stress σ'_{yy}, using:

$$\tan\phi'_{ds} = \frac{\tau_{yx}}{\sigma'_{yy}} \tag{4.12}$$

Following the assumptions discussed in 3.2 referring to the reliability of boundary measurements in symmetrical direct shear tests to interpret the shearing resistance of

granular materials, the direct shear measured boundary stresses and the Mohr's circle of strain increments can be combined to determine the plane strain frictional shearing resistance of granular material ϕ'_{max} from the geometry of Mohr's circle of stress using Davis (1968):

$$\sin\phi_{ps} = \frac{\tan\phi_{ds}}{\cos\psi\left(1+\tan\psi\tan\phi_{ds}\right)} \tag{4.13}$$

The variations of ϕ'_{max} as a function of D_{50} for all the distributions considered are presented in Fig. 4.4a at different combination of normal pressures and initial relative densities. It is clear from the results presented in Fig. 4.4a that the material peak strength decreased with the increase of D_{50} at the dense state (D_r = 90%) and the lowest normal pressure of 50 kPa. With the increase in the applied normal stresses and the initial void ratios of the tested samples, the peak strengths converged towards an approximate constant value irrespective of the D_{50} of interest. At the same D_{50}, Fig. 4.4a shows also that the increase in C_u yields a minor decrease in ϕ'_{max}; namely within 2 degrees, in agreement with earlier results reported by Kirkpatrick (1965) and Zelasko et al. (1975) who observed the minor effect of C_u on the shear strength of granular materials.

Assuming that all dilatations occur within a uniform shear zone of thickness t, ψ_{max} can be estimated from the rate of change of vertical displacement, υ_y, with respect to horizontal displacement, υ_x through:

$$\tan\psi_{max} = \frac{-d\varepsilon_{yy}}{d\gamma_{yx}} = \frac{d\upsilon_y/t}{d\upsilon_x/t} = \frac{d\upsilon_y}{d\upsilon_x} \tag{4.14}$$

The ψ_{max} values for all distributions at two different combinations of normal pressures and initial relative densities are presented in Fig. 4.4b. As the majority of samples exhibited contractive behavior at the highest normal stress (400 kPa) and the lowest relative density (D_r = 50%), the ψ_{max} results of samples at this condition is not presented in Fig. 4.4b. Similar to the results presented in Fig. 4.4a, it is obvious from Fig. 4.4b that the ψ_{max} values are also influenced by particle size, as well as the material initial density and stress level. The experimental data shows also that for a given D_{50}, ψ_{max} decreased steadily as a function

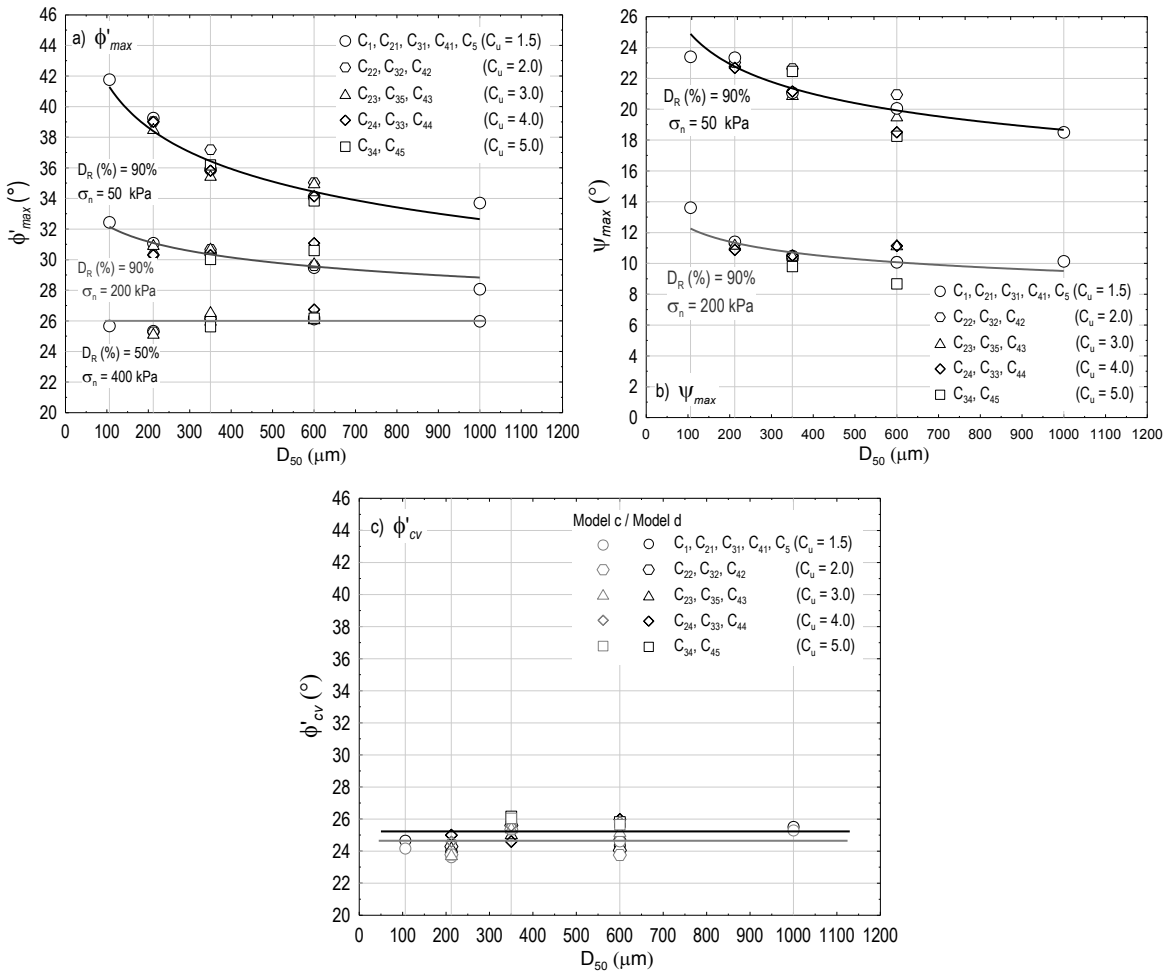

Figure 4.4. Effects of D_{50} on: a) ϕ'_{max} for $(D_R = 90\%, \sigma_n = 50kPa)$, $(D_R = 90\%, \sigma_n = 200kPa)$, and $(D_R = 50\%, \sigma_n = 400kPa)$ b) ψ_{max} for $(D_R = 90\%, \sigma_n = 50kPa)$, and $(D_R = 90\%, \sigma_n = 200kPa)$ c) ϕ'_{cv} of basalt beads.

of normal pressure with the medium-dense samples having a much lower ψ_{max} than the dense samples.

At large horizontal displacement when the sample is sheared at a constant volume, the critical state friction angle, $(\phi'_{cv})_{ds}$, is mobilized. This parameter represents the minimum shear strength the soil can display. An appropriate evaluation of $(\phi'_{cv})_{ds}$ as a fundamental soil parameter constitutes an important step towards a robust development/validation of any strength-dilatancy formulation. In direct shear tests, the critical state shearing resistance can be obtained through several methods using the results of single or multiple tests. Among the five different methods available in the literature and presented in Table

Table 4.3. Detail of methods used to predict $(\phi'_{cv})_{ds}$

Method	Description
a	The direct measurement of the mobilized friction angle at large strains and zero dilation rate
b	Plot $\tau/\sigma + dy/dx$ against x, $(\phi'_{cv})_{ds} = sin^{-1}(int\ ercept\ at\ x = 0)$
c	Plot τ/σ against dy/dx, $(\phi'_{cv})_{ds} = sin^{-1}(int\ ercept\ at\ dy/dx = 0\ for\ best\ fit\ 1:1\ slope)$
d	Plot $(\phi_p)_{ds}$ against ψ_{max}, $(\phi'_{cv})_{ds} = sin^{-1}(int\ ercept\ at\ \psi_{max} = 0\ for\ best\ fit\ 1:1\ slope)$
e	Angle of repose of loose hip of soil

4.3, methods c and d using multiple tests were suggested by many researchers (Bolton 1986; Jewell 1989; Pedley 1990; Simoni and Houlsby 2006) to evaluate the $(\phi'_{cv})_{ds}$ values, since they minimize the influence of errors compared to the single test methods. In addition, direct shear test can produce meaningful data at peak state and using the measurements taken at this point are expected to be more reliable than at large strains as required for method a.

Following the procedures of methods c and d, $(\phi'_{cv})_{ds}$ was determined for each distribution from a series of tests at different combination of relative densities and normal pressures. Finally, the plane strain friction angles ϕ'_{cv} for all distributions at the critical state, when the dilation angle is zero, are obtained from:

$$tan(\phi'_{cv})_{ds} = sin(\phi'_{cv})_{ps} \tag{4.15}$$

The variations of ϕ'_{cv} with D_{50} are presented in Fig. 4.4c. Fig. 4.4c shows that the maximum difference between ϕ'_{cv} values obtained from methods c and d are less than 0.5 degrees, and both the methods show the independency of ϕ'_{cv} to the particle size distribution elements, D_{50} and C_u. This observation is in agreement with previous studies, which illustrated the dependency of ϕ'_{cv} only on the mineral constituting the particles (Negussey et al. 1988; Wijewickreme 1986).

Similar procedures have been followed to obtain shear parameters for Péribonka and Eastmain sands. The measured ϕ'_{max}, ψ_{max}, and ϕ'_{cv} values are used in following sections to describe the interactions dominating the contribution of dilatancy to the peak friction angle, $(\phi'_{max} - \phi'_{cv})$, for various values of D_{50}, using Eqs. (4.8)-(4.11).

4.4.2 Evaluating the contribution of particle size distribution to Bolton's flow rule

In this Section, a systematic investigation has been done to observe if the maximum shear resistance of granular materials can be described by a unique function of maximum dilation or dilatancy index, regardless of particle characteristics. As a first step, the ϕ_{max}^{meas} values of tested samples made up of basalt beads and sands were, respectively plotted in Fig. 4.5 versus ϕ_{max}^{pred} values using Eqs. (4.8) and (4.9). It worths to mention that 25% of the tested samples showed contractive behavior at high normal stresses and low relative densities. The scatter of data in Fig. 4.5 are somewhat large confirming the imperfection of Bolton's equations for an accurate evaluation of ϕ'_{max} based on the constant proportion of dilatancy. Figs. 4.5a and 4.5c show that most of the calculated ϕ'_{max} values using Eq. (4.8) fall within around 23% deviation from the measured values. The corresponding data using Eq. (4.9) (Figs. 4.5b and 4.5d) shows lesser degree of agreement between the calculated and measured ϕ'_{max} values with deviations of even up to 45%.

At the first look, it is likely that the potential source of scatters in Fig. 4.5 may be attributed to the fact that Eqs. (4.8) and (4.9) were developed neglecting the explicit consideration of the soil grain characteristics. To examine the sensitivity of Eqs. (4.8) and (4.9) to particle size and grading , the percentage error $(\%Error)$ in predicting the value of ϕ'_{max} using Eqs.(4.8) and (4.9) was calculated for each test as the percentage deviation of ϕ_{max}^{pred} from ϕ_{max}^{meas}, $\left[\left(\phi_{max}^{meas}-\phi_{max}^{pred}\right)/\phi_{max}^{meas}\right]\times 100$. The average percentage prediction errors for all tests on a given particle-size distribution were then calculated for three different groups of ϕ'_{max} values: (1) $(Ave-\%Error)_{All}$ represents the average percentage prediction errors of all tests performed on each particle-size distribution; (2) $(Ave-\%Error)_{<\phi_{Ave}}$ and (3) $(Ave-\%Error)_{>\phi_{Ave}}$ are the averages percentage errors for ϕ'_{max} values which are respectively smaller and larger than $(\phi'_{max})_{Average}$, where $(\phi'_{max})_{Average}$ is the average of all ϕ'_{max} values obtained for a given particle-size distribution. These three introduced $(Ave-\%Error)$ values were calculated for all distributions and presented in Fig. 4.6.

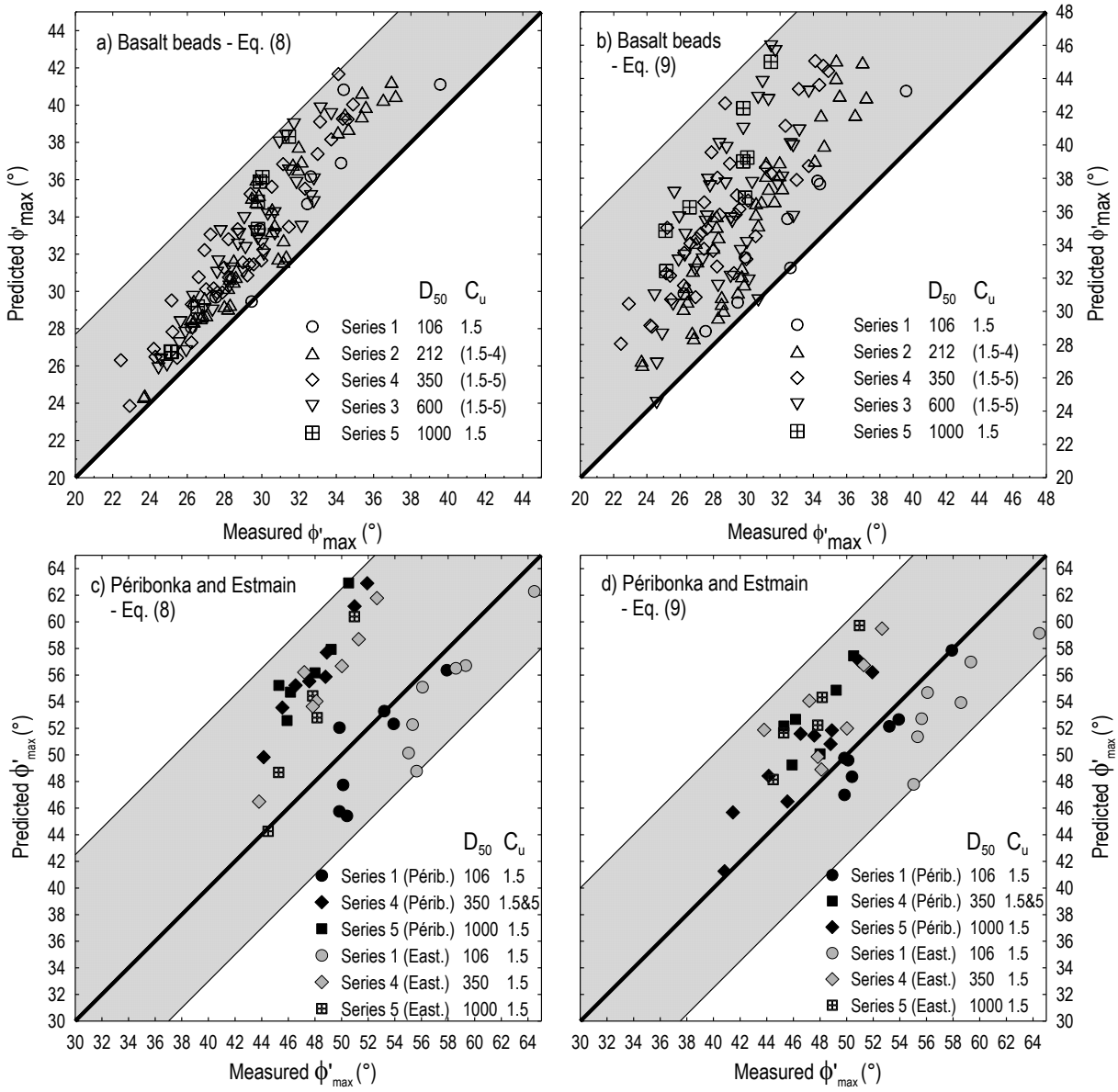

Figure 4.5 Comparison of ϕ'_{max} predictions: by a) Eq. (4.8) and b) Eq. (4.9), respectively with ϕ'_{max} data of basalt beads and comparison of ϕ'_{max} predictions: by c) Eq. (4.8) and d) Eq. (4.9), respectively with ϕ'_{max} data of Péribonka and Eastmain sands.

The comparison of $(Ave-\%Error)$ values in Fig. 4.6 clearly demonstrates the effect of particle-size distribution on the deviation between measured and predicted ϕ'_{max} values using Eqs. (4.8) and (4.9). The scrutiny of the error bars plotted in Fig. 4.6a reveals the increasing trend of $(Ave-\%Error)$ values with the increase of D_{50} for all samples made up of rounded and angular particles. Besides, Fig. 4.6a shows the increase of $(Ave-\%Error)$

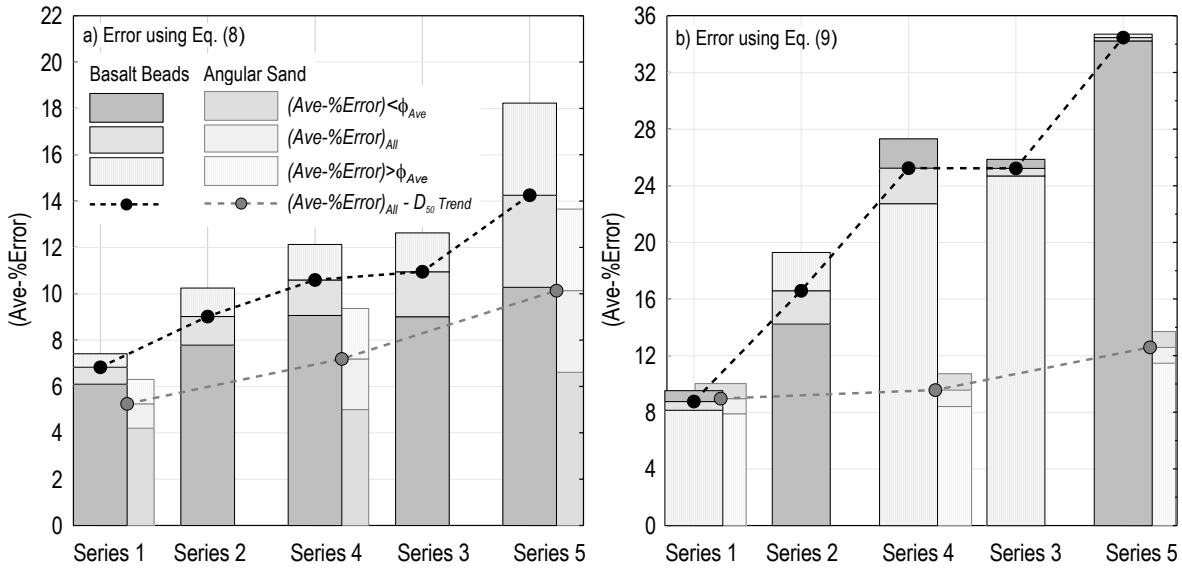

Figure 4.6 The average of the percentage errors for series 1 to 5 of basalt beads and sands using: a) Eq. (4.8) and b) Eq.(4.9).

values with the increase of ϕ'_{max} for a given particle-size distribution. The difference between $(Ave-\%Error)_{>\phi_{Ave}}$ and $(Ave-\%Error)_{<\phi_{Ave}}$ is affected by the particle-size distribution, so that their deviation increases more than 8% and 5% respectively for basalt beads and angular sands from series 1 ($D_{50}=106\mu m$) to series 5 ($D_{50}=1000\mu m$). Comparing the $(Ave-\%Error)$ values for each series of particle-size distribution in Fig. 4.6a, indicates that the $(Ave-\%Error)$ values decreases with increasing angularity of the grains so that for a given particle-size distribution the $(Ave-\%Error)$ values for sands composed of angular grains are smaller than those of basalt beads. However, as mentioned above the sensitivity of $(Ave-\%Error)$ values to particle-size effect still exist for angular material.

In Fig 4.6b, the $(Ave-\%Error)$ values predicted by Eq. (4.9) have been provided. In general, the $(Ave-\%Error)$ values presented in Fig 4.6b are found to be larger than those predicted by Eq. (4.8), but similarly having the increasing trend with the increase in D_{50}. It is apparent from the Fig 4.6b that the $(Ave-\%Error)$ values using Eq.(4.9) are more pronounced for basalt beads than angular sands. Note that the maximum variation of $(Ave-\%Error)$ values due to increase of D_{50} is roughly 3.5% for angular sands.

These observations clearly demonstrate the importance of the grain-size characteristics while predicting ϕ'_{max} values with Bolton's Equations. Thus, more appropriate revising of the constant coefficient in Eq. (4.8) and Eq. (4.9) is needed based on various particle-size distribution elements to quantify their effects in the correlation between the maximum shear resistance and dilation.

4.4.3 Implementing the particle size parameters in to equations (4.8) and (4.9) over a wide range of stresses and densities

The results mentioned in sections above show that when employing the constant proportion of dilatancy or dilatancy index in Bolton's Equations, the ϕ'_{max} values are over-predicted for plane strain strengths. In addition, a hypothesis is also established based on the initial investigation of direct shear data presented in previous Section. This hypothesis assumes that disregarding the particle characteristics in Bolton's equations with constant coefficients might be the source of scatter and over-prediction of ϕ'_{max} values. In order to evaluate this hypothesis in Eqs. (4.8) and (4.2) more closely, the sensitivity of each side of these equations to the particle-size parameters, D_{50} and C_u, are examined over a wide range of stresses and densities using the state parameter proposed by Been and Jefferies (1985), define as $(e-e_{cr})$. This parameter combines the influence of void ratio and stress level with reference to a steady state and allows the quantification of many aspects of granular material behavior using a single parameter.

Fig. 4.7 displays the available data of $(\phi'_{max}-\phi'_{cv})$ values versus the state parameter, $(e-e_{cr})$, for series 3 ($C_u = 1.5 to 5$) and series 1 to 5 ($C_u = 1.5$) distribution curves. It may be seen in this figure that for a given $(e-e_{cr})$, the value of $(\phi'_{max}-\phi'_{cv})$ is highly dependent on the D_{50}, where the slope of the regression lines gradually decreasing by around 3.5 times with increasing D_{50} from an absolute value of more than 681 for $D_{50} = 106\mu m$, to a value of about 194 for distribution having $D_{50} = 1000\mu m$. Moreover for series 2 to 4, the regression lines for the $(\phi'_{max}-\phi'_{cv})$ values of particle size distribution curves with equal D_{50} but different C_u fall together, showing the C_u -independence of $(\phi'_{max}-\phi'_{cv})$ values for $1.5 < C_u < 5$. Similar trends have also been observed for series 2 and 4.

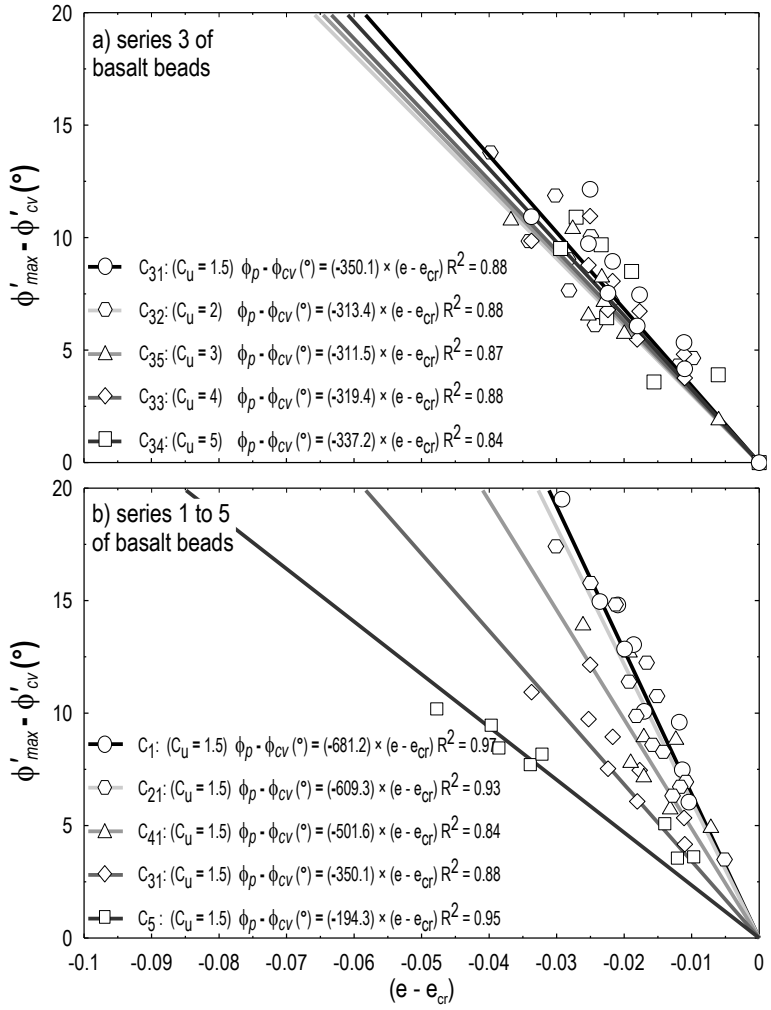

Figure 4.7. $(\phi'_{max} - \phi'_{cv})$ as a function of $(e - e_{cr})$ for a) series 3 (D_{50} = 600 μm), and b) series 1 to 5 (C_u = 1.5) of basalt beads.

An alternative equation (Eq.(4.10)) was formulated by Collins et al. (1992) based on Eqs. (4.8) and (9), proposing the correlation between $(\phi'_{max} - \phi'_{cv})$ and the state parameter, using the data of triaxial tests performed by Been and Jefferies (1985). In Eq.(4.10), the angles are measured in radians, and A is a parameter in the range of 0.6 to 0.95 depending on the type of the sands. Unfortunately, Collins et al. (1992) did not specified the particle characteristics that may cause the variation of parameter A in Eq.(4.10). In Fig. 4.7a, the line of $(\phi'_{max} - \phi'_{cv})$ values versus $exp(-\xi)$ predicted by Collins et al. (1992) with the constant $0.60 < A < 0.95$ is provided for basalt beads. As expected (similar to Fig. 4.7), the decrease of A value with increasing D_{50} is observed in Fig. 4.8a. Moreover, the variation of the $0.33 < A < 1.20$ parameter A ($0.33 < A < 1.20$) with D_{50} in the direct shear test conditions was

found to be out of the range suggested by Collins et al. (1992) $0.60 < A < 0.95$. The difference in the A ranges between the current study and Collins et al's recommendations is mainly attributed to the higher values of $(\phi'_{max} - \phi'_{cv})$ in the plane strain test compared to that in the triaxial test. In fact, the plane strength $(\phi'_{max} - \phi'_{cv})$ is generally higher than the triaxial strengths, over a wide range effective stresses and initial relative densities, an observation that has long been recognized and noted by many researchers (Bolton 1986; Lee and Seed 1967; Rowe 1969). So that, the original expression of Collins et al. (1992) for which $0.60 < A < 0.95$, may under-estimate the $(\phi'_{max} - \phi'_{cv})$ values, especially for $63\mu m < D_{50} < 245\mu m$. In addition, the A value in Eq. (4.10) was assigned based on a limited range of D_{50}, $140\mu m < D_{50} < 390\mu m$ and causes over-estimation for samples made up of larger particles.

The $(\phi'_{max} - \phi'_{cv})$ values were also calculated for some particle-size distribution of Péribonka and Eastmain sands (Table 4.2) and plotted versus $exp(-\xi)$ in Fig. 4.8b. The decrease of $(\phi'_{max} - \phi'_{cv})$ values versus $exp(-\xi)$ with increasing D_{50} is apparent in Fig. 4.8b. However, the lower A values has been reached for sands, which is attributed to the effect of particle shape. Generally, in sand made up of angular particles, interlocking between angular particles is degraded with increasing the axial strain. On the other hand, as the interlocking of the angular particles restrains the relative sliding and rotation between particles, larger shear deformation is required to break the interlocking before relative particle movement associated with dilation can take place. The coupled effect of dilatation and the degradation of interlocking during shearing leads to higher value of $(e - e_{cr})$, and consequently $exp(-\xi)$ for sands to mobilize the maximum shear resistance, ϕ'_{max}, and the flatter regression lines associated with $(\phi'_{max} - \phi'_{cv})$ and dilation angle values for a given particle-size distribution.

Next, a correlation of $(\phi'_{max} - \phi'_{cv})$ with the dilatancy index I_R were developed through to the Bolton's Eq. (4.9). The function was fitted to the data for each particle-size distribution of basalt bead and sands presented in Figs. 4.8c-d. The decrease of $(\phi'_{max} - \phi'_{cv})$ with the increase of D_{50} for a given I_R value is also apparent in these figures. Figs. 4.8c-d reveal

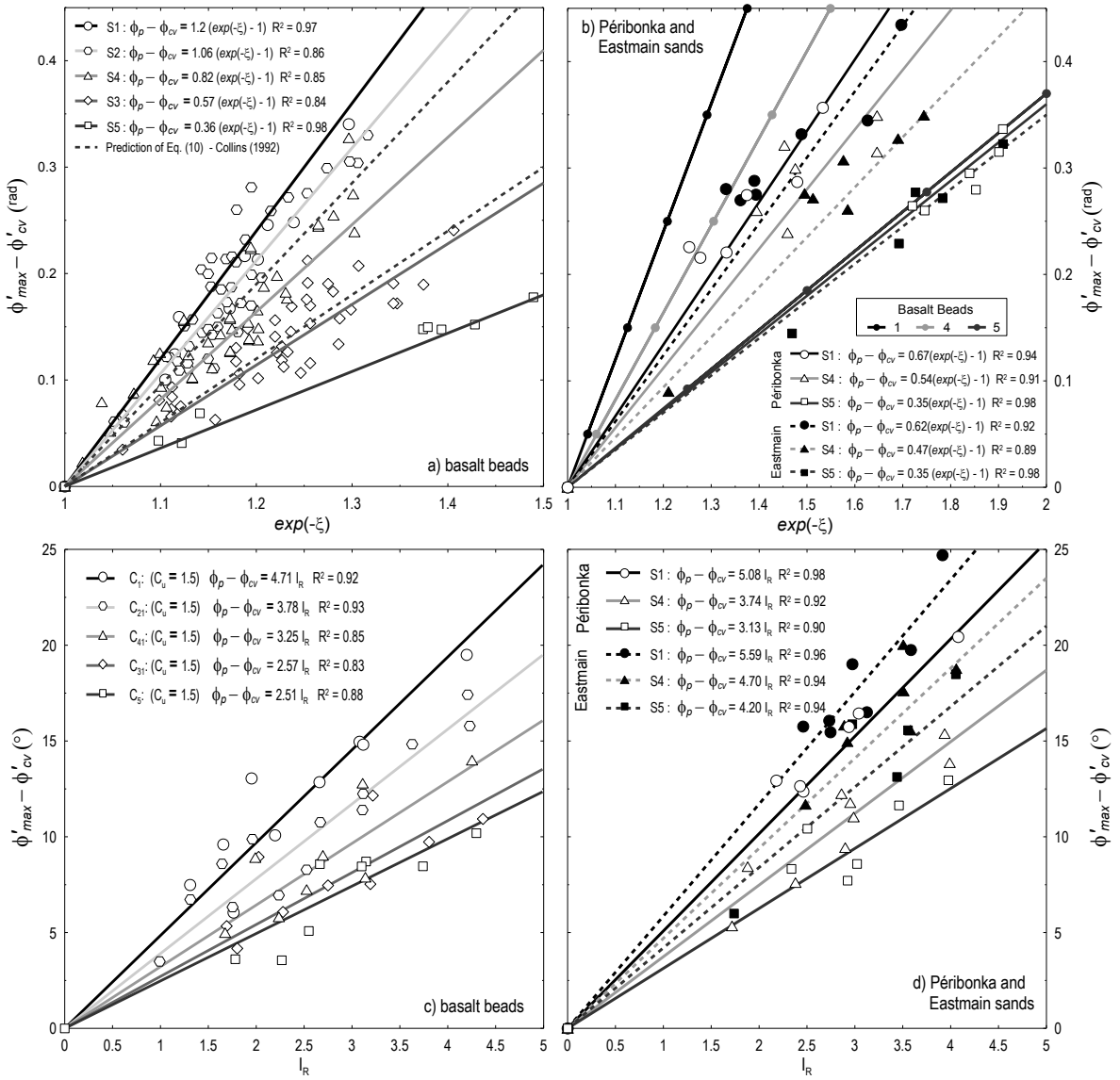

Figure 4.8 $(\phi'_{max} - \phi'_{cv})^{rad}$ as a function of $exp(-\xi)$ for: a) basalt beads and b) Péribonka and Eastmain sands and $(\phi'_{max} - \phi'_{cv})$ as a function of I_R for: c) basalt beads and d) Péribonka and Eastmain sands.

that the coefficient c describing the density and pressure dependence of $(\phi'_{max} - \phi'_{cv})$ values varies in the range of $2.51 < c < 5.59$ with respect to the particle-size and angularity.

To investigate if the maximum dilatation angle, ψ_{max}, of the 16 grain-size distributions of samples made up of basalt beads can be described by a unique function of D_{50}, ψ_{max} values are plotted versus $(e - e_{cr})$ in Figs. 4.9a-b. The regression line passing the ψ_{max} values of the samples with $D_{50} = 106\mu m$ are located at the higher boundary of data points while the

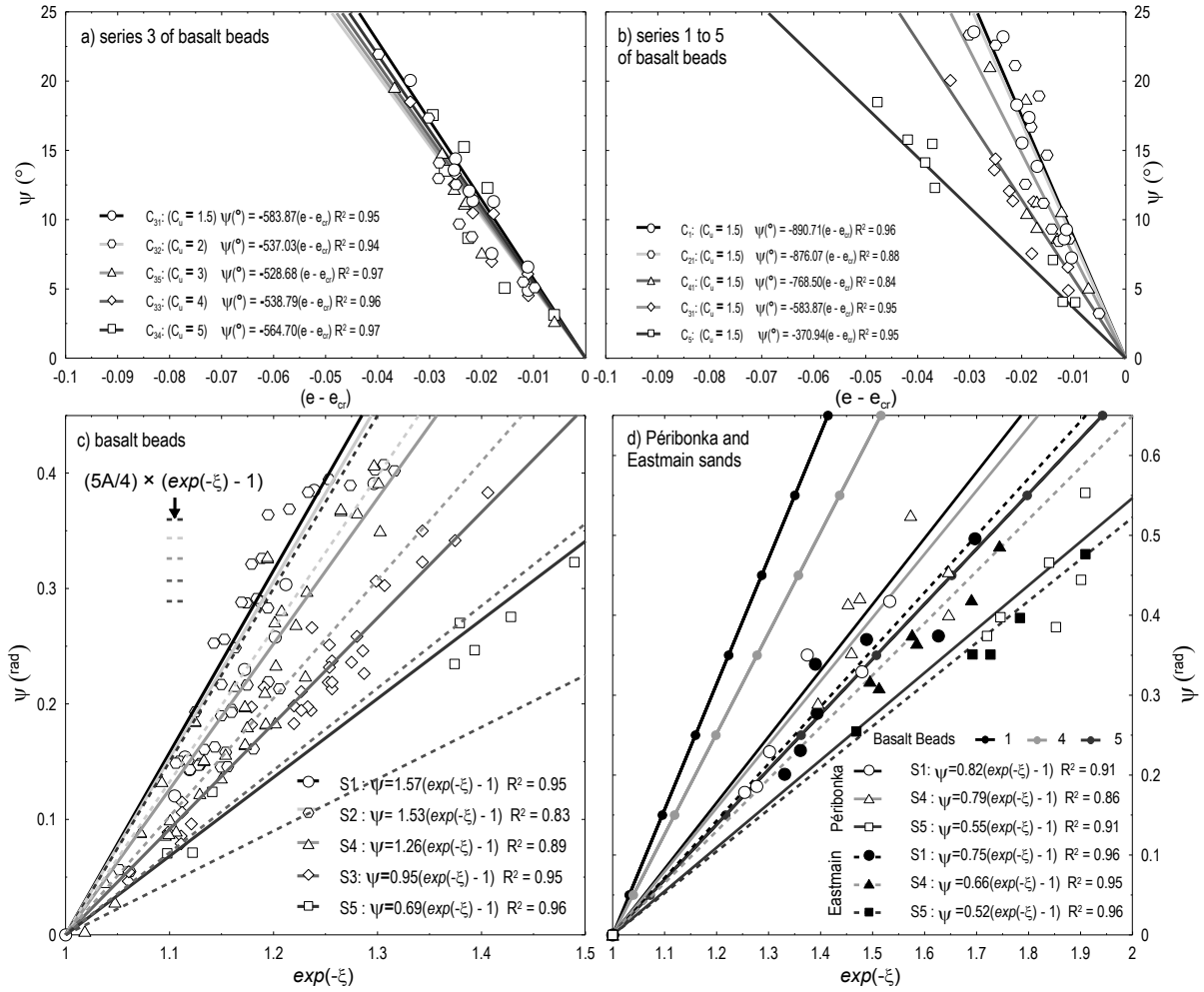

Figure 4.9 ψ_{max} as a function of $(e-e_{cr})$ for: a) series 3 and b) series 1 to 5 of basalt beads and ψ_{max}^{rad} as a function of $exp(-\xi)$ for: c) basalt beads and d) Péribonka and Eastmain sands.

regression line corresponds to the ψ_{max} values of the samples with $D_{50} = 1000\mu m$ tend to lay at the lower boundary. That means that for a given $(e-e_{cr})$ value, ψ_{max} decreases with increasing D_{50}. Similar to Fig. 4.7, no clear tendency concerning the influence of C_u could be found from the ψ_{max} values of series 2 to 4.

In order to illustrate how the effect of D_{50} can be manifested in Eq. (4.11) by Collins et al. (1992), for all mentioned distributions of basalt beads and sands, the $\psi_{max} - exp(-\xi)$ correlations are plotted in Figs. 4.9c-d. An initial perusal of the regression lines corresponds to the ψ_{max} values for each series of basalt beads shows that the original expression of Collins et al. (1992), for which $B = (5A/4)$, was insufficient as a measure of

the dilatacy potential. Considering $B=(5A/4)$ provides a reasonable estimate for sample with $D_{50}=106\mu m$ whereas it under-estimates ψ_{max} of material made up of larger particles, so that the under-estimation increases by increasing D_{50}.

Comparing the $\psi_{max}-exp(-\xi)$ correlation of glass beads with Fig. 4.9d reveals that the coefficient B is also affected by the shape of the grains as well as the size of the particles. In addition, it is also obvious from this figure that Collins et al. (1992) did not establish a reliable relationship between ψ_{max} and $exp(-\xi)$ based on the coefficient $B=(5A/4)$ even for sands made up of angular shaped particles, as far as like what was observed for basalt beads it under-estimates the ψ_{max} values, especially for sands with larger D_{50}.

To update Eqs. (4.8)-(4.11) proposed by Bolton (1986) and Collins et al. (1992) to account for the particle characteristics in prediction of ϕ'_{max}, correlations of parameters b, c, A and B in these equations with the mean particle size D_{50} were developed and presented in the next section.

4.4.4 Proposing correlation for $(\phi'_{max}-\phi'_{cv})$ and ψ_{max}

The data in Figs. 4.7 and 4.9a-b and Figs. 4.8b and 4.9d can be alternatively replotted as a correlation between the $(\phi'_{max}-\phi'_{cv})$ and maximum dilation angle, ψ_{max}. By fitting the points to linear regression lines for each D_{50}, it can be seen that the results of tests on each series, regardless of C_u, were consistent in terms of $(\phi'_{max}-\phi'_{cv})$ and ψ_{max} (Fig. 4.10). However, the range of the obtained b values is not coincident with Bolton's equation with $b=0.8$ for plane strain condition, and is observed to decrease as a function of the increase in D_{50}, for materials made up of rounded to angular particles. Comparing Figs. 4.7 and 4.9a-b shows that, for a given state parameter $(e-e_{cr})$, $(\phi'_{max}-\phi'_{cv})$ decreased by more than ψ_{max} as D_{50} increased, causing a significant drop in the proportion b of the contribution of dilation to peak shear resistance. As shown in Fig. 4.11a, for distributions with $63\mu m<D_{50}<2000\mu m$, the correlation between $(\phi'_{max}-\phi'_{cv})$ and ψ_{max} can be described asx:

$$\phi'_{max}-\phi'_{cv}=b\psi_{max} \tag{4.16}$$

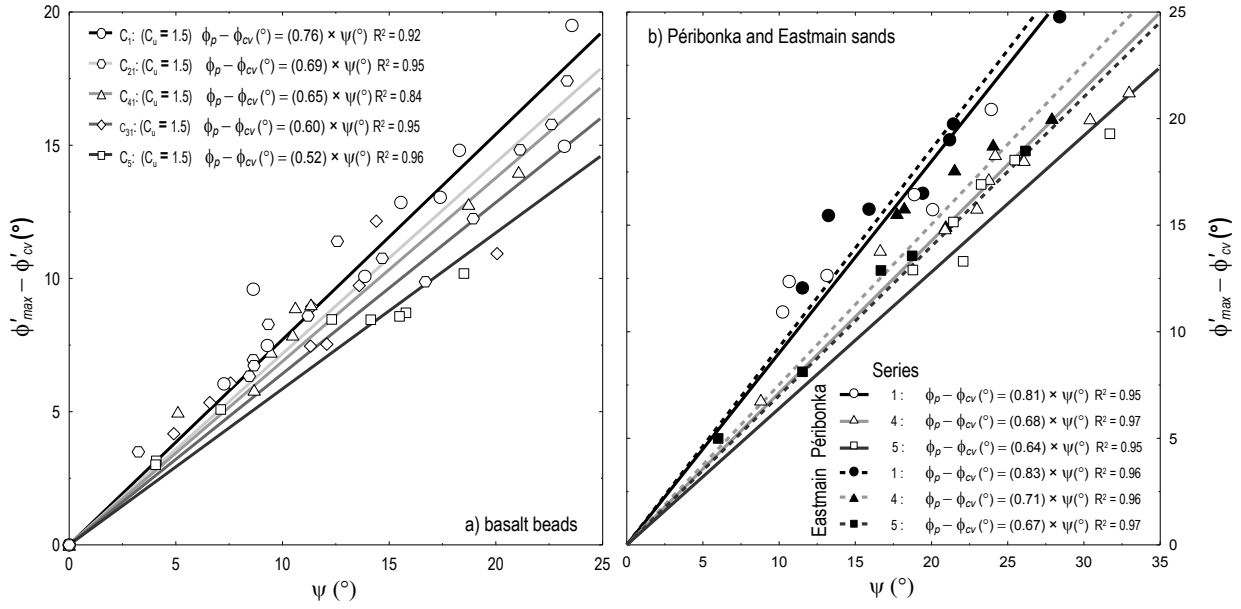

Figure 4.10 ($\phi'_{max} - \phi'_{cv}$) versus ψ_{max} for samples made up of: a) basalt beads and b) Péribonka and Eastmain sands.

where parameter b varies with D_{50} as:

$$b = c_1 (D_{50})^{-c_2} \tag{4.17}$$

The decrease of the b value with increasing D_{50} is described by a power function (Eq. 4.17), with constant $c_1 = 1.60$ and $c_2 = 0.16$ for material made up of rounded particles. These constants decrease to $c_1 = 1.28$ and $c_2 = 0.09$ with increasing the particle angularity. The parameters c_1, c_2, and b are calculated from Eq. (4.17) for each series considered and summarized in columns 7-9 of Table 4.2.

The ϕ'_{max} values predicted by Eq. (4.16) with the parameter b obtained from Eq. (4.17) are plotted versus the measured ones in Figs. 4.12a-b. Since the deviation of the data from the line $\phi'^{pred}_{max} = \phi'^{meas}_{max}$ are small, averaged 0.77 ± 0.54 degrees for basalt beads and 1.12 ± 0.85 degrees for sands, the good prediction of the proposed correlation is confirmed. Note that the average variation of the predicted values from the measured ones is roughly 6% for both rounded beads and angular sands. A comparison between the ϕ'_{max} values predicted

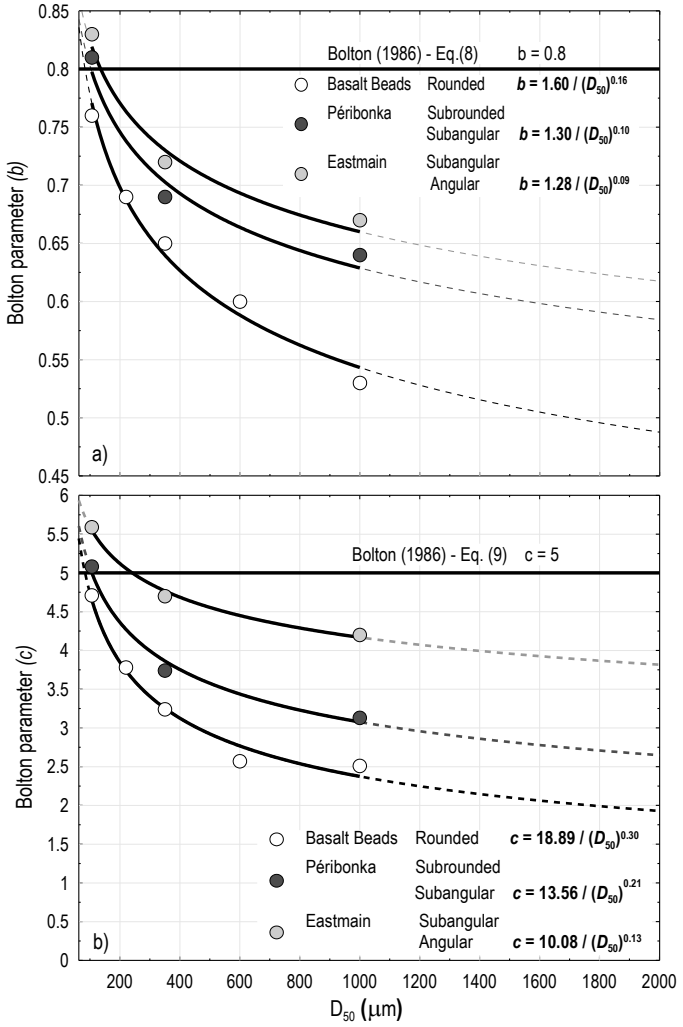

Figure 4.11. Parameter b and c in dependence of D_{50}.

by Bolton's Eq. (4.8) with its commonly used constant and those estimated by Eq. (4.16) using the coefficient b as a function of D_{50} shows that, for a particle-size distribution with large D_{50} of $1000\,\mu m$, Bolton's Eq. (4.8) predicts ϕ'_{max} of 1.14 ± 0.046 (rounded particles) and 1.11 ± 0.040 (angular particles) times larger than ϕ'_{max} values obtained from Eq. (4.16). For $D_{50} = 600\,\mu m$, these factors are reduced to 1.11 ± 0.046 and 1.09 ± 0.021 in rounded and angular particles, respectively. The deviation for $D_{50} = 106\,\mu m$ is further reduced by factors of 1.07 ± 0.012 and 0.095 ± 0.015 in rounded and angular particles, respectively). The increase of the deviation between ϕ'_{max} values obtained from Bolton's equation and those estimated using Eq. (4.16) with D_{50} is in agreement with observations illustrated in Fig. 4.6.

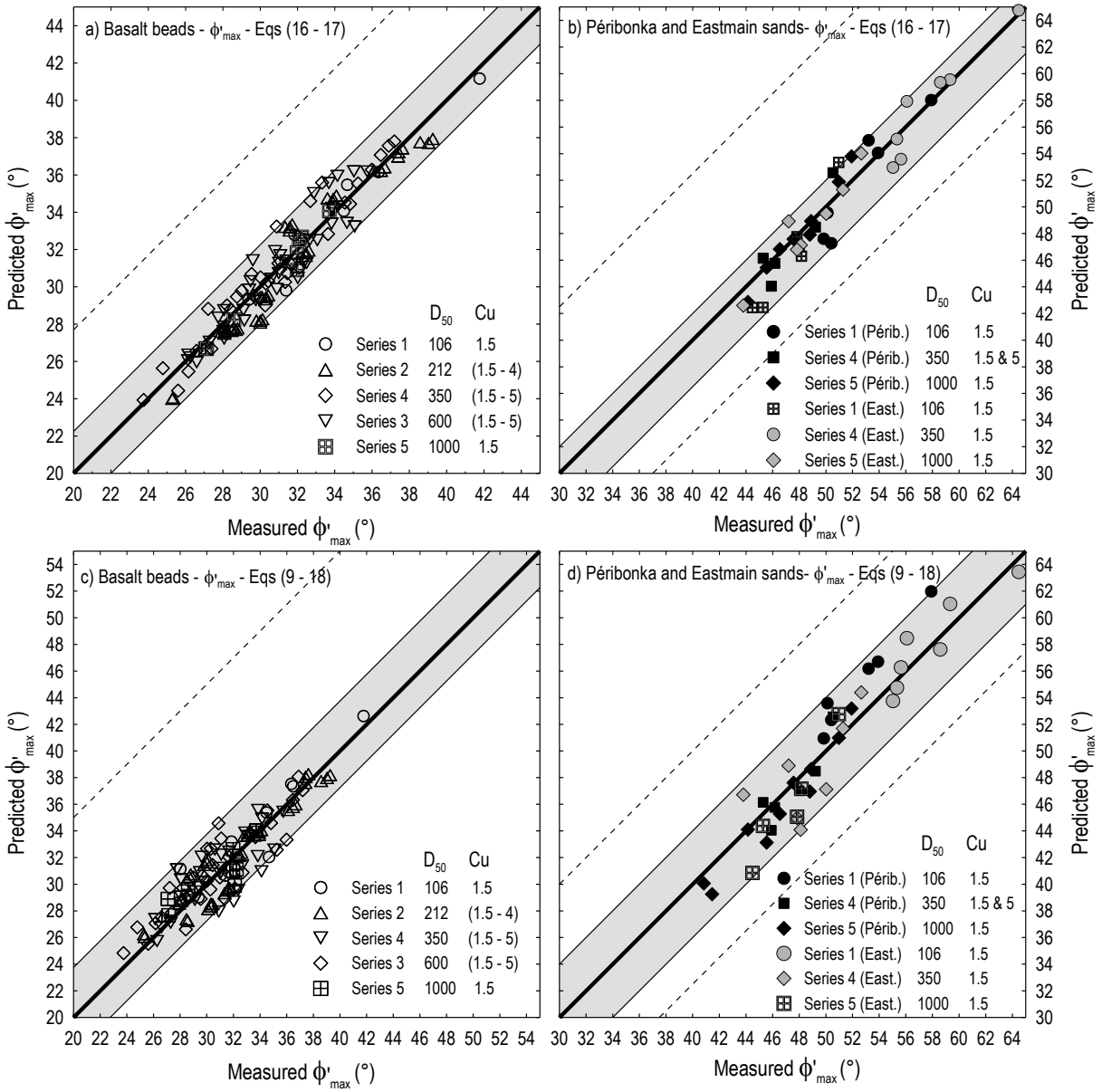

Figure 4.12. Comparison of ϕ'_{max} predictions by Eqs. (4.16)-(4.17) with ϕ'_{max} data of: a) basalt beads and b) Péribonka and Eastmain sands and Comparison of ϕ'_{max} predictions by Eqs. (4.9) and (4.18) with ϕ'_{max} data of: a) basalt beads and b) Péribonka and Eastmain sands.

In addition, a new correlation between $(\phi'_{max} - \phi'_{cv})$ and the relative dilatancy index I_R was develop for all tested series. In Fig. 4.11b, the parameter c is observed to decrease with the increase in D_{50} and cannot be considered as constant equal to 5 for plane strain condition

as proposed by Bolton (1986). According to Fig. 4.11b, the parameter c can be expressed as a function of D_{50} as:

$$c = c_3 (D_{50})^{-c4} \tag{4.18}$$

This function was fitted to the data of the tested materials, resulting in constants $c_3 = 18.89$ and $c_4 = 0.30$ for materials made up of rounded particles. These constants decreased by increasing angularity of the particles to $c_3 = 13.56$ and $c_4 = 0.21$ for materials with sub-rounded to sub-angular particles, and to $c_3 = 10.08$ and $c_4 = 0.13$ for materials with sub-angular to angular particles. As apparent from Figs. 4.12c-d the difference between the values of ϕ'^{pred}_{max} and ϕ'^{meas}_{max} decreased considerably if Eqs. (4.9) and (4.18) are compiled (maximum error of 12% compared to 45% using Bolton's equation with constant c). However, the prediction of ϕ'_{max} by Eqs. (4.9) and (4.18) is a relatively less accurate (averaged 1.14 ± 0.88 degrees for basalt beads and 1.67 ± 1.1 for sands) compared to the prediction of Eqs. (4.16)-(4.17), especially for sands made up of angular particles.

In Collins et al.'s Eqs. (4.10)-(4.11) the dependence of coefficients A and B on D_{50} are presented in Fig. 4.13. The decrease of these coefficients with increasing D_{50} can be approximated by logarithmic functions:

$$A = c_5 \cdot ln(D_{50}) + c_6 \tag{4.19}$$

$$B = c_7 \cdot ln(D_{50}) + c_8 \tag{4.20}$$

$$B = c_9 \cdot A + c_{10} \tag{4.21}$$

The constants c_5 to c_8 for each series are summarized in column 13-14 and 16-17 of Table 4.2. The quite good prediction of ϕ'_{max} values using Eqs. (4.10) and (4.19) for coefficient A can be seen in Figs. 4.14a-14b for both basalt beads (averaged 1.07 ± 0.66 degrees) and angular sands.

(averaged 1.74 ± 0. 85 degrees). In addition, comparing Eqs. (4.19) and (4.20) shows that a correlation can be developed between coefficients A and B, regardless of D_{50} (Table 4.2,

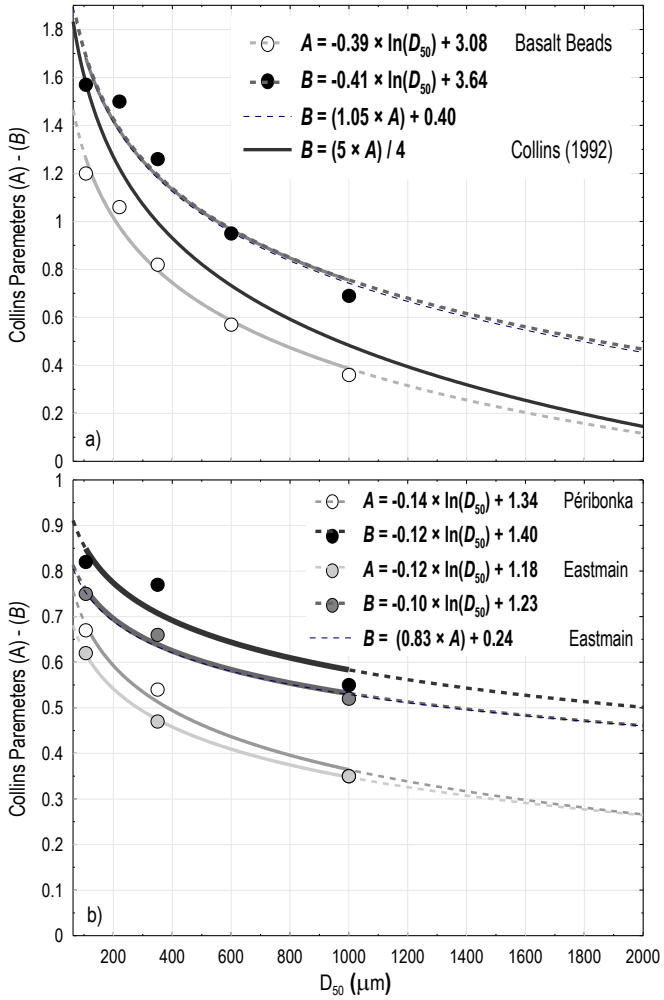

Figure 4.13. Parameter A and B in dependence of D_{50}.

columns 15 and 20). The ψ_{max} values predicted by Eq. (4.21) are plotted versus the measured ones in Figs. 14c-d, showing the small deviation of the data from the line $\phi'^{pred}_{max} = \phi'^{meas}_{max}$ for basalt beads (averaged 1.50 ± 1.18 degrees) and angular sands (averaged 1.07 ± 1.68 degrees).

Overall, the empirical formula for ϕ'_{max} which is formulated based on the state parameter $(e - e_{cr})$(Eq. 4.10) with the parameter A as a function D_{50} (Eq. 4.19) shows generally the same precision as Bolton's Eqs. (4.9) with Eq. (4.18). In the absence of the valid dilation information, depending on the availability of data (current e, and critical void ratios e_{cr} for Eqs. (4.10) and (4.19), or relative density D_R, and mean effective stress p' for Eqs. (4.9) and (4.18)), these equations (Eq. 4.9 with Eq. 4.18 and Eq. 4.10 with Eq. 4.19) can be used interchangeably.

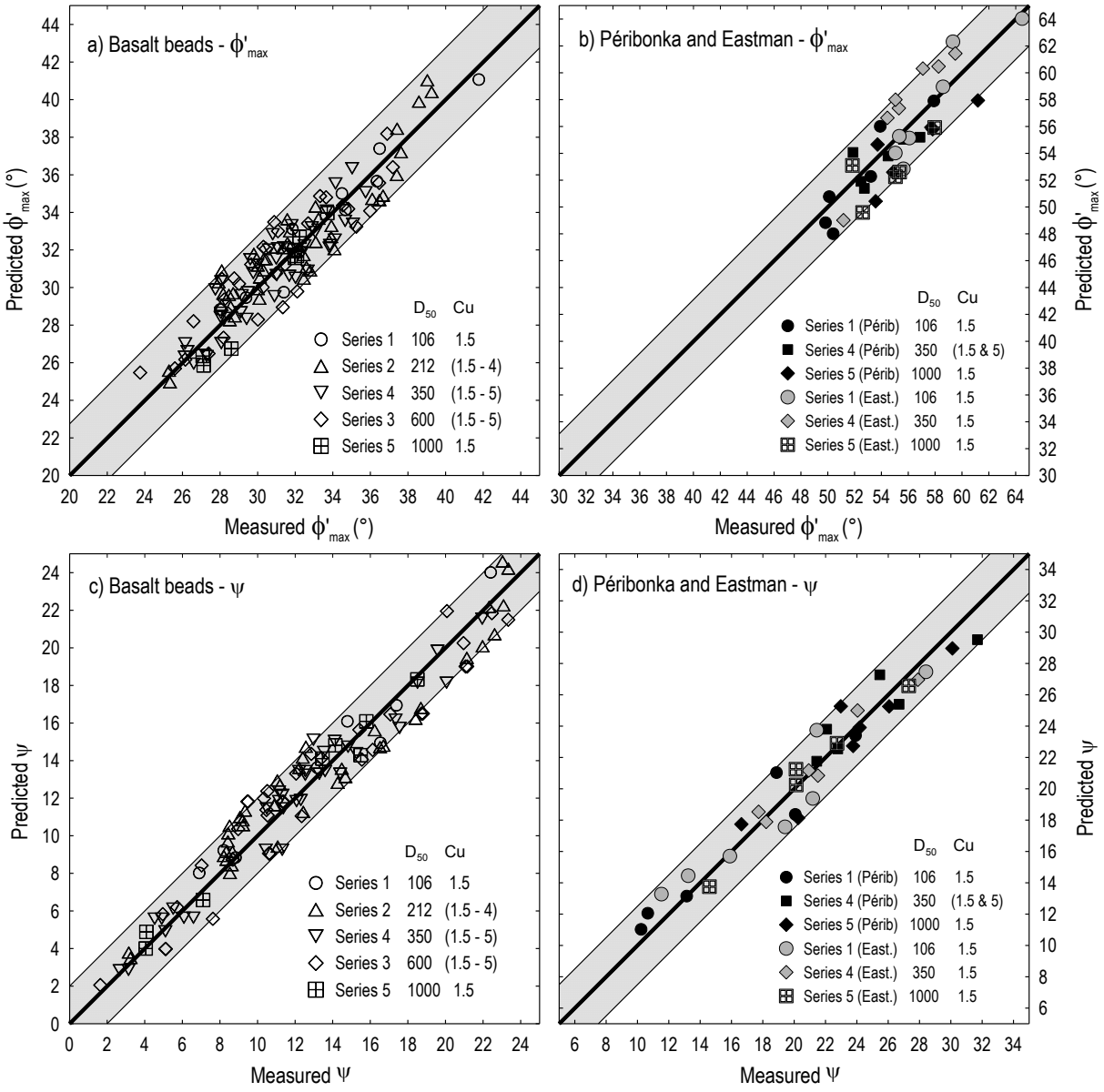

Figure 4.14. Comparison of ϕ'_{max} predictions by Eqs. (4.10) and (4.19) with ϕ'_{max} data of: a) basalt beads and b) Péribonka and Eastmain sands**.** Comparison of ψ_{max} predictions by Eqs. (4.11) and (4.21) with ψ_{max} data of: a) basalt beads and b) Péribonka and Eastmain sands.

4.4.5 Comparing the measured ϕ'_{max} data from the literature with ϕ'_{max} predictions by the proposed correlations

Similar to Fig. 4.1, Fig. 4.15 displays the comparison of ϕ'_{max} values predicted either by Eqs. (4.16) or by Eq. (4.9) using the coefficients $b(D_{50})$ and $c(D_{50})$, with ϕ'_{max} data from the

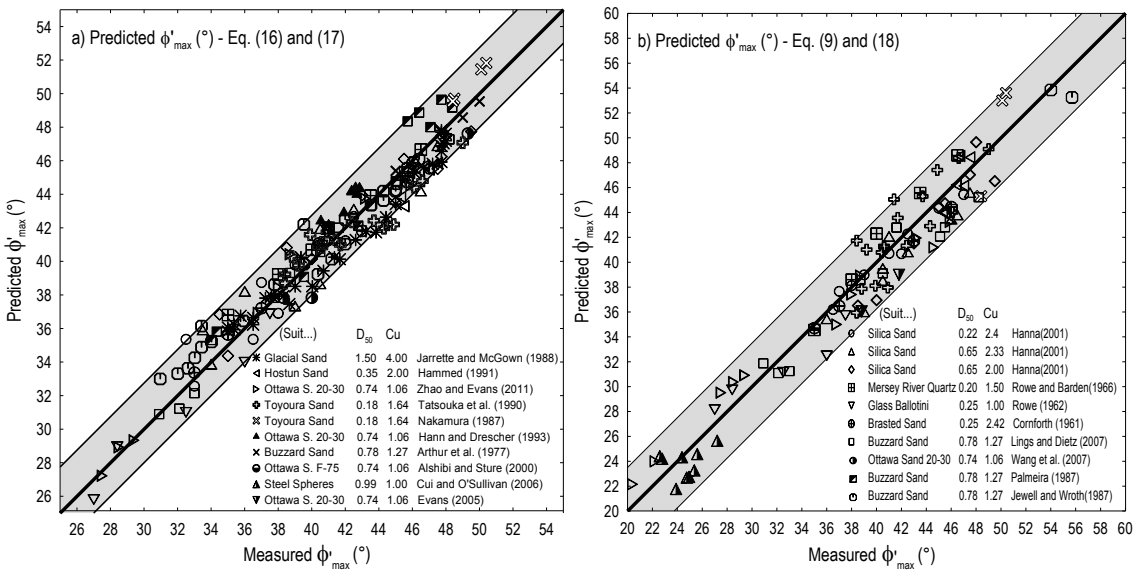

Figure 4.15 Comparison of ϕ'_{max} predictions by a) Eqs. (4.16) and (4.17) and b) Eqs (4.9) and (4.18), respectively with ϕ'_{max} data from the literature.

literature. The prediction of Eqs. (4.16)-(4.17) is shown in Fig. 4.15a. Considering the grain shape as well as the D_{50} value for each tested material, most of the data points plot close to the $\phi'^{pred}_{max} = \phi'^{meas}_{max}$ line with an average deviation of 1.00 ± 0.68 degrees. That implies that the measured and the predicted ϕ'_{max} values using these Equations coincide well. In addition, based on Figs. 4.1 and 4.15 it may be concluded that for materials with small D_{50} values, both Eqs. (4.8) and (4.16) deliver quite reasonable results, while for materials with large D_{50} Eqs. (4.16)-(4.17) works three times better.

The prediction of Eqs. (4.9) and (4.18) areis given in Fig. 4.15b. For gathered tested materials, most of the data points are plotted close to the bisecting line with a maximum deviation of 3.65 degrees (averaged 1.57 ± 0.94 degrees). The average of ϕ'_{max} deviation from the bisecting line is around 3.5 times smaller than when the original Bolton's equation was used in agreement with the observations in Fig. 4.6. However, limited ϕ'_{max} data with p', and D_R information were available from literature and more data for angular sands with higher C_u values would be beneficial in future.

4.5 Conclusion

Comparing ϕ'_{max} values predicted using Bolton's strength-dilation formulations to the corresponding ϕ'_{max} data reported in the literature reveals that due to the fixed coefficients used in Bolton's equations the estimated ϕ'_{max} values are generally over-predicted, and the scatter between ϕ'^{meas}_{max} and ϕ'^{pred}_{max} is quite significant. A total of 276 symmetrical direct shear test were performed on three granular materials to describe the particle characteristics parameters dominating the contribution of dilatancy to the peak friction angle of 16 different particle size distributions. It has been demonstrated that in the investigated range of $1.5 \leq C_u \leq 5$, and $106\mu m \leq D_{50} \leq 1000\mu m$, the maximum shear resistance of the tested materials ϕ'_{max} cannot be described by a unique function of maximum dilation or dilatancy index, and the coefficients b and c in Bolton's equations significantly decreases with increasing mean particle size D_{50}, and does not depend on the coefficient of uniformity C_u. Accordingly, the well-known Bolton's and Collins formulations have been developed to express the effect of particle-size distribution in the relationship between the friction angle and the dilation of granular materials at different relative densities and normal pressures. More specifically, the parameters b, c, A, and B of Bolton's and Collins et al.'s equations (Eqs. (4.16) to (4.21)) have been correlated with D_{50}. In addition, an extension of the proposed correlations considering the influence of the particles angularity has been done by testing Péribonka and Eastmain sands made up of sub-rounded to angular particles. The proposed correlations predict quite well most of the ϕ'_{max} values tested in the laboratory, or reported in the literature for sands with rounded to angular particle shape.

It should be noted that this study only tested the particle-size distribution with a linear curve in the semi-logarithmic scale. Moreover, the data gathered from the literature correspond to standard sands having rather uniform particle-size distributions. In the future, testing more naturally shaped particle-size distribution curves, from poorly graded to well graded, would be beneficial. The influence of the fines content $FC(\%)$ in shear strength-dilation relationship can also be studied and integrated into the proposed correlations.

CHAPITRE 5. Influence de la taille des particules et de la gradation sur la relation de contrainte de cisaillement- dilatance de cisaillement des matériaux granulaires en condition de triaxial consolidé-drainé.

Avant-propos

Auteurs et affiliation :

Samaneh Amirpour Harehdasht: Étudiante au doctorat, Université de Sherbrooke, Sherbrooke, Faculté de génie, Département de génie civil.

Mourad Karray: Professeur, Université de Sherbrooke, Faculté de génie, Département de génie civil.

Mahmoud N. Hussien: Chercheur postdoctoral, Université de Sherbrooke, Sherbrooke, Faculté de génie, Département de génie civil.

Mohamed Chekired: Chercheur, Institut de Recherche d'Hydro-Québec, Varennes (Québec).

Date de soumission : Août 2016
État de la soumission : en évaluation par le comité de lecture de la revue.

Revue : International Journal of Geomechanics, ASCE

Titre français : Influence de la taille des particules et de la gradation sur la relation de contrainte de cisaillement- dilatance de cisaillement des matériaux granulaires en condition de triaxial consolidé-drainé.

Contribution au document

Ce chapitre inclut des analyses et l'examen des résultats expérimentaux des essais de compression triaxiale drainée. Ce chapitre examine de manière plus approfondie l'impact

potentiel de l'information microstructurale imposée par la géométrie interne des particules (par exemple, la taille des particules, la forme des particules et la gradation des particules) sur la contrainte de cisaillement–dilatance de cisaillement du matériau granulaire pendant l'essai triaxial conventionnel. Dès lors, l'effet microstructural pris en compte dans le calcul de l'équation de la contrainte de cisaillement–dilatance de cisaillement et dans son ajustement empirique en état de condition triaxiale en étant traité en tant que contrainte imposée par la taille des particules et l'obliquité constitutives. En outre, les données expérimentales triaxiales des divers matériaux granulaires sont recueillies à partir de la littérature de manière à élargir les preuves à l'appui des contraintes mises en application dans des relations de la contrainte de cisaillement–dilatance de cisaillement.

Résumé français

Le présent article examine l'influence de la taille et de la gradation des particules sur la contrainte de cisaillement–dilatance de cisaillement des matériaux granulaires à partir des résultats de 35 tests des triaxiaux consolidés-drainés. Sept granulométries de deux matériaux différents sur une échelle de 63 μm à 2000 μm ont été testées à différentes pressions normales et densités initiales relatives. Il a été démontré que la relation contrainte de cisaillement–dilatation n'est pas influencée par la variation du coefficient d'uniformité C_u. Toutefois, elle décroît significativement avec l'augmentation de la taille moyenne des particules D_{50}. Les coefficients des équations de Vaid et Sasitharan, et Wan et Guo ont été dès lors ajustés en tenant compte du D_{50}. Une comparaison des prédictions des formules proposées avec les données de la relation contrainte de cisaillement de cisaillement –dilatations de cisaillement issues de la littérature prouvent également que la prise en compte de la taille du grain amène des résultats plus cohérentess que lorsque la taille des particules n'est pas considérée.

Mots-clés: la taille de la particule, la contrainte de cisaillement, le comportement de dilatation, essai triaxial consolidé-drainé, sable

Abstarct

This paper examines the potential influence of particle-size distribution on the stress-dilatancy behavior of granular material based on the results of 35 conventional drained triaxial compression tests. Seven different grain-size distribution curves of two different materials (glass beads, Péribonka sand) in the range of 63 μm to 2000 μm were tested at different normal pressures and initial relative densities. It is demonstrated for a given relative density and confining pressure that while the shear strength and volumetric response of the tested materials do not depend on the coefficient of uniformity C_u in the investigated range, it is significantly influenced by the variation of the mean particle-size D_{50}. Based on the triaxial test results, a correlation between the material constant α of Wan and Guo's modified stress-dilatancy equation and D_{50} of the tested materials has been developed. In addition, the coefficients of Vaid and Sasitharan's equations as an experimental adjustment of the famous Rowe's stress-dilatancy equation have been fine-tuned to account for D_{50}. A comparison of the predictions by the proposed empirical formulas with the stress-dilatancy data from the literature and a micromechanical explanation of the experimental results are also provided.

Key words: Particle-size, shear strength, dilation, drained triaxial, sand

5.4 Introduction

The mechanical behavior of granular materials naturally revolves around dilatancy and its relationship with the shearing resistance, which is governed by a number of factors such as void ratio, confining stresses, previous deformation history as well as the stress path (Gudehus 1996; Houlsby 1991b; Nakai 1997; Pradhan et al. 1989; Vaid and Sasitharan 1992; Wan and Guo 1999). Endeavors to establish stress-dilatancy relations can be traced as far back as the early works of Casagrande (1936), that developed thereafter by other researchers based on theoretical energy principals (De Josselin de Jong 1976; Newland and Allely 1957; Rowe 1962; Schofield and Wroth 1968; Taylor 1948) and laboratory experiments (Bolton 1986; Collins et al. 1992; Vaid and Sasitharan 1992).

By far, most popular description of stress-dilatancy theories still hinge on the energy principals as in the pioneering work of Rowe (1962), who developed the stress-dilatancy relation by neglecting particle crushing and elastic strains, and applying the principle of energy minimization. Despite questioning the applicability of the minimum energy principle to frictional materials, De Josselin de Jong (1976) did prove, with an alternative approach based on the laws of friction, that Rowe's final conclusion and his stress–dilatancy relationship were valid, and defined as:

$$R = KD \tag{5.1}$$

where $R = \sigma_1/\sigma_3$, σ_1 and σ_3 are the major and minor principal effective stresses, respectively; $D = 1 - d\varepsilon_v/d\varepsilon_a$ is the dilatancy factor, $d\varepsilon_v$ and $d\varepsilon_a$ are the major principal strain rate and volumetric strain rate, respectively. $K = tan^2\left(\pi/4 + \phi_f/2\right)$ is the material parameter with ϕ_f as the mobilized friction angle at the onset of dilation. Although Rowe's theoretical relation has been used as a flow rule in a number of soil plasticity models to simulate the stress–strain behavior of granular materials (Hughes et al. 1977; Molenkamp 1981; Wan and Guo 1998), its complexities in general present a major obstacle towards successful and robust implementation into soil models. In addition, many experiments show that dilatancy changes during deformation history cannot be fully described by Rowe's original stress-dilatancy equation, without explicit consideration of density, pressure, and micro-structure dependencies (Nemat-Nasser 2000; Wan and Guo 1998, 2000). These shortcomings encouraged researchers to use other theoretical and experimental approaches to modify the original Rowe's stress dilatancy equation or to find a constitutive experimental adjustment for it. Some of the outcomes of these researches are listed in Table 5.1. It can be seen in this table that, while the importance of confinement and density has been clearly implemented into Rowe's stress-dilatancy relation and its experimental adjustments, experimental studies with a focus on microstructural issues are scares (e.g., experimental Eq.(5.13)-(5.15) for plane strain condition and Eq. (5.10)).

For this purpose, the present paper examines more closely the potential impact of particle geometry (e.g. particle-size, particle shape, and particle gradation) on the stress-dilatancy

Table 5.1 Summary of experimental and theoretical approach to modified original Rowe's stress-dilatancy equation.

Author(s)	Proposed relation		Notes
Vermeer and de Borst (1984)	$\sin\psi_{max} = \frac{\sin\phi'_{max} - \sin\phi'_{cv}}{1 - \sin\phi'_{max}\sin\phi'_{cv}}$ [1]	(5.2)	● Rowe's stress-dilatancy theory in terms of the cardinal parameters. ● Considered ϕ_f equal to ϕ'_{cv} for simplicity.
Bolton (1986)	Plane strain condition $\phi'_{max} - \phi'_{cv} = 0.8\psi_{max}$ $\phi'_{max} - \phi'_{cv} = f(D_R, p') = cI_R$ [2] $I_R = D_R(Q - \ln p') - R$	(5.3) (5.4)	● Empirical flow rule as operationally matches the theoretical Rowe's Equation. ● $c = 3$ triaxial compression, $c = 5$ plane strain. ● $R = 1$, $Q = 10$.
Vaid and Sasitharan (1991)	$\phi'_{max} - \phi'_{cv} = 0.33\psi_{max}$	(5.5)	● Linear empirical relation similar to Bolton (1986) for triaxial condition.
Collins et al. (1992)	$(\phi'_{max} - \phi'_{cv}) \equiv f(\xi) = A[\exp(-\xi) - 1]$ [3] $\psi_{max} \equiv g(\xi) = B[\exp(-\xi) - 1]$	(5.6) (5.7)	● Constitutive empirical relation to Bolton's equation. ● $0.6 \le A \le 0.95$ and $B = (5A/4)$.
Wan and Guo (1999)	$\sin\psi_{max} = \frac{\sin\phi'_{max} - (e/e_{cr})^{\alpha}\sin\phi'_{cv}}{1 - (e/e_{cr})^{\alpha}\sin\phi'_{max}\sin\phi'_{cv}}$ [4] $\sin\phi_f = (e/e_{cr})^{\alpha}\sin\phi_{cv}$	(5.8) (5.9)	● Modified original Rowe's equation to include stress and density dependency.
Wan and Gue (2000)	$\sin\phi_f = \frac{X\left(\frac{F_{33}}{F_{11}}\right) + \gamma^{p*}}{a + \gamma^{p*}}(e/e_{cr})^{\alpha}\sin\phi_{cv}$ [5]	(5.10)	● Modified original Rowe's equation to include fabric dependency.
Chakraborty and Salgado (2010)	$\phi'_{max} - \phi'_{cv} = 0.62\psi_{max}$ $\phi'_{max} - \phi'_{cv} = f(D_R, p') = 3.8I_R$	(5.11) (5.12)	● Amended empirical Bolton's equation for low confining pressures. $R = 1$. $Q = 7.4 + 0.60\ln\sigma'_c$. $Q = 7.1 + 0.75\ln\sigma'_c$.
Amirpour Harehdasht et al. (2016)			● Adjusted the coefficients of Bolton's and Collins et al.'s equations to account for D_{50} and angularity in plane strain condition.
	$\phi'_{max} - \phi'_{cv} = b\psi_{max}$ $b = f(D_{50})$	(5.13)	From rounded to angular $b = c_1(D_{50})^{-c_2}$: $1.60 \ge c_1 \ge 1.28$; $0.16 \le c_2 \le 0.09$
	$\phi'_{max} - \phi'_{cv} = f(D_R, p') = cI_R$ $I_R = f(D_{50})$	(5.14)	$c = c_3(D_{50})^{-c_4}$: $18.89 \ge c_3 \ge 10.08$; $0.30 \ge c_4 \ge 0.13$ $A = c_5\ln(D_{50}) + c_6$: $-0.39 \le c_5 \le -0.12$; $3.08 \ge c_6 \ge 1.18$
	$(\phi'_{max} - \phi'_{cv}) \equiv f(\xi) = A[\exp(-\xi) - 1]$ $\psi_{max} \equiv g(\xi) = B[\exp(-\xi) - 1]$ A and $B = f(D_{50})$	(5.15)	$B = c_7\ln(D_{50}) + c_8$: $-0.41 \le c_7 \le -0.10$; $3.64 \ge c_8 \ge 1.23$ or $B = c_9A + c_{10}$: $1.05 \ge c_9 \ge 0.83$; $0.40 \ge c_{10} \ge 0.24$

Note:

[1] ϕ'_{max} maximum friction angle; ϕ'_{cv} critical state friction angle; ψ_{max} maximum dilation angle.

[2] D_R relative density; p' effective stress.

[3] $\xi = (e - e_{cr})$ state parameter (Been and Jefferies 1985); e current void ratio and e_{cr} critical void ratio.

[4] ϕ_f mobilized friction angle at the onset of dilation, $\phi_\mu \le \phi_f \le \phi_{cv}$; α material constant.

[5] F_{33} and F_{11} fabric tensor components in the axial and radial directions; γ^{p*} the true plastic shear strain; X and a material constants

of granular materials during conventional triaxial test. A total of 35 drained triaxial compression tests have been carried out on samples made up of glass microspheres (rounded particles), and Péribonka sand consisting of sub-rounded to sub-angular particles in the range of 63 μm to 2000 μm, and over a wide range of normal pressures and initial relative densities. Thereafter, the microstructural effect was implemented into stress-dilatancy equations (Eqs. (5.8)-(5.9)) and their empirical adjustment in triaxial condition like Eq. (5.5) by treating it as constraints imposed by constituent particle-size and angularity. In addition, experimental triaxial data of various granular materials were gathered from the literature to provide evidence in support of the implemented constraints into existing stress-dilatancy relations.

5.4 Material and testing program

5.3.4 Material

The majority of the present work was performed on glass microspheres produced by Whitehouse Scientific Ltd, England, in 20 individual narrow distribution grades between 63 and 2000 μm each with good sphericity. These gradations were mixed to produce the 7 particle-size distribution curves presented in Fig 5.1. The curves are linear in semi-logarithmic scale. The influence of grain size represented by D_{50} on the shearing behavior of the glass beads was studied using tests on uniform distributions C_1 to C_5 with identical coefficients of uniformity

Table 5.2 Parameters D_{50}, C_u, e_{max}, and e_{min} of the tested particle-size distribution curves; Summary of constants used in different correlations (5.18) and (5.21).

							Eq. (5.18)			Eq. (5.21)		
			D_{50}	C_u	e_{max}	e_{min}	c_1	c_2	α	c_3	c_4	b
Glass Microspheres, G_s= 2.9 (gr/cm^3)	1	C_1	106	1.5	0.77	0.57	0.13	0.28	0.51	1.14	0.21	0.42
	2	C_2	212	1.5	0.75	0.56			0.63			0.37
	4	C_4	350	1.5	0.72	0.54			0.72			0.32
		C_{45}	350	5.0	0.58	0.41						
	3	C_3	600	1.5	0.70	0.50			0.86			0.30
		C_{32}	600	5.0	0.69	0.49						
	5	C_5	1000	1.5	0.69	0.51			0.98			0.26
Péribonka G_s= 2.7 (gr/cm^3)	1	C_1	106	1.5	0.88	0.55	0.68	0.10	1.11	1.13	0.20	0.43
	4	C_4	350	1.5	0.82	0.56			1.32			0.36
		C_{45}	350	5.0	0.64	0.46						
	5	C_5	1000	1.5	0.85	0.6			1.41			0.27

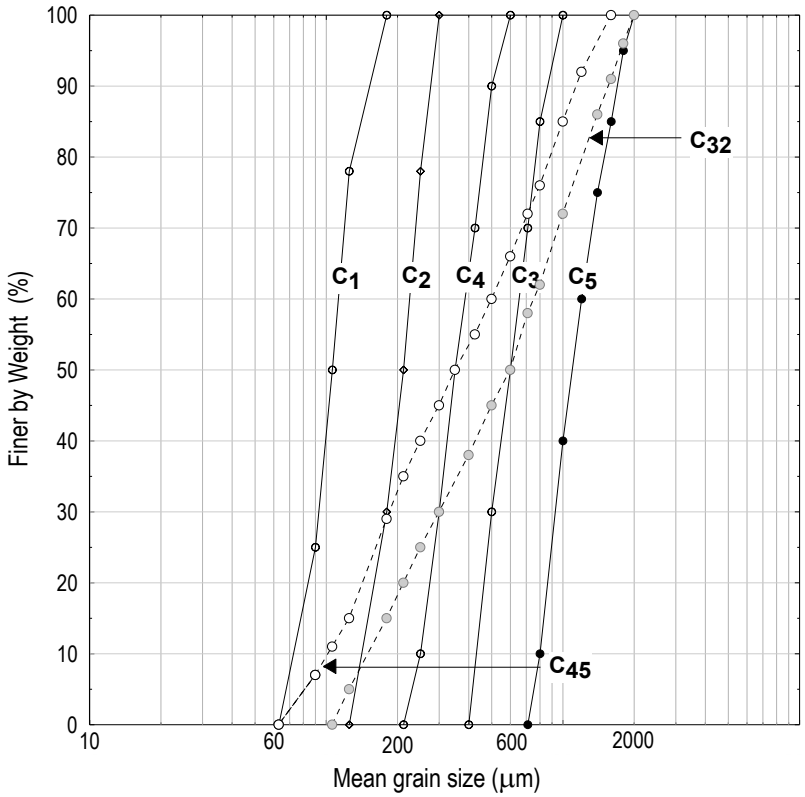

Figure 5.1 Tested grain-size distribution curves: a) C_1 to C_5, $C_u = 1.5$ and b) C_{45} and C_{32}, $C_u = 5$

($C_u = 1.5$) and D_{50} values ranging between 106 μm to 1000 μm. An investigation into the effects of grading was also performed on the same material using two different distributions (i.e., C_{32} and C_{45} with $C_u = 5$).

In order to investigate whether the trend of the results obtained for the uniform glass beads could also be applied in other materials with different particle shapes, a number of additional tests were performed on Péribonka sand with different particle angularities and deliberately prepared particle-size distribution curves as shown in Table 5.2. Péribonka sand is quartz sand made up of sub-rounded to sub-angular particles. The sphericity and roundness value of Péribonka sand based on image analysis of 30 grains are 0.60 and 0.44, respectively. The particle shapes of this material are shown in Fig. 5.2, where the images for grains smaller than 250 μm were obtained from scanning electron microscope (SEM). Sieve analyses on the two tested materials were carried out before and after the tests and no obvious evidence of particle crushing was observed.

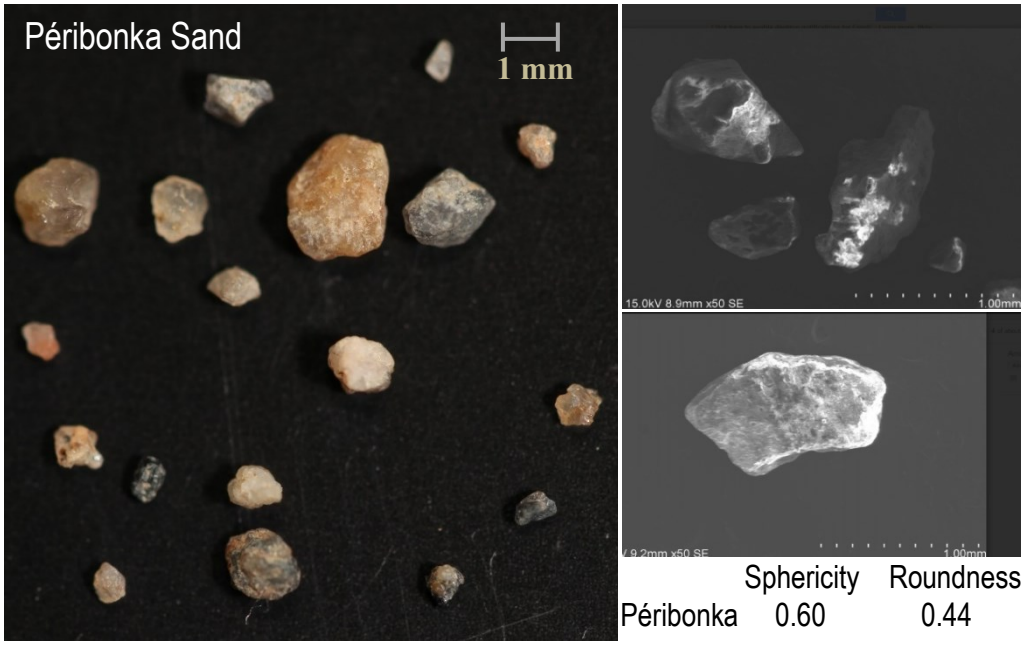

Figure 5.2 Particles of Péribonka sand in the range of 63 μm to 2000 μ

To achieve desirable relative densities for triaxial tests, the maximum and minimum densities of each distribution were measured in the dry state, according to the method specified by Muszynski (2006). Many conventional (ASTM, American Society for Testing and Materials 2001a; b; c) and alternative methods (Oda 1976; Yoshimine et al. 1998; Youd 1973) of obtaining limit densities exist, but they generally require a relatively large specimen and were therefore not applicable to the small amount of material available for each distribution (maximum 150 grams). The minimum and maximum void ratios obtained are also summarized in Table 5.2.

5.3.4 Triaxial testing device, specimen preparation and testing procedure

A total of 35 drained triaxial compression tests were carried out in the conventional triaxial test apparatus on cylindrical specimens 77.44+/-2 mm in length and 38.72+/-2 mm in diameter. During sample preparation, a latex membrane was placed along the interior wall of a split mold and held aligned by a vacuum pressure. Specimens of 50-95% relative density were prepared using multi-layer funnel deposition, followed by lateral tapping of the mold separately for each layer in a symmetrical pattern. When each placed layer is tapped, some of the tapping energy is transmitted to the lower layers. So that, not only the layer being placed, but also is the layers below likely to be densified. Therefore, in order to achieve uniform relative density through the

sample the layers would be placed with the relative densities increasing from the bottom to the top.

After a specimen was prepared and installed in the triaxial cell, which was filled with de-aired water, saturation of specimens was performed in three stages. Carbon dioxide gas was first flushed through the specimen in the upward direction for 20 minutes. Thereafter, de-aired water was flushed followed by the backpressure application with maintained effective stress of 10 kPa. During these stages, samples saturation was verified using the pore-pressure parameter $B = \Delta u / \Delta \sigma$ not less than 0.95 +/-2.

When the saturation phase of the test is completed, the maximum back pressures was hold constant and the cell pressure was increased until the difference between the cell pressure and the back pressure equals the desired consolidation pressure. For each set of particle distribution, samples are tested at different consolidation pressures of 50 and 200 kPa. After final consolidation phase, each sample was sheared under drained condition (CD test). During shearing, the cell pressure was kept constant while advancing the axial load piston downward against the sample cap with strain rate of 0.005 mm/min. All tests were terminated when strain to failure reached a predetermined value of 20% axial strain. Data acquisition was used to measure the load, effective stress, volume change and axial deformation.

5.4 Test results and discussion

5.3.4 Effect of particle-size distribution on stress-strain and volume change response of tested material

Figs. 5.3 and 5.4 shows the triaxial shear strength and volumetric response of samples made up, respectively of glass beads and Péribonka sand with different mean particle-sizes of 106 μm to 1000 μm. All samples in these figures were sheared at the same initial relative density of 90%, and under a normal stress of 50 kPa. For the glass beads samples in Fig. 5.3, following the initial volumetric compression at small axial strain, a significant dilation occurs, until the mobilized stress ratio approaches its maximum value. It is apparent from Fig. 5.3 that the peak strength decreases as the D_{50} of samples increases, while after peak for sample with $D_{50} = 106 \mu m$, the

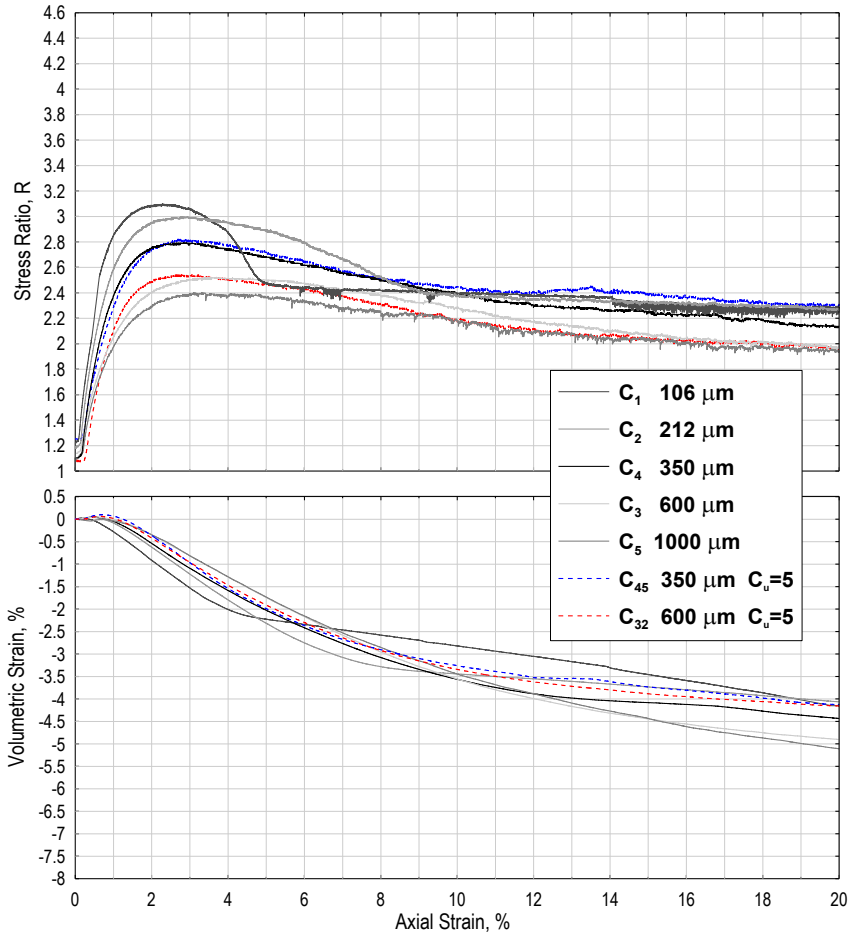

Figure 5.3 Typical data of stress ratio and volumetric strain plotted against axial strain for glass beads at $D_R = 90\%$ and $\sigma_n = 50kPa$.

stress ratio decreases quickly with continuous shearing. However, the sudden drop in stress ratio tend to reduce with the increase of D_{50}, almost vanishes for sample with $D_{50} = 1000\mu m$. In addition, comparing the test results of C_{32} and C_{45} ($C_u = 5$) presented in this figure with C_3 and C_4 ($C_u = 1.5$), it appears that for a given D_{50}, the coefficient of uniformity C_u does not influence the shear strength and volumetric behavior of the samples, at least in the range of the tested D_{50} and C_u values. The independency of shearing behavior of the tested granular material to the coefficient of uniformity C_u is in agreement with the observations during symmetrical direct shear tests (Amirpour Harehdasht et al. 2016), consequently the coefficient of uniformity will not considered in the empirical correlations presented in this paper.

The clear differences between the stress-strain behaviors of samples with different particle-size distributions, under dense conditions and low normal stress, might be attributed to their dilation mechanism, concentrated mainly within their shear zone. As experimentally shown (Jewell and Wroth 1987; Tatsuoka et al. 1990; Wu et al. 2008), the shear zones experience the most intense disturbance during shearing, which is related to the formation and failure of the particle bridges (Sammis et al. 1987) supporting the load in a sheared granular material. The volumetric change in the sample, as well as the shear strain, contributes to the mechanism of these bridge formations where individual voids and high values of void ratio develop in proportion to particle-size (Li et al. 2012; Oda and Kazama 1998).

For dense samples with small D_{50}, small particles dominated the system. Pores were not very evident during shearing (Morgan 1999), and the assemblage appeared quite densely packed before particle columns were formed in the shear zone. Thus, at the initial phase of shearing the increase in stress ratio occurred at very slight vertical displacement. Through further increases in the stress ratio, highly concentrated stress chains with similar orientations were developed in the shear zone (Morgan 1999; Oda and Kazama 1998; Oda 1972), and the dilation started to appear. Around the peak, individual slip planes were very sharply defined, comprising single rows of small particles (Li et al. 2012; Morgan 1999). These chains likely collapsed under approximately the same shear displacement, corresponding to the maximum shear stress ratio, and failure subsequently occurred through sudden slip along a plane of particles accompanied by macroscopic stress drop (Mair et al. 2002).

In dense samples with a larger D_{50}, inter-particle contacts were dominated by large particle pairs, leaving large pores between them while generating diffuse webs of load-bearing particles (Morgan 1999; Oda, M, Konishi 1974; Oda and Kazama 1998), and caused more vertical and shear displacement than the samples with a smaller D_{50} before reaching the maximum shear resistance. When stresses built up, the particle columns failed and reformed repeatedly; the pores expanded and the shear zone dilated, leading to relatively wide and diffuse zones of slip plane dominated by large particles (Anthony and Marone 2005; Mair et al. 2002; Morgan 1999). Therefore, the deformation in these samples was very irratic and the shear zone was normally looser than in samples with a smaller D_{50}, making the post-peak strain softening smoother than in samples with a sharp, well-defined slip plane (Li et al. 2012; Morgan 1999).

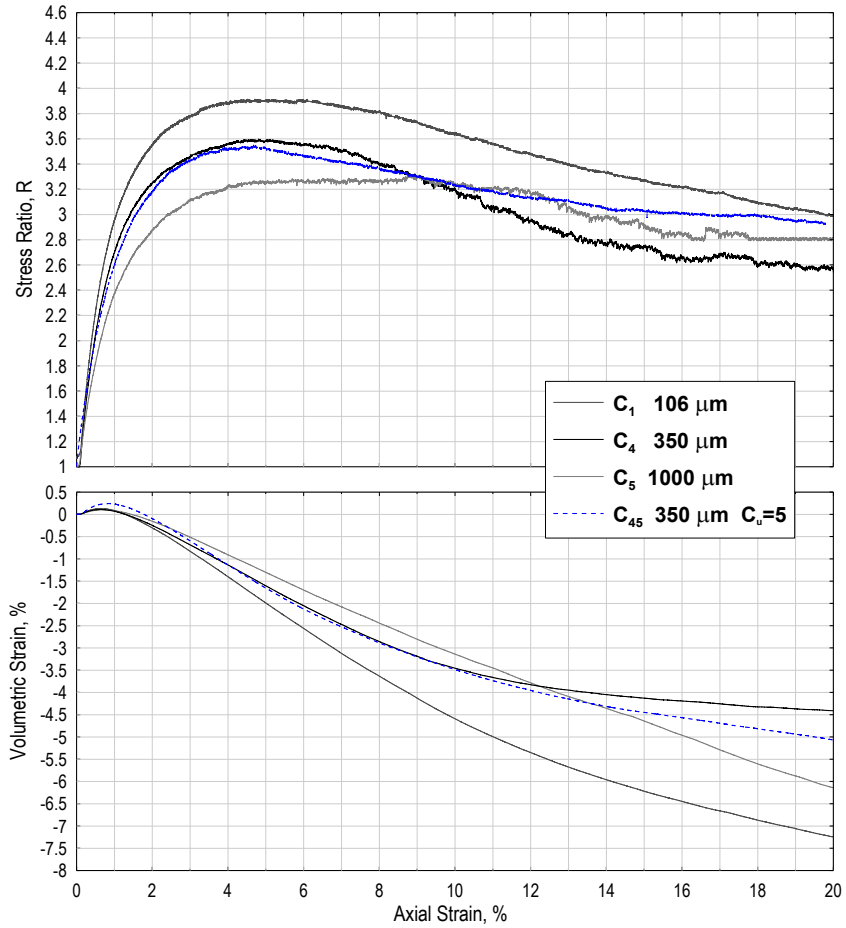

Figure 5.4. Typical data of stress ratio and volumetric strain plotted against axial strain for Péribonka sand at $D_R = 90\%$ and $\sigma_n = 50kPa$.

Comparing the shearing response of glass beads with Péribonka sand for a given particle-size distribution in Fig. 5.4 shows that for a given distribution, the dilation of Péribonka sand starts at an axial strain larger than that of for glass beads. In addition, a closer examination reveals that Péribonka sand requires larger axial strains to mobilize the maximum shear resistance than glass beads, where the post-peak strain softening is gentle than that of beads. This behavior can be interpreted according to Guo and Su (2007) as the difference between glass beads and Péribonka sand arises from the interparticle locking of angular particles that restrains their relative sliding and rotations in Péribonka sand. So that, larger shear stress is required for Péribonka sand to break the interlocking before the relative particles movements associated with diatancy occurs. In other words, the observed plateau on the stress ratio-strain curves of samples

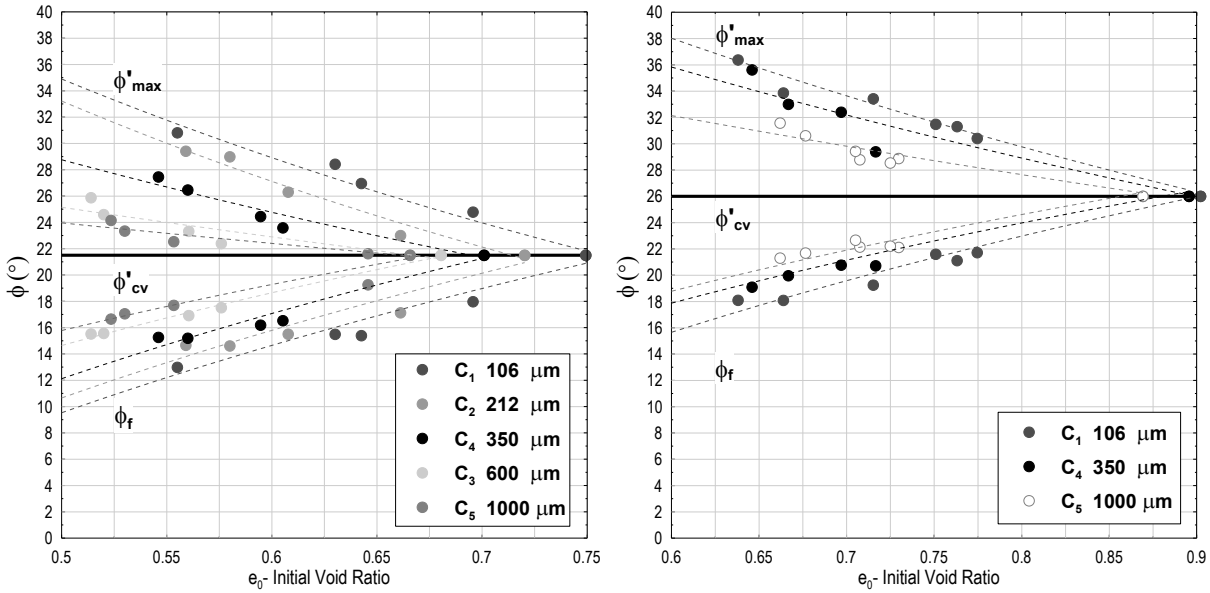

Figure 5.5 Measured shear strength ϕ'_{max}, ϕ'_{cv}, and ϕ'_f of a) glass beads and b) Péribonka sand at different initial void ratios.

made up of angular particles (Fig. 5.4) is attributed to the coupled effect of the dilation and the degradation of interlocking.

Fig. 5.5 summarizes the variation of the friction angle at the onset of dilation ϕ'_f and the peak friction angle ϕ'_{max} against the initial void ratio for glass beads and Péribonka sand. Among the five different methods available in the literature and presented in Table 5.3, methods c and d using multiple tests were suggested by many researchers (Bolton 1986; Jewell 1989; Pedley 1990; Simoni and Houlsby 2006) to evaluate the friction angle at large strain ϕ'_{cv} values, since they minimize the influence of errors compared to the single test methods. According to these methods, the critical friction angle of glass beads and peribonka sand in this study are D_{50}-independence, equal to 21.5° and 26°, respectively. For a given particle-size distribution, the decline of ϕ'_{max} with increasing initial void ratio e_0 is apparent in both Figs. 5.5a and 5.5b, while the $\phi'_{max} \approx Ae^{ne_0}$ curves describing the void ratio dependence of peak shear resistance are different for each particle-size distribution. For all tested distribution curves, the dilation ϕ'_f gradually approaches ϕ'_{cv} as e_0 increases. However, the experimental results in both figures show that the difference between ϕ'_f and ϕ'_{cv} decreases with the increase in D_{50} for a given e_0.

Table 5.3 Detail of methods used to predict ϕ'_{cv}.

Method	Description
a	The direct measurement of the mobilized friction angle at large strains and zero dilation rate
b	Plot $\tau/\sigma + dy/dx$ against x, $(\phi'_{cv})_{ds} = sin^{-1}(int\ ercept\ at\ x = 0)$
c	Plot τ/σ against dy/dx, $(\phi'_{cv})_{ds} = sin^{-1}(int\ ercept\ at\ dy/dx = 0\ for\ best\ fit\ 1:1 slope)$
d	Plot $(\phi_p)_{ds}$ against ψ_{max}, $(\phi'_{cv})_{ds} = sin^{-1}(int\ ercept\ at\ \psi_{max} = 0\ for\ best\ fit\ 1:1 slope)$
e	Angle of repose of loose hip of soil

It has to be noted that, the friction angle ϕ'_f at the onset of dilation is obtained from stress-dilatancy plots where the dilatancy factor $D = 1.$ Examples of these plots presenting the stress ratio R versus dilatancy factor $D = 1 - d\varepsilon_v / d\varepsilon_a$ for glass beads and Péribonka sand are shown, respectively in Figs. 5.6 and 5.7.

5.3.4 Effect of particle-size distribution on stress-dilatancy response of tested material

Fig. 5.6a compares the stress-dilatancy evolution of 5 distribution C_1 to C_5 of glass beads, under the effective confining stress of $\sigma_3 = 50kPa$ and initial relative density of $D_R = 90\%$. Independent of D_{50}, prior to the maximum dilation, the stress-dilatancy curves of all distributions show a consistent increase of the stress ratio $R = \sigma_1/\sigma_3$ with the dilatancy factor $D = 1 - d\varepsilon_v / d\varepsilon_a$. After the peak point, both R and D decrease gradually and reach a critical state at which no further volume change take place. However, the discussion in the previous section clearly reveals that the shear strength and volumetric behavior of tested material would vary with D_{50}, which in turn would be manifested in their stress-dilatancy plots. As expected, the disparity in the stress-dilatancy response exhibited by glass bead samples with different D_{50} is evident in this figure, so that the corresponding $(R-D)_{max}$ decreases with increase of D_{50}. Independent of the mean particle-size D_{50} of samples, all $R-D$ curves are confined within an upper and a lower bounds correspond to the $K_{cv} = tan^2(\pi/4 + \phi_{cv}/2)$ and $K_{\mu} = tan^2(\pi/4 + \phi_{\mu}/2)$ lines, in agreement with the classical stress-dilatancy results presented by Rowe (1962). It should be noted that in this study

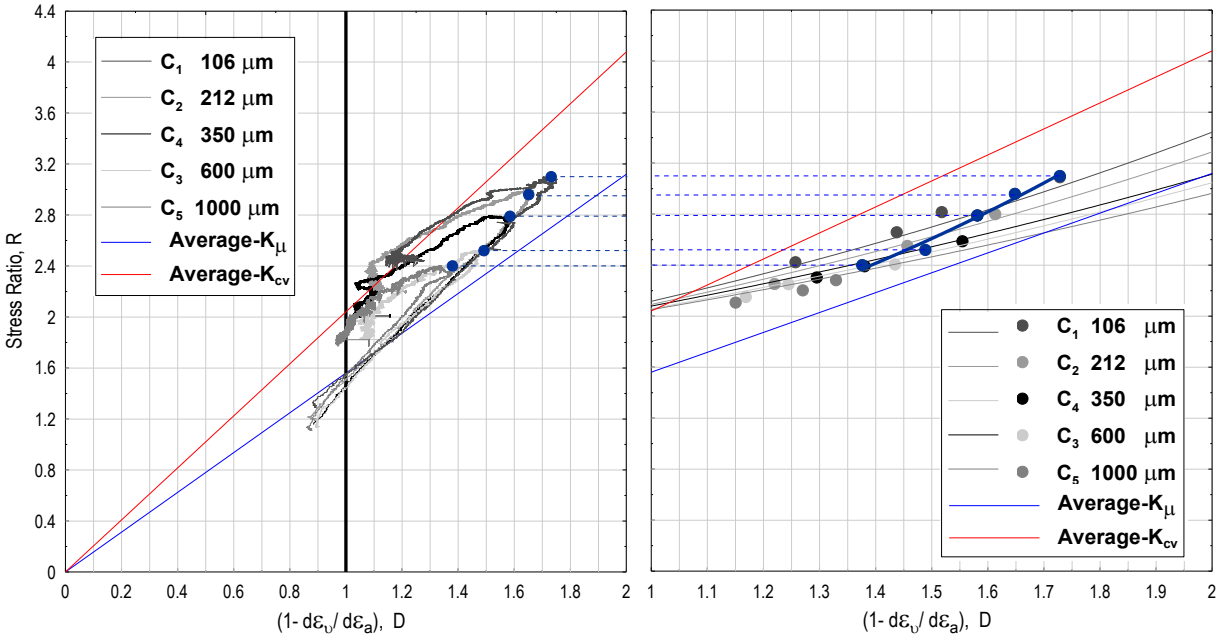

Figure 5.6 a) Stress-dilatancy curves for particle size distributions of glass beads C_1 to C_5 at $D_R = 90\%$ and $\sigma_n = 50kPa$, and b) $(R-D)_{max}$ values of distributions C_1 to C_5 independent of the confining pressure and relative density.

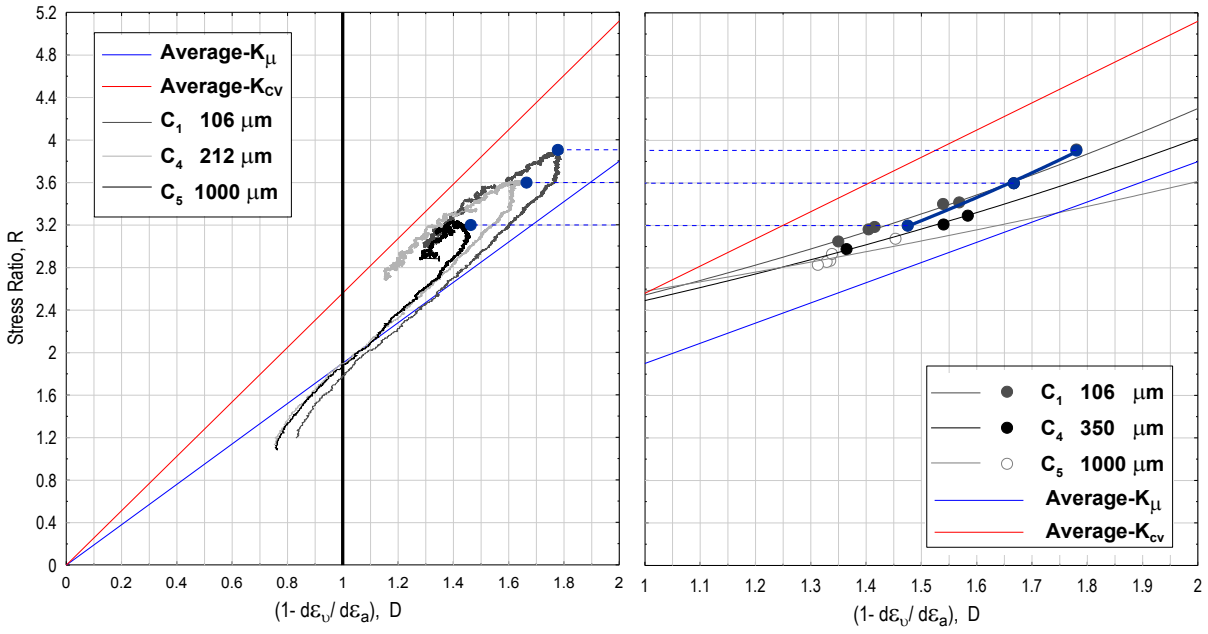

Figure 5.7 a) Stress-dilatancy curves for particle size distributions of Péribonka sand C_1, C_4, and C_5 at $D_R = 90\%$ and $\sigma_n = 50kPa$, and b) $(R-D)_{max}$ values of distributions C_1, C_4, and C_5 Independent of the confining pressure and relative density.

the inter-particle friction angle ϕ_μ for each distribution was back-calculated from the stress dilatancy plot of very dense specimens. So that, ϕ_μ decreases from 14° to 11.5° for distributions C_1 to C_5, in agreement with earlier results found in the literature (Bowden et al. 1943; Lee and Seed 1967; Rowe 1962), where there is a decrease in ϕ_μ with the increase of the size of the load per particle (i.e., increase of particle-size) for a given material while crushing of particles did not occur. Similar behavior have been observed in Fig. 5.7a for samples made up of angular particles, where ϕ_μ decreases from 18° to 16° for distribution C_1 to C_5.

Finally, in Figs. 5.6b and 5.7b the data of the test series on the influence of D_{50} are combined, independent of the confining pressure and relative density, where $50kPa \le \sigma_n \le 200kPa$ and $50\% \le D_R \le 90\%$. $(R-D)_{max}$ data of all distributions of glass beads and Péribonka sand with equal C_u but different D_{50} confined between the two regression line passing through $D_{50} = 106\mu m$ and $D_{50} = 1000\mu m$ data, confirming the D_{50}-dependence of $(R-D)_{max}$. The highlighted points in this figure also show an example of how the $(R-D)_{max}$ values of different D_{50} at a given combination of confining stress and relative density are placed on regression-$(R-D)_{max-D_{50}}$ line, while decreasing with the increase of D_{50}.

5.3.4 Implementation of D_{50} on modified Rowe's stress-dilatancy equation (material constant α)

Wan and Guo (1999) using triaxial data from King and Dickin (1970) clearly revealed that there is no single linear relationship between stress ratio R and dilatancy D as implied by Row's Equation and as can be also seen in Figs. 5.6 and 5.7. As shown in Figs 5.6 and 5.7, while the $(R-D)_{max}$ values depend on the initial void ratio and the applied confining pressure, the stress-dilatancy curves are confined between two straight lines with different slopes; namely K_μ and K_{cv}. According to Wan and Guo (1999) the equivalent friction angle ϕ_f cannot be arbitrary considered constant equal to ϕ'_{cv} as commonly accepted in Eq. 5.2, since it is bound to vary with both density and internal structure during the deformation process. After a careful examination of their experimental data and theoretical investigation, Wan and Guo (1999) suggested a

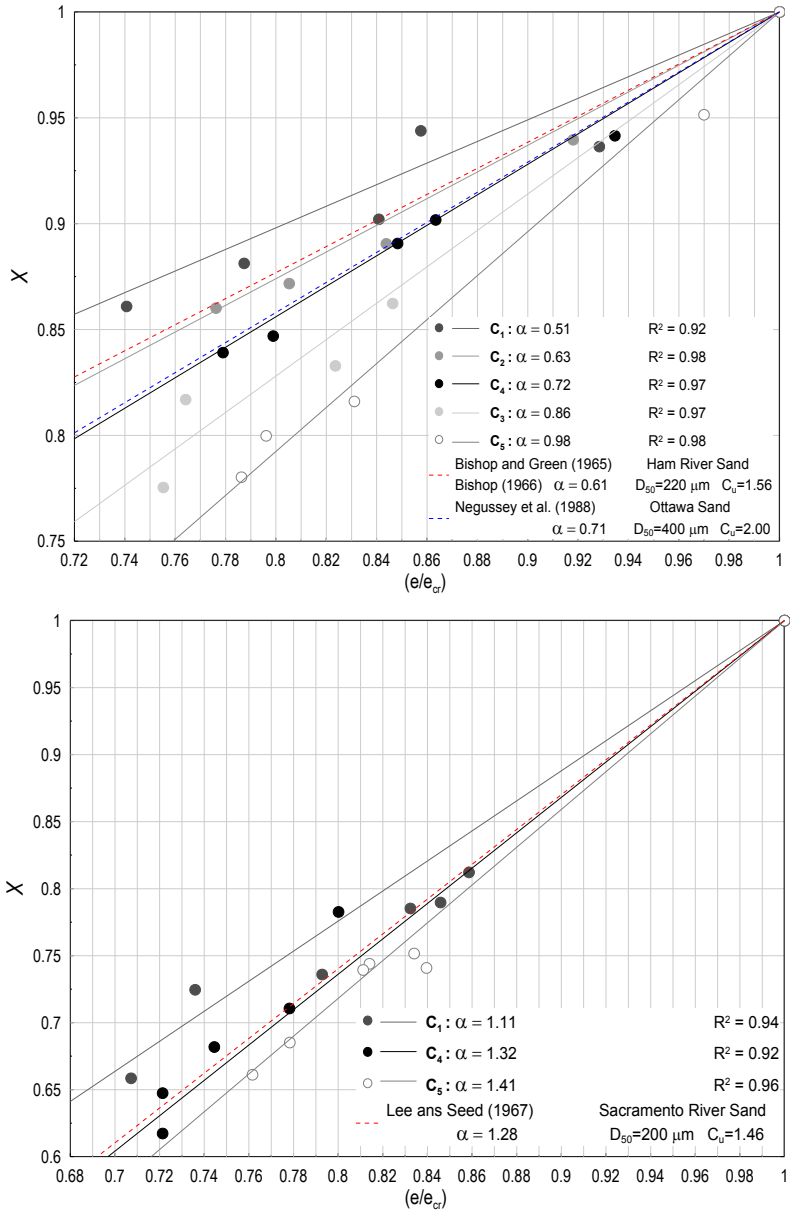

Figure 5.8 Determination of parameter α for particle size distributions a) C_1 to C_5 of glass beads b) C_1, C_4, and C_5 of Péribonka sand

modified Rowe's stress-dilatancy equation where dilation process, and ϕ_f was linked to the deviation of the current void ratio from the mean stress dependent critical void ratio (Eqs. (5.8) and (5.9)). Wan and Guo (1999) introduced the parameter α as a material constant in their formula that can be deducted by rearranging the Eq. (5.8) irrespective of the initial void ratio and the confining pressure, as:

$$\alpha = \frac{\log X}{\log\left(e/e_{cr}\right)} \tag{5.16}$$

where $X = \frac{\sin\phi'_{max} - \sin\psi_{max}}{\left(1 - \sin\phi'_{max}\sin\psi_{max}\right)\sin\varphi'_{cv}}$ (5.17)

In order to evaluate the effect of particle geometry on the parameter α, the variation of X values are plotted with respect to $\left(e/e_{cr}\right)$ at peak state in Figs. 5.8a and 5.8b, irrespective of both material density and confining pressure for glass beads and Péribonka sand, respectively. Fig 5.8 clearly demonstrates that for a given material, Eq. (5.8) cannot be fully described using a unique parameter α, which is affected by the size of the particles as well as the shape of the constituent grains.

The variation of the parameter α with D_{50} can be described by a power function as:

$$\alpha = c_1 (D_{50})^{c_2} \tag{5.18}$$

where the constants $c_1 = 0.13$ and $c_2 = 0.28$ for material made up of rounded particles (glass beads). The values of these constants change to $c_1 = 0.68$ and $c_2 = 0.10$ for Péribonka sand with sub-rounded to sub-angular particles. The parameter α is calculated from Eq. (5.18) for each series considered and summarized in Fig. 5.9 and columns 8-10 of Table 5.2.

The obtained parameters $\alpha(D_{50})$ are compared to α values determined for three different sands using conventional triaxial compression test data borrowed from the literature as depicted in Fig. 5.9. However, the effect of particle-size distribution and shape are isolated here from other factors (e.g. surface texture, particle crushing, and fine particle content) that might affect the parameter α. Therefore, their influence on parameter α should be investigated and integrated into the proposed correlations by testing more naturally shaped particle-size distributions ranging from poorly to well graded curves.

5.3.4 Implementation of D_{50} on experimental adjustment of Rowe's stress-dilatancy equation

Vaid and Sasitharan (1992) defined the angle of dilataion ψ_{max} as:

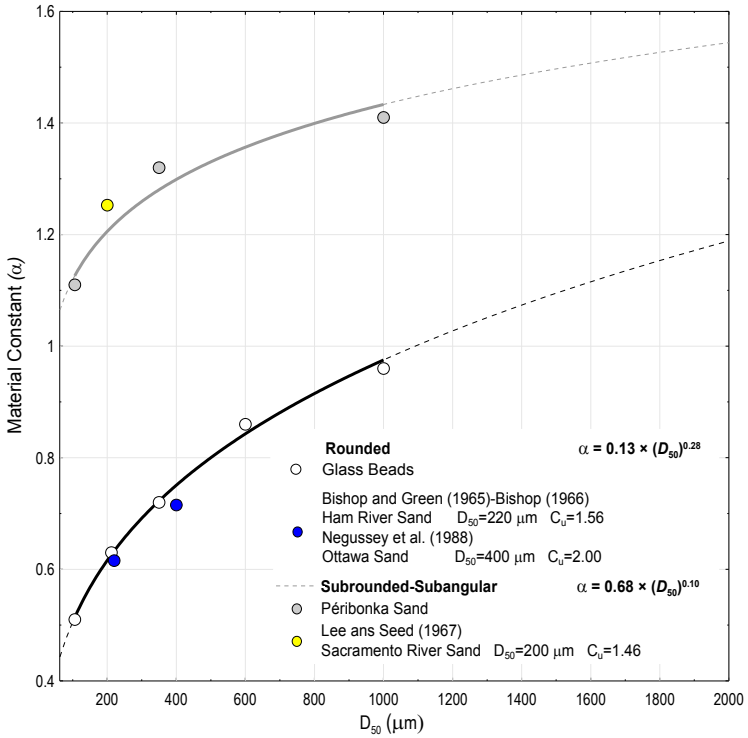

Figure 5.9 Parameter α as a function of D_{50}.

$$\psi_{max} = sin^{-1}\left(\frac{2}{\frac{3}{\left|d\varepsilon_v / d\varepsilon_a\right|}+1}\right) \tag{5.19}$$

and proposed a relationship similar to Bolton's Eq. (5.3) as an experimental alternative of Rowe's stress-dilatancy equation for conventional triaxial condition. When defining the angle of dilation ψ_{max} according to Eq. (5.19) , the data in Figs. 5.6b and 5.7b can be alternatively replotted as the correlation between $(\phi'_{max} - \phi'_{cv})$ and the maximum angle of dilation ψ_{max} suggested by Bolton (1986) and Vaid and Sisitharan (1991). By fitting the points to linear regression lines for each D_{50}, it can be seen that the results of tests on each distribution are consistent in terms of $(\phi'_{max} - \phi'_{cv})$ and ψ_{max} (Fig. 5.10). However, the range of the obtained b values is not coincident with the Vaid and Sasitharan's equation $b = 0.33$ for triaxial condition, and is observed to decrease as a function of the increase in D_{50}, for materials made up of rounded

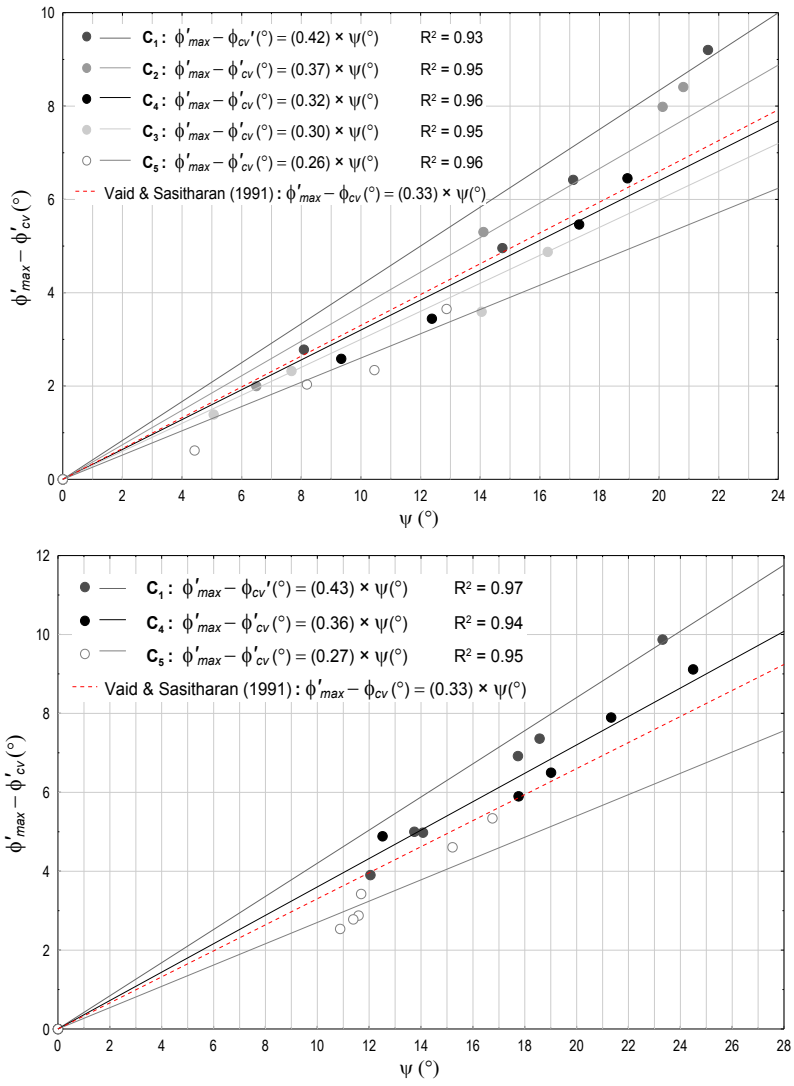

Figure 5.10 $(\phi'_{max} - \phi'_{cv})$ versus ψ_{max} for samples made up of: a) glass beads and b) Péribonka sand.

to angular particles. To clarify the causes of the drop in coefficient b with D_{50}, the sensitivity of each side of these equations to D_{50} was examined over a wide range of stresses and densities, using the state parameter proposed by Been and Jefferies (1985), defined as $(e - e_{cr})$. This parameter combines the influence of void ratio and the stress level with reference to a steady state and allows the quantification of many aspects of granular material behavior using a single parameter.

It can be seen in Figs. 5.11a that for a given $(e-e_{cr})$, the value of $(\phi'_{max}-\phi'_{cv})$ is highly dependent on the D_{50}, where the slope of the regression lines gradually decreasing by around 3.5 times with increasing D_{50} from an absolute value of more than 67 for $D_{50}=106\mu m$, to a value of about 18 for distribution having $D_{50}=1000\mu m$ for glass beads. The decrease of $(\phi'_{max}-\phi'_{cv})$ values versus $(e-e_{cr})$ with increasing D_{50} by 1.84 times is also apparent for Péribonka sand in Fig. 5.12a. Similarly, the regression line passing the ψ_{max} values of the samples made up of glass beads and Péribonka sand with $D_{50}=106\mu m$ are located at the higher boundary of data points while the regression line corresponds to the ψ_{max} values of the samples with $D_{50}=1000\mu m$ tend to lay at the lower boundary (Figs. 5.11b and 5.12b). Comparing the $(\phi'_{max}-\phi'_{cv})$ and ψ_{max} data versus the state parameter $(e-e_{cr})$ in these figures shows that for a given state parameter, $(\phi'_{max}-\phi'_{cv})$ decreased more than ψ_{max} as D_{50} increased, causing a significant drop in the proportion b of the contribution of dilation to peak shear resistance. As shown in Fig. 5.13, for the distribution curves with $63\mu m<D_{50}<2000\mu m$, the correlation between $(\phi'_{max}-\phi'_{cv})$ and ψ_{max} for triaxial condition can be described as:

$$\phi'_{max}-\phi'_{cv}=b\psi_{max} \tag{5.20}$$

where parameter b varies with D_{50} as:

$$b=c_3(D_{50})^{-c_4} \tag{5.21}$$

The decrease of b value with increasing D_{50} is described by a power function (Eq. (5.12)), with constant $c_3=1.14$ and $c_4=0.21$ for material made up of rounded particles. Similar to what was observed in Amirpour Harehdasht et al. (2016) for plane strain condition, these constants decrease with increasing the particle angularity (to $c_3=1.12$ and $c_4=0.19$ in triaxial condition). The parameter b is calculated for each series considered and summarized in columns 11-13 of Table 5.2.

The triaxial $\psi_{max}-(\phi'_{max}-\phi'_{cv})$ data of various granular materials with different D_{50} values and particle angularity also gathered from the literature, and their corresponding obtained b values are plotted in Fig. 5.13. The obtained b values of a material made up of rounded to sub-angular

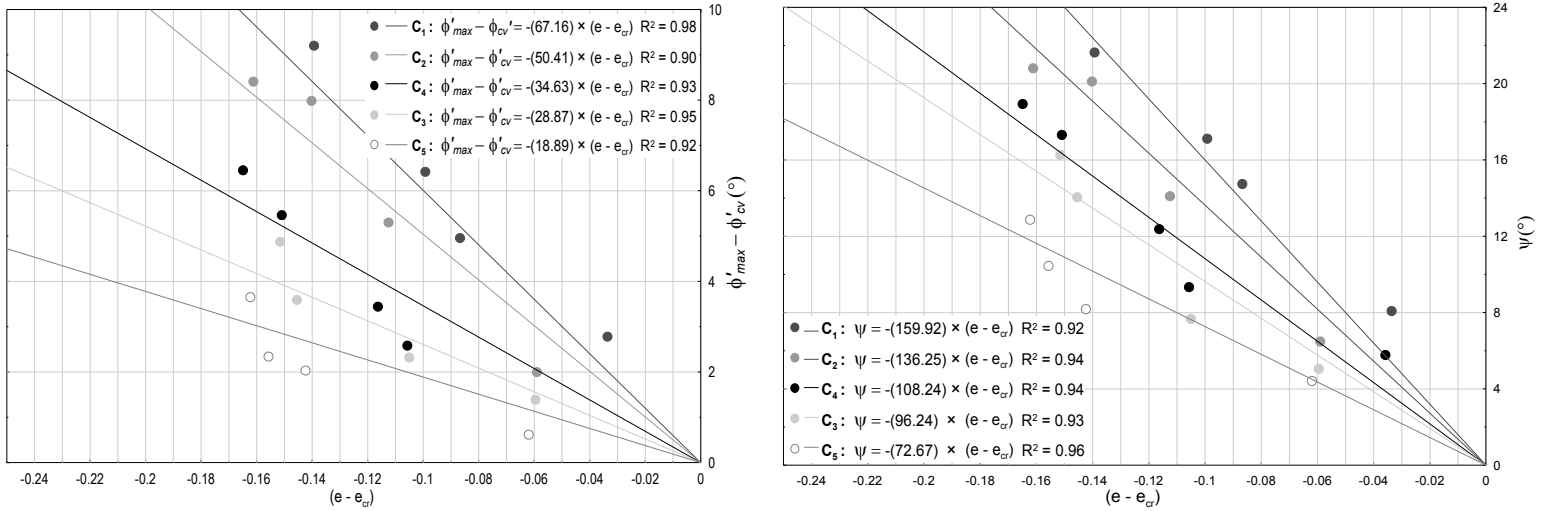

Figure 5.11. $(\phi'_{max} - \phi'_{cv})$ and ψ_{max} as a function of $(e - e_{cr})$ for glass beads.

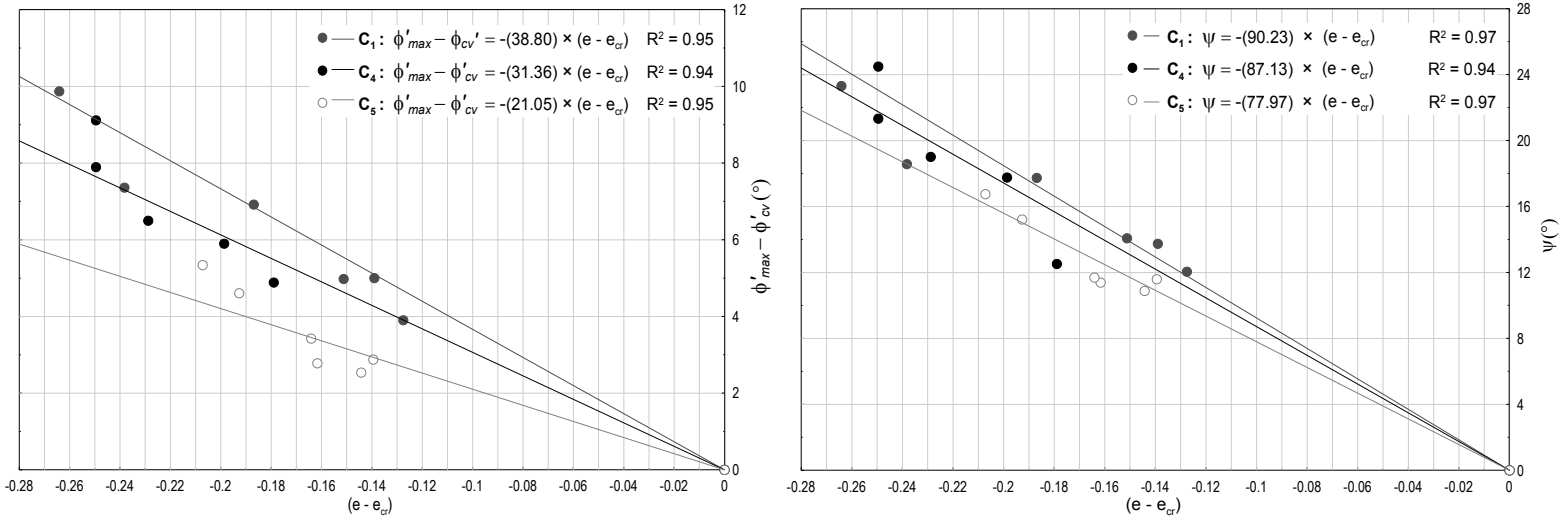

Figure 5.12 $(\phi'_{max} - \phi'_{cv})$ and ψ_{max} as a function of $(e - e_{cr})$ for Péribonka sand

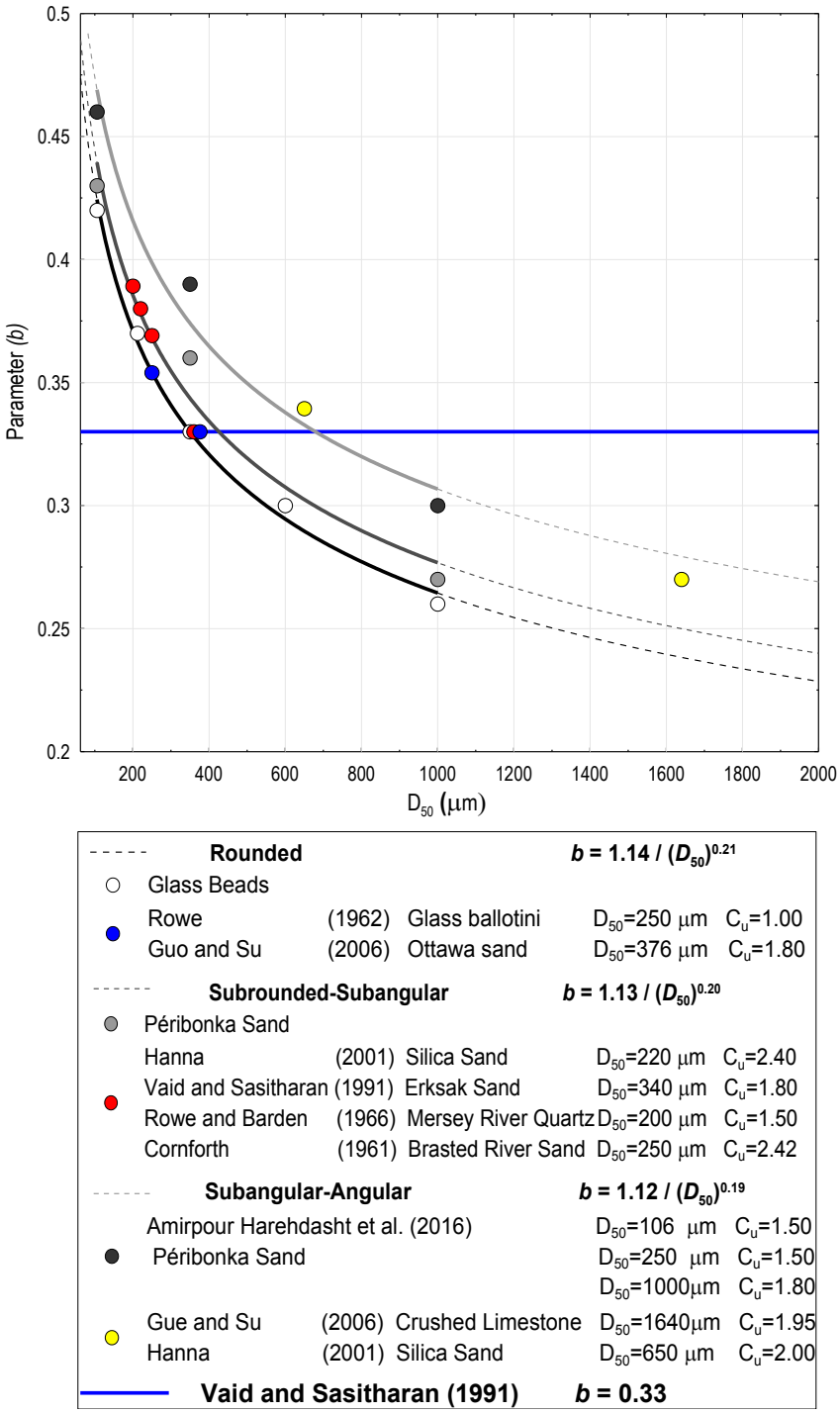

Figure 5.13 Parameter b in dependence of D_{50} for samples made up of rounded to angular particles.

particles are located on the regression line passing through the b points of glass beads and Péribonka sand, in agreement with the b values obtained from Eq. (5.21). In addition, the $\psi_{max}-(\phi'_{max}-\phi'_{cv})$ data of various materials with sub-angular to angular particles were used to obtain their corresponding b parameter. As can be seen in Fig. 5.13 the b values obtained from these materials formed a unified power function curves with c_3 and c_4 values of 1.12 and 0.19, respectively.

5.4 Conclusion

A total of 35 drained triaxial compression tests have been performed on two granular materials to describe the particle characteristics parameters dominating the stress-dilatancy behaviour of 7 differentparticle-size distributions. It has been demonstrated that in the investigated range of and $106\mu m \leq D_{50} \leq 1000\mu m$, stress-dilatancy behavior of the tested materials significantly influenced by the variation of D_{50}.

Based on the triaxial test results, the material constant α of the Wan and Guo's stress-dilatancy equation have been adjusted and correlated with D_{50}. However, an extension of the proposed correlations considering the influence of other factors such as surface texture, particle crushing, and fine particle content seems necessary.

A correlation of parameter b with D_{50} in Vaid and Sasitharan's equation as an experimental adjustment of Rowe's stress-dilatancy equation has also been proposed. The proposed $b(D_{50})$ correlations predict quite well most of the b values using conventional triaxial compression test data borrowed from the literature with rounded to angular particle shapes.

CHAPITRE 6. Conclusions and Recommendations

6.1. Conclusions and Recommendations (Français)

6.2.1. Sommaire et conclusions

L'étude examine de manière approfondie l'impact potentiel des caractéristiques des particules (taille, gradation et forme des particules) sur des corrélations empiriques et théoriques existantes bien connues entre l'angle de frottement et le comportement de dilatation des matériaux granulaires dans des conditions de déformation plane et triaxiale. Après examen de la sensibilité des relations de contrainte de cisaillement-dilatance de cisaillement aux caractéristiques des particules, les coefficients ont été ajustés pour tenir compte des caractéristiques des particules, et des limites de taille de particule ont été imposées à leurs validités. 276 essais de cisaillements symétriques directs et 35 essais de compression triaxiale drainée sur 16 distributions de taille de particules différentes de différents matériaux granulaires ont été exécutés dans ce but. Une analyse respective des données de force et de dilatation rassemblées à partir de la littérature est également présentée dans cette étude pour fournir des preuves appuyant des contraintes mises en application dans des relations existantes.

À une première étape de cette étude, l'exécution de l'appareil physique de cisaillement direct est optimisée en explorant des modifications de la configuration de test symétrique (par exemple, bloc à charge fixe sur le bâti supérieur, collier de serrage modifié, espace initial entre les armatures de la boîte de cisaillement et utilisation de la membrane mince), basée sur le bref examen de la littérature sur les accomplissements progressifs de l'interprétation des données et du développement de la DSA. Les caractéristiques les plus généralement abordées dans ces études sont la tendance à tourner du bloc à charge fixe et du bâti supérieur pendant le test conventionnel. Ensuite, la fiabilité et l'applicabilité des limites de mesure à l'aide de tests physiques de cisaillements symétriques directs dans l'interprétation de la résistance au cisaillement frictionnel en déformation plane des matériaux granulaires ont été discutées et confirmées par l'usage la Méthode d'Éléments Discrets (Discrete Element Method [DEM]) (3D), SiGran. Dans la boîte de cisaillement direct virtuelle, les frontières supérieures et

inférieures sont libres de se déplacer verticalement, mais pas de tourner. Pendant toutes les simulations, aucun mouvement hors-plan n'a été autorisé. Les accomplissements de cette étude secondaire sont classés par catégorie en deux parties - numériques et expérimentales - comme suit:

1. L'évaluation numérique des limites de mesure dans le test de cisaillement symétrique direct.

L'objectif principal de cette étude était d'analyser le comportement macro- et micromécanique du matériau granulaire (particules polydispersées) testé dans le cisaillement symétrique direct au moyen de la méthode d'éléments discrets tridimensionnelle (DEM-3D). Les résultats numériques ont été comparés à leurs contreparties expérimentales à la macro-échelle sous différentes contraintes normales appliquées de 50, 200, et 400 kPa. La partie expérimentale de cette étude a été exécutée en employant la norme polydispersée de particules, ayant une taille de gamme 500μm -2000μm. La même distribution de dimension particulaire de 102248 sphères en verre ont été employées à titre de tests expérimentaux pour des simulations. Dans les modèles de la DEM, les micro-paramètres assignés dans les modèles autres que ceux directement mesurés ont été choisis de sorte à produire les macro-propriétés désirées du matériau examiné en laboratoire. Dans les échantillons physiques et virtuels, la charge de cisaillement est appliquée à l'appareil à la manière de déplacement contrôlé à une vitesse constante de 0.0051 mm/s.

- Il y a une similitude marquée entre le comportement de macro-échelle des deux 'ensembles de cisaillement simple (Stroud 1971) et l'arrangement virtuel et physique amélioré de cisaillements symétriques directs pour les billes en verre sous les contraintes normales de 50 kPa. Cependant, les angles de dilatation maximaux mesurés et calculés déduits des limites de mesure sous-estiment légèrement de 2.5° de moins que $\Delta\psi$ à l'intérieur de la zone de cisaillement.

- Le nombre de coordination diminue rapidement pendant le déplacement de cisaillement initial et s'aplatit d'une valeur relativement régulière tandis que la valeur critique est atteinte. Des valeurs de contrainte normales plus élevées peuvent aider le spécimen avec un plus grand CN à soutenir une valeur plus élevée d'effort de cisaillement.

- La distribution du contact normal et des forces de contact manifeste les mêmes modèles d'évolution de l'anisotropie sous différentes contraintes normales appliquées. Cependant, des anomalies significatives sont notées dans les distributions de grandeur de forces de contact normales et tangentielles

- Il y a une bonne concordance entre les courbes rapprochées (τ/σ_n) obtenues à partir des paramètres d'anisotropie et du rapport de contrainte à partir des limites des échantillons virtuels, qui confirme la coaxialité des composantes des forces de contact et des anisotropies de contact normales pendant le cisaillement.

- Le rapport entre l'énergie de rotation et l'énergie tangentielle est de moins de 3% pour les trois cas. Cependant, il est énoncé comme bon indicateur de la localisation du cisaillement menant à l'établissement de bandes de cisaillement. La distribution spatiale de l'énergie de rotation à différentes étapes de déformation du cisaillement prouve que la localisation des déformations démarre des limites et se prolonge vers le milieu de la boîte de cisaillement tout en développant une bande de cisaillement continue et uniforme tout au long du plan moyen de la boîte.

- Une légère différence, de moins de 1°, entre les angles de frottement de déformation plane calculés à partir de l'équation conventionnelle de Davis (1968) et ceux obtenus à partir de l'équation prolongée de Wang et al. (2007) indique l'effet mineur de la non-coaxialité dans les trois cas numériques en état maximal.

Les résultats de micro-échelle présentés dans le troisième chapitre suggèrent que les paramètres d'états maximaux obtenus à partir de l'arrangement symétrique sont très proches de celui d'un cisaillement simple idéal, car il permet une déformation uniforme à l’intérieur de la bande de cisaillement développée, une orientation horizontale de la prolongation linéaire nulle, et une coaxialité des principales contraintes et de la déformation incrémentielle à l'état maximal. De sorte que les mesures faites aux limites du test de cisaillement symétrique direct modifié sonnent tout à fait appropriées pour déterminer le comportement de résistance au cisaillement et de changement de volume des sols granulaires.

2. Influence de la taille des particules et de la gradation sur la relation de résistance au cisaillement -Dilatation des matériaux granulaires en condition de déformation plane et de compression triaxiale

La comparaison des valeurs de résistance au cisaillement en employant les formulations de résistance au cisaillement -dilatation de Bolton avec les données ϕ'_{max} correspondantes rapportées dans la littérature indiquent qu'en raison des coefficients fixes employés dans les équations de Bolton, les valeurs ϕ'_{max} estimée sont généralement surévaluées. Une recherche systématique au sujet du cisaillement symétrique direct modifié et des résultats de test triaxial drainé démontre également l'inefficacité relative de Collins et al. (1992), et Vaid et Sasitharan (1992), comme ajustements empiriques de l'équation de contrainte de cisaillement– dilatance de cisaillement de Rowe pour des conditions de déformation plane et de compression triaxiale, dans le but de prévoir exactement l'angle de frottement maximale du sol ϕ'_{max}.

- L'étude du comportement de cisaillement de 35 tests triaxiaux drainés sur des billes en verre montre que pendant les essais de compression triaxiale, dans la gamme étudiée de $1.5 \le C_u \le 5$, et $106\mu m \le D_{50} \le 1000\mu m$, la contrainte de cisaillement– dilatance de cisaillement du matériau examiné est sensiblement influencée par la variation de D_{50}.

- Pour les conditions de déformation plane et de compression triaxiale, la résistance au cisaillement maximum des matériaux examinés ϕ'_{max} ne peut pas être décrite par une fonction unique d'index de dilatation maximale comme proposé par des équations bien connues de force-dilatation (Bolton 1986; Collins et al. 1992; Vaid et Sasitharan 1992). De sorte que, les coefficients d'équations empiriques sont sensiblement affectés par la variation de la taille moyenne des particules, D_{50}, et ne dépendent pas du coefficient d'uniformité C_u .

- Après examen de la sensibilité des formulations empiriques de la contrainte de cisaillement– dilatance de cisaillement bien connues dans des conditions de déformation plane et de compression triaxiale vis-à-vis des caractéristiques des particules, leurs coefficients ont été ajustés afin de rendre compte des caractéristiques des particules, en particulier pour D_{50}.

- L'examen des sables de Péribonka et d'Eastmain pendant le cisaillement direct et les essais triaxiaux montre le même comportement de contrainte de cisaillement– dilatance de cisaillement pour des matériaux composés de particules sub-arrondies et angulaires (des sables de Péribonka et d'Eastmain). La prolongation des corrélations empiriques proposées considérant l'influence de l'obliquité des particules a été faite, car le résultat du cisaillement montre que le coefficient des rapports empiriques est affecté par la forme des particules aussi bien que par la taille des particules.

- Les corrélations proposées prévoient assez bien la plupart des valeurs de résistance au cisaillement et de dilatation examinées en laboratoire, ou rapportées dans la littérature pour des sables avec une forme de particules arrondies à angulaires.

Les formules de force-dilatation ajustées peuvent être salutaires pour évaluer indépendamment la cohérence des forces de cisaillement déterminées expérimentalement, et pour introduire des lois d'écoulement plus raffinées au sein des analyses géotechniques analytiques et numériques.

6.2.2. Recommandations pour les travaux futures

Les résultats de la recherche numérique présente dans le chapitre 3 proposent des voies de recherche potentiellement importante pour mieux comprendre le comportement micromécanique tridimensionnel des milieu granulaires. La modification mineure du programme SiGran permettra à des expériences numériques d'être effectuées sur des ensembles non-cohésifs plus complexes.

- Les résultats numériques présentés dans cette thèse mènent à une meilleure compréhension du rôle du comportement micromécanique des matériaux granulaires pendant le cisaillement symétrique direct. En prenant en note de la limitation de l'analyse tridimensionnelle sur le matériau composé de la forme idéale utilisée, la validation au moyen d'un modèle mobilisant des particules plus réalistes serait exigée, dans le but du développement de modèles constitutifs abordant l'influence des caractéristiques des particules à la lumière des résultats de la microstructure.

- Des facteurs tels que la texture, la forme et la gradation des particules peuvent être implémentés dans le code informatique de SiGran pour étudier l'influence des inter-particules de verrouillage due aux vraies caractéristiques du sol sur la dilatation et le comportement de cisaillement des matériaux granulaires.

Les études expérimentales présentées dans les chapitres 4 et 5 de cette thèse ont étudié l'influence de la distribution de la taille de la particule sur les caractéristiques de cisaillement et de dilatation des matériaux granulaires. Les résultats expérimentaux de trois matériaux se composant de particules à obliquité différente sont présentés dans ces chapitres afin de proposer des corrélations de contrainte de cisaillement– dilatance de cisaillement basées sur les caractéristiques de dimension des particules. Ces corrélations prévoient assez bien la plupart des valeurs ϕ'_{max} rapportées dans la littérature pour des sables à la forme de grain arrondie à angulaire. . Cependant, les travaux et améliorations suivants sont considérés nécessaires dans les recherches à venir :

- L’adaptabilité des équations proposées à des courbes de distribution de taille de particules plus compliquées doit être vérifiée. Jusqu'ici, seulement des courbes de distribution de taille de particules ayant une forme linéaire à l’échelle semi-logarithmique ont été testées. Les courbes à distribution de taille de particule en forme de s et à granulométrie discontinue ainsi que des courbes formées plus naturellement peuvent être examinées à l'avenir. En outre, l'applicabilité des corrélations proposées dans ces études à des courbes à distribution de taille de particules plus naturelle peut être étudiée.

- L'efficacité de la base de corrélations proposées sur des facteurs de distribution de la taille des particules dans les chapitres 4 et 5 a été validée en employant les données recueillies de la littérature. Cependant, ces données correspondent seulement à un certain nombre de données D_{50} de sables standard et de matériaux ayant une distribution de dimension particulaire plutôt uniforme. Par conséquent, plus de données de matériaux granulaires ayant des distributions de taille de particules différentes seraient salutaires pour refléter la dépendance des valeurs ϕ'_{max} prédites à partir des équations de taille-distribution de particules proposées.

- D'autres essais peuvent être effectués concernant l'influence des facteurs de la forme de grain et du contenu fin sur les corrélations $\phi'_{max}(D_{50})$ et $\psi_{max}(D_{50})$. De sorte que l'influence du contenu fin et des facteurs de forme puisse être intégrée dans les corrélations proposées.

- La constante matérielle α dans la corrélation contrainte de cisaillement– dilatance de cisaillement de Wan et Guo modifiée a été seulement évaluée pour la distribution de taille de particules des matériaux examinés. Cependant, la constante matérielle α peut être affectée par d'autres caractéristiques de particules telles que la rugosité et la forme des particules aussi bien que la distribution de la taille des particules. De sorte que la corrélation $\alpha(D_{50})$ proposée dans le chapitre 6 peut être améliorée sur base de ces facteurs dans de futures recherches.

- La corrélation résistance au cisaillement-dilatation développée sur base de la distribution de la taille des particules peut être mise en application dans des analyses géotechniques, où la contrainte de cisaillement– dilatance de cisaillement est un facteur clé dans la description des matériaux granulaires. Les résultats peuvent être comparés à l'analyse dans laquelle les rapports empiriques et théoriques conventionnels ont été employés. Cette comparaison peut être salutaire pour évaluer l'efficacité de la nouvelle description des corrélations contrainte de cisaillement– dilatance de cisaillement sur l'exécution de modèles constitutifs.

6.2. Conclusions and Recommendations (Anglais)

6.2.1. Summary and conclusions

This study closely examines the potential impact of particle characteristics (e.g. particle size, particle shape, and particle gradation) on the well-known existing empirical and theoretical correlations between the friction angle and the dilation behavior of granular materials in plane strain and triaxial conditions. After examining the sensitivity of strength-dilation relations to the particle characteristics, the coefficients have been adjusted to account for particle characteristics, and particle-size limits are imposed on their validities. The 276 direct shear tests and 35 drained triaxial tests on 16 different particle-size distributions of different granular materials were conducted for purpose. An analysis of strength and dilation data collected from the literature is also presented in this study to provide evidence in support of the implemented constraints into existing relations.

As a first step of this study, the performance of the physical direct shear apparatus was optimized by exploring modifications to the symmetrical test configuration (e.g., fix load pad to the upper frame, modified collar attachment, initial gap between the shear-box frames, and the use of thin membrane), based on the brief review of literature on the gradual achievements of data interpretation and DSA development. The characteristics most commonly addressed in these studies is the tendency for the load pad and upper frame to rotate during conventional testing. Thereafter, the reliability and applicability of boundary measurements in physical symmetrical direct shear tests to interpret the plane strain frictional shearing resistance of granular material were discussed and confirmed using three-dimensional (3D) discrete element method (DEM) computer code SiGran. In a virtual direct shear box, the top and bottom boundaries are free to move vertically, but not to rotate. During all simulations, no out-of-plane motion was permitted. Achievements of this study are sub-categorized into numerical and experimental aspects as follows:

1. Numerical assessment of boundary measurements in symmetrical direct shear test

The prime objective of this study was to analyze the macro and micromechanics behavior of granular material (polydisperse particles) tested in symmetrical direct shearing by means of

three-dimensional (3D) discrete element method (DEM). The numerical results were compared to their experimental counterparts at the macro-scale under applied normal stresses of 50, 200, and 400 kPa. The experimental part of this study was performed using the polydisperse particle standard, having the range size of 500-2000 μm. The same particle size distribution of 102248 glass spheres as experimental tests were used for the simulations. In DEM models the assigned micro-parameters in the models other than those directly measured were chosen so as to produce the desired macro-properties of the material being tested in the laboratory. In both physical and virtual samples, shear load was applied to the apparatus in the displacement-controlled fashion at a constant velocity of 0.0051 mm/s.

- There was a marked similarity between macro-scale behavior of the two sets of simple shear (Stroud 1971) and both virtual and physical improved arrangement of symmetrical direct shear for glass beads under the normal stresses of 50 kPa. However, the measured and the calculated peak dilatancy angles deducted from the boundaries measurements underestimate slightly by $\Delta\psi$ less than 2.5° than that inside the shear zone.

- The coordination number CN decreases rapidly during the initial shear displacement, and flatten off to a relatively steady value while the critical values is attained. Higher normal stress value may assist specimen with a larger CN to sustain higher shear stress value.

- The distribution of the contact normal and the contact forces exhibits the same evolution patterns of anisotropy under different applied normal stresses. However, significant discrepancies were noted in the distributions of the magnitude of the normal and the tangential contact forces.

- There is a good agreement between the approximated (τ/σ_n) curves obtained from the anisotropy parameters and the stress ratio from the boundaries of the virtual samples, which confirms the coaxiality of the contact force components and contact normal anisotropies during shearing.

- The ratio of the rotational energy to the tangential energy is less than 3% for the three cases. However, it stated as a good indicator of shear localization leading to the establishment of shear bands. The spatial distribution of rotational energy at different stages of shear

distortion shows that the strain localization initiates from the boundaries and extends towards the middle of the shear box while developing a continuous and uniform shear band along the middle plane of the box.

- A slight difference, less than 1°, between the plane strain friction angles calculated from the conventional Dave's equation (Davis, 1968) and those obtained from the extended equation of Wang et al. (2007) reveals the minor effect of non-coaxiality in the three numerical cases at peak states.

The micro-scale results presented in chapter three suggest that the peak state parameters obtained from the symmetrical arrangement are very close to those of an ideal simple shear, as it permits a uniform deformation within the developed shear band, a horizontal orientation of the zero linear extension, and a coaxiality of principal stresses and incremental strains at the peak state. So that, measurements at the boundaries of the modified symmetrical direct shear test are quite appropriate for determining strength and volume change behavior of granular soils.

2. Influence of particle size and gradation on the shear strength-dilation relation of granular Materials in plain strain and triaxial condition

Comparing shear resistance values using Bolton's strength-dilation formulations with the corresponding ϕ'_{max} data reported in the literature reveals that due to the fixed coefficients used in Bolton's equations the estimated ϕ'_{max} values are generally over-predicted. A systematic investigation of modified symmetrical direct shear and drained triaxial test results also demonstrates the relative inefficiency of Collins et al. (1992), and Vaid and Sasitharan (1992). The empirical adjustments of Rowe's stress-dilatancy equation for plane strain and triaxial condition, to accurately predict the soil peak friction angle ϕ'_{max}.

- Investigating the shearing behavior of 35 drained triaxial tests on glass beads shows that during triaxial compression tests, in the investigated range of $1.5 \leq C_u \leq 5$, and $106\mu m \leq D_{50} \leq 1000\mu m$, the tress-dilatancy behavior of the tested material was significantly influenced by the variation of D_{50}.

- For both plane strain and triaxial conditions, the maximum shear resistance of the tested materials ϕ'_{max} cannot be described by a unique function of maximum dilation or dilatancy index as proposed in well-known strength-dilation equations (Bolton 1986; Collins et al. 1992; Vaid and Sasitharan 1992). Thus, the coefficients of empirical equations are significantly affected by the variation of mean particle size D_{50}, and not depend on the coefficient of uniformity C_u.

- After examining the sensitivity of the well-known empirical shear strength-dilation formulations in plane strain and triaxial conditions to the particle characteristics, their coefficients have been adjusted to account for particle characteristics, in particular for D_{50}.

- Examining the Péribonka and Eastmain sands during direct shear and triaxial tests shows the same shear–strength-dilation behavior for materials made up of sub-rounded to angular particles (Péribonka and Eastmain sands). The modification of the proposed empirical correlations considering the influence of the particles angularity was completed, as the shear results shows the coefficient of the empirical relationships are affected by the particle shape as well as the particle-size distribution.

- The proposed correlations predict quite well most of the shear strength and dilation values tested in the laboratory, or reported in the literature for sands with a rounded to angular particle shape.

The adjusted strength-dilation formulas may be beneficial for independently assessing the consistency of the experimentally-determined shear strengths, and introducing more refined flow rules into analytical and numerical geotechnical analyses.

6.2.2. Recommendation for future research

The results of the current numerical investigation in chapter 3 pose potentially rewarding avenues of research into the three dimensional .micromechanical behavior if granular media. Minor modifications to the program SiGran will allow numerical experiments to be carried out on more complex cohessionless assemblies.

- Numerical results presented in this thesis lead to a better understanding of the role of micro-mechanical behavior of granular materials during symmetrical direct shearing. Noting that the limitation of the three dimensional analysis on material made up of ideal shape employed, validation with a model with more realistic particles would be required, for the development of the constituent models addressing the influence of particle characteristics in the light of the microstructure findings.

- Factors such as surface texture, shape and grading of particles can be implemented in SiGran computer code to investigate the influence of inter-particles locking owing to the real soil characteristics on dilatancy and shearing behavior of granular materials.

The experimental studies presented in chapter 4 and 5 of this thesis investigated the influence of particle size distribution on shearing and dilatancy characteristics of granular materials. The experimental results of three material consisting of particles with different angularity are presented in these chapters to propose shearing strength-dilatation correlations based on particle-size characteristics. These correlations predict quite well most of the ϕ'_{max} values reported in literature for sands with rounded to angular grain shape. However, following works and improvements are considered necessary in future studies:

- The suitability of the proposed equations for more complicated grain-size distribution curves has to be evaluated. Up to now, only grain-size distribution curves with a linear shape in the semilogarithmic scale have been tested. S-shaped and gap-graded grain-size distribution curves as well as more naturally shaped curves can be tested in the future. In addition, the applicability of the proposed correlations in these studies to more naturally grain-size distribution curves can be studied.

- The efficiency of the proposed correlations base on particle-size distribution factors in chapters 4 and 5 have been validate using the data gathered from the literature. However, these data correspond to only to limited D_{50} data of standard sands and materials having a rather uniform particle size distribution. Therefore, more data of granular materials having different particle size distributions would be beneficial to reflect the dependence of ϕ'_{max} values predicted from proposed equations on particle size-distributions.

- Further tests can be conducted regarding the influence of the grain shape factors and fine content on $\phi'_{max}(D_{50})$ and $\psi_{max}(D_{50})$ correlations. So that, the influence of the fine content and shape factors can be integrated into the proposed correlations.

- The material constant α in Wan and Guo modified stress-dilatancy correlation has been only evaluated for particle-size distribution of the tested materials. However, the material constant, α can be affected by other particle characteristics such as particle roughness and shape as well as particle-size distribution. So that, the proposed $\alpha(D_{50})$ correlation in chapter 6 can be improved based on these factors.

- The developed shear-strength-dilation correlation based on particle-size distribution can be implemented in geotechnical analysis, where stress-dilatancy is a key factor for describing granular materials. The results can be compared to analysis in which the conventional empirical and theoretical relationships have been used. This comparison can be beneficial to evaluate the efficiency of new description of stress-dilatancy correlations on the performance of constitutive models.

LISTE DES RÉFÉRENCES

Al-Douri, R. et Poulos, H. (1992). Static and cyclic direct shear tests on carbonate sands. *Geotechnical Testing Journal*, 15(2), 138–157.

Anthony, J. L., et Marone, C. (2005). Influence of particle characteristics on granular friction. *J. Geophys. Res.*, 110(B08409).

Arthur, J.R.F., Dunstan, T., Al-Ani, G.A.J.L. , et Assadi, A. (1997). Plastic deformation and failure in granular media. *Géotechnique*, 27(1), 53–74.

Arthur, JRF, Dalili, A, et Dunstan, T. (1988). Discussion on the engineering application of direct and simple shear testing. *Géotechnique*, 38(1), 140–144.

ASTM (American Society for Testing and Materials). (1990). Standard Test Method for Direct Shear Test of Soils Under Consolidated Drained Conditions. *ASTM D 3080*, West Conshohocken, PA, 417–422.

ASTM (American Society for Testing and Materials). (2001a). Standard test methods for laboratory compaction characteristics of soil using modified effort (56,000 ft-lbf/ft3, 2,700 kN-m/m3). *ASTM D 1557-00*, West Conshohocken, PA.

ASTM (American Society for Testing and Materials). (2001b). Standard test methods for maximum index density and unit weight of soils using a vibratory table. *ASTM D 4253-00*, West Conshohocken, PA.

ASTM (American Society for Testing and Materials). (2001c). Standard test Methods for minimum index density and unit weight of soils and calculation of relative density. *ASTM D 4254-00*, West Conshohocken, PA.

Baligh, M. M. (1976). Cavity expansion in sands with curved envelopes. *J. Geotech. Eng., ASCE*, 102(11), p. 1131–1145.

Bardet, J. P. (1990). Hypoplastic model for sands. *J. Engi. Mech.*, 116(9), 1973–1994.

Bardet, J. P. (1994). Observations on the effects of particle rotations on the failure of idealized

granular materials. *Mechanics of Materials*, 18(2), 159–182.

Bathurst, R. (1985). A study of stress and anisotropy in idealized granular assemblies. Ph.D. Dissertation, Queen`s University, Kingston, Ontario, Canada.

Bathurst, R. J., et Rothenburg, L. (1990). Observations on stress-force-fabric relationships in idealized granular materials. *Mechanics of Materials*, 9(1), 65–80.

Been, K., et Jefferies, M. (1985). A state parameter for sands. *Géotechnique*, 35(2), 99–112.

Billam, J. (1972). Some Aspects of the Behaviour of Granular Materials at High Pressure-Stress-Strain Behaviour of Soils. *Proc. Roscoe Memorial Symp.*, Cambridge, UK, 69–80.

Bishop, A. W. (1948). A large shear box for testing sands and gravels. *Proc. 2nd international Conf. Soil Mech. Found. Eng.*, 207–211.

Bishop, A. W. (1954). The pore pressure coefficients A and B. *Géotechnique*, 4(4), 143–147.

Bolton, M. D. (1986). The strength and dilatancy of sands. *Géotechnique*, 36(1), 65–78.

Bowden, F. P., Moore, A. J. W., et Tabor, D. (1943). The ploughing and adhesion of sliding metals. *Journal of Appl. Phys.*, 14(80), 80–91.

Bowles, J. E. (1996). *Foundation analysis and design.* 5th Ed., McGraw- Hill Companies, Inc., New York, US.

Briaud, J. L., et Gibbens, R. M. (1999). Behavior of five large spread footings in sand. *J. geotech. geoenviron. eng.*, 125(9), 787–796.

Bromwell, L. G. (1966). The Friction of Quartz in High Vacuum. Research report R66-18, Massachusetts Institute of Technology, Cambridge, Mass.

Budhu, M. (2007). *Soil mechanics and foundations.* 2nd Ed., John Wiley and Sons, Inc., New Jersey, US.

Carnek, B., Dvorak, A., Hlavacek, J., Klein, K., et Patrasek, J. (1973). New apparoaches to problems of bearing capacity and settlement of piles. *Proc. 8th Int. Conf. Soil. Mech.*

Found. Eng., Moscow, Russia, 67–74.

Casagrande, A. (1936). Characteristics of Cohesionless Soils Affecting the Stability of Slopes and Earth Fills. *J. Boston Soc. Civ. Eng.*, 23(1), 13–32.

Casagrande, A., et Albert, S. G. (1930). *Research on the Shearing Resistance of Soils.* Massachusetts Institute of Technology Report, Cambridge, MA,United States.

Cavarretta, I., Coop, M., et O'Sullivan, C. (2010). The influence of particle characteristics on the behaviour of coarse grained soils. *Géotechnique*, 60, 413–423.

Cerato, AB, et Lutenegger, A. L. (2006). Specimen size and scale effects of direct shear box tests of sands. *Geotechnical Testing Journal*, 29(6), 1–10.

Chan, L. C. Y., et Page, N. W. (1997). Particle fractal and load effects on internal friction in powders. *Powder Technol.*, 90, 259–266.

Clark, J. I. (1998). The settlement and bearing capacity of very large foundations on strong soils: 1996 R.M. Hardy keynote address. *Can. Geot. J.*, 35, 131–145.

Collins, I. E., Pender, M. J., et Wang, Y. (1992). Cavity expansion in sands under drained loading conditions. *Int. J. Numer. Anal. Met. Geomech.*, 16(1), 3–23.

Coulomb, C. A. (1773). In Memories de Mathematique et de Physique. *Academie Royal des Sciences par divers sans)*, 7, 343–382.

Cubrinovski, M., et Ishihara, K. (1999). Empirical correlation between SPT N-value and relative density for sandy soils. *Soils Found.*, 39(5), 61–71.

Cubrinovski, M., et Ishihara, K. (2002). Maximum and minimum void ratio characteristics of sands. *Soils Found.*, 42(6), 65–78.

Cui, L., et O'Sullivan, C. (2006). Exploring the macro- and micro-scale response of an idealised granular material in the direct shear apparatus. *Géotechnique*, 56(7), 455–468.

Cundall, P. A., et Strack, O. D. L. (1979). A discrete numerical model for granular assemblies.

Géotechnique, 29(1), 47–65.

Davis, E. H. (1968). Theories of plasticity and the failure of soil masses. *Soil mech.: Selected tops.*, K. l. Lee, ed., London, UK, 341–380.

Dyer, MR, et Milligan, G. W. E. (1984). A photoelastic investigation of the interaction of a cohesionless soil with reinforcement placed at different orientations. *International Conference on In-Situ Soil Rock Reinforcemen*, Paris, France.

Dyer, M. R. (1985). *Observation of the stress distribution in crushed glass with applications to soil reinforcement*. Ph.D. Dissertation, University of Oxford, Oxford, UK.

Eslami, A., Fellenius, B. H., et Veiskarami, M. (2004). Problems on determination of shallow foundations bearing pressure by analytical approach. *Proc. 1st National Congress of Civil Engineering*, Sharif University of Technology, Tehran, Iran.

Fellenius, B. H., et Altaee, A. (1994). Stress and settlement of footings in sand. *Proc. Conference on Vertical and Horizontal Deformations for Foundations and Embankments, ASCE, Geotechnical Special Publication, GSP ,* College Station, TX, USA, 2(40), 1760–1773.

Frank, R., et Tadjbakhsh, S. (1986). Finite element study of pile axial behaviour in elasto-plastic dilating media. *Proc. 3rd Int. Conf. on Numerical Methods in Offshore Piling.*, Nantes, France, 201–217.

Gibson, R. E., et Anderson, W. F. (1961). In-situ measurement of soil properties with the pressuremeter. *Civil Eng. Public Works Rev.*, 56(658), 615–618.

Goddard, J. D., et Bashir, Y. B. (1990). On Reynolds dilatancy. *Recent developments in structured continua*, D. DeKee and P. N. Kaloni, eds., Pitman Res. Notes in Math. Series No. Pitman Res. Notes in Math. Series No. 229, Vol. 5, Longmans Greene/Wiley, New York, 23–35.

Goddard, J. D., et Didwania, A. K. (1998). Computations of dilatancy and yield surfaces for assemblies of rigid frictional spheres. *J. Mech. and App. Math.*, 51(1), 14–43.

Gudehus, G. (1996). A comprehensive constitutive equation for granular materials. *Soils Found.*, 36(1), 1–12.

Guo, P. J. (2000). Modelling granular materials with respect to stressdilatancy and fabric: A fundamental approach. PhD dissertation, Civil Engineering Dept., Univ. of Calgary, Alberta, Canada.

Guo, P., et Su, X. (2007). Shear strength, interparticle locking, and dilatancy of granular materials. *Can. Geot. J.*, 44(5), 579–591.

Gutierrez, M. S., et Wang, J. (2010). Discrete element simulations of direct shear specimen scale effects. *Géotechnique*, 60(5), 395–409.

Hansen, C. E. B. (1958). Line ruptures regarded as narrow rupture zones - Basic equations based on kinematic considerations. *Proc. Brussels Conf. on Earth Pressure Problems*, 39–48.

Haruyama, M. (1969). Effects of surface roughness on the shear characteristics of granular materials. *Soils Found.*, 9(4), 48–67.

Head, K. H. (1982). *Manual of soil laboratory testing. Volume 2: Permeability, shear strength and compressibility tests.* Pentech Press, London, UK.

Holtz, R. D., et Kovacs, W. D. (1981). *An introduction to geotechnical engineering*. Prentice-Hall Inc, New Jersey, US.

Horne, H. M., et Deere, D. U. (1962). Frictional Characteristics of Minerals. *Géotechnique*, 12(4), 319–335.

Houlsby, G. T. (1991a). *How the dilatancy of soils affects their behaviour*. Soil Mechanics Report Number 121/91, University of Oxford, Department of Engineering Science, Oxfor, UK.

Houlsby, G. T. (1991b). How the dilatancy of soils affects their behaviour. *Proce. 10th Europ. Conf. of Soil Mech. and Found. Eng.*, 4, 1189–1202.

Hughes, J. M. O., Wroth, C. P., et Windle, D. (1977). Pressuremeter test in sands. *Géotechnique*,

27(4), 455–477.

Ishihara, K. (1993). Liquefaction and Flow Failure during Earthquake. *Géotechnique*, 43, 351–415.

Ismael, N. F. (1985). Allowable pressure from loading tests on kuwaiti soils. *Can. Geot. J*, 22, 151–157.

Jahanandish, M., Veiskarami, M., et Ghahramani, A. (2010). Effect of stress level on the bearing capacity factor, Nγ , by the ZEL method. *KSCE Journal of Civil Engineering,* 14(5), 709–723.

Jardine, R., et Christoulas, S. (1991). Recent deveopments in defining and measuring static piling parameters. *Int. Conf. on deep foundations*, Paris, France.

Jewell, R. A. (1989). Direct Shear Test on Sand. *Géotechnique*, 39(2), 309–322.

Jewell, R. A., et Wroth, C. P. (1987). Direct shear tests on reinforced sand. *Géotechnique*, 37(1), 53–68.

Johnson, I. W., Carter, J. P., Novello, E. A., et Ooi, L. H. (1988). Constant normal stiffness direct shear testing of calcarenite. *Proc. Int. Conf. on Calcareous Sediments*, Perth, Australia, 541–554.

De Josselin de Jong, G. (1976). Rowe's Stress-Dilatancy Relation based on Friction. *Géotechnique*, 26(3), 527–534.

King, G. J. W., et Dickin, E. A. (1970). Comparison of stress dilatancy theory. *J. Soil Mech. Foun. Div., ASCE*, 96(5), 1697–1714.

Kirkpatrick, W. M. (1965). Effect of grain size and grading on the shearing behavior of granular materials. *Proc. 6th Int. Conf. Soil Mech. Found. Engi.*, Montreal, Canada, 273–277.

Koerner, R. M. (1970). Effect of particle characteristics on soil strength. *J. Soil Mech. Foun. Div., ASCE*, 96(4), 1221–1234.

Krey, H. . (1926). *Erddruck, Erdwiderstand und Tragfähigkeit des Baugrundes.* Wilhelm Ernest and Son, Berlin, Berlin, Germany.

Lade, P. V., Liggio, C. D., et Yamamuro, J. A. (1998). Effects of non-plastic fines on minimum and maximum void ratios of sand. *Geotech. Test. J., ASTM*, 21(4), 336–347.

Lee, K. l., et Seed, H. (1967). No TitleDrained strength characteristics of sands. *J. Soil Mech. Found. Div., ASCE*, 93(6), 117–141.

Li, Y. R., Aydin, A., Xu, Q., et Chen, J. (2012). Constitutive behavior of binary mixtures of kaolin and glass beads in direct shear. *KSCE J. Civil Eng.*, 16(7), 1152–1159.

Lings, M. L., et Dietz, M. S. (2004). An improved direct shear apparatus for sand. *Géotechnique*, 54(4), 245–256.

Liu, S., et Matsuoka, H. (2003). Microscopic interpretation on a stress-dilatancy relationship of granular materials. *Soils Found.*, 43(3), 73–84.

Maeda, K., et Miura, K. (1999). Confining stress dependency of mechanical properties of sands. *Soils Found.*, 39(1), 53–67.

Mair, K., Frye, K. M., et Marone, C. (2002). Influence of grain characteristics on the friction of granular shear zones. *J. Geophys. Res.*, 107(B10), 1–9.

Marshall, A. M., Farrell, R. P., Klar, A., et Mair, R. J. (2012). 2012. Tunnels in sands the effect of size, depth, and volume loss on greenfield displacements. *Géotechnique*, 62(5), 385–399.

Masson, S., et Martinez, J. (2001). NoMicromechanical analysis of the shear behavior of a granular material. *ASCE Journal of Engineering Mechanics*, 127(10), 1007–1016.

Matsuoka, H. (1974). Dilatancy characteristics of soils. *Soils Found.*, 14(3), 45–53.

Meyerhof, G. G. (1963). Some recent research on the bearing capacity of foundations. *Can. Geot. J.*, 1, 16–26.

Michalowski, R. L. (1997). An estimate of the influence of soil weight on bearing capacity using limit analysis. *Soils Found.*, 37(4), 57–64.

Miura, K., Maeda, K., Furukawa, M., et Toki, S. (1997). Physical characteristics of sand with different primary properties. *Soils Found.*, 37(3), 53–64.

Miura, K., Maeda, K., Furukawa, M., et Toki, S. (1998). Mechanical characteristics of sands with different primary properties. *Soils Found.*, 38, 159–172.

Molenkamp, F. (1981). *Elasto-plastic double hardening model Monot.* LGM Report CO-218595, Delft Geotechnic, Delft, Netherland.

Morgan, J. (1999). Numerical simulations of granular shear zones using the distinct element method: 2. Effects of particle size distribution and interparticle friction on mechanical behavior. *J. Geophys. Res.*, 104(B2), 2721–2732.

Morgenstern, N. R., et Tchalenko, J. S. (1967). Microscopic structure in kaolin subjected to direct shear. *Géotechnique*, 17(4), 309–328.

Muszynski, M. R. (2006). Determination of maximum and minimum densities of poorly graded sands using a simplified method. *Geotech.Test. J., ASTM*, 29(3), 263–272.

Nakai, T. (1997). Dilatancy characteristics of geomaterials. *Deformation and Progressive Failure in Geomaterials, IS-Nagoya'97*, A. Asaoka, T. Adachi, and F. Oda, eds., 899–906.

Negussey, D., Wijewickreme, W. K. D., et Vaid, Y. P. (1988). Constant volume friction angle of granular materials. *Can. Geot. J.*, 25(1), 50–55.

Nemat-Nasser, S. (1980). On behaviour of granular soils in simple shear. *Soils Found.*, 20(1), 59–73.

Nemat-Nasser, S. (2000). A micromechanically-based constitutive model for frictional deformation of granular materials. *J. Mech. Phys. Solids*, 48, 1541–1563.

Newland, P. L., et Allely, B. H. (1957). Volume changes in drained triaxial tests on granular materials. *Géotechnique*, 7(1), 17–34.

Ni, Q, Powrie, W., Zhang, X., et Harkness, R. (2000). Effect of particle properties on soil behaviour: 3-D numerical modelling of shear box tests. *ASCE Geotechnical Special Publication*, 96, 58–70.

Nova, R., et Wood, D. M. (1979). A constitutive model for sand in triaxial compre.ssion. *Int J. Numer. Analyt. Meth. Geomech.*, 255–278.

Oda, M, et Konishi, J. (1974). Microscopic deformation mechanism of granular material in simple shear. *Soils Foundations*, 14(4), 25–38.

Oda, M. (1972). The mechanism of fabric changes during compressional deformation of sand. *Soils Found.*, 12(2), 1–18.

Oda, M. (1976). *Fabric and their effects on the deformation behavior of sand.* Special Issue: Department of Foundation Engineering, Faculty of Engineering, Saitama University, Japan.

Oda, M. (1977). Co-irdination number and its relation to shear strength of granular material. *Soils and Foundations*, 17(2), 29–42.

Oda, M., et Kazama, H. (1998). Microstructure of shear bands and its relation to the mechanisms of dilatancy and failure of dense granular soils. *Géotechnique*, 48(4), 465–481.

Pedley, M. J. (1990). *Experimental study of soil reinforcement interactions.* Ph.D. Dissertation, University of Oxford, Oxford, UK.

Peña, A. A., García-Rojo, G., et Herrmann, H. J. (2007). Influence of particle shape on sheared dense granular media. *Granul. Matter*, 9, 279–291.

Perkins, S. W., et Madson, C. R. (2000). Bearing capacity of shallow foundations on sand: a relative density approach. *J. geotech. geoenviron. eng.*, 126(6), 521–530.

Potts, D., Dounias, G., et Vaughan, P. R. (1987). Finite element analysis of the direct shear box test. *Géotechnique*, 37(1), 11–23.

Pradhan, T. B. S., Tatsuoka, F., et Sato, Y. (1989). Experimental stress dilatancy relations of

sand subjected to cyclic loading. *Soils Found.*, 29, 450–64.

Procter, D. C., et Barton, R. R. (1974). Measurements of the angle of interparticle friction. *Géotechnique*, 24(4), 581–604.

Reynolds, O. (1885). On the dilatancy of media composed of rigid particles in contact. *Philos. Mag.*, 5(2), 469–482.

Roscoe, K. H. (1970). The influence of strains in soil mechanics. *Géotechnique*, 20(2), 129–170.

Rothenburg, L. (1981). *Micromechanics of idealized granular systems*. Ph.D. Dissertation, Ottawa, Ontario, Canada: Carleton University;1981

Roubtsova, V., Chekired, M., Karray, M., et Amirpour, S. (2015). Work-energy balance for discrete element method. *Congresso de Métodos Numéricos em Engenharia*, Lisboa, Portugal.

Roubtsova, V., Chekired, M., Morin, B., et Karray, M. (2011). 3D virtual laboratory for geotechnical applications: Another perspective. *Proc. 2nd Int. Conf. Particle-Based Meth.*, 342–353.

Rowe, P. W. (1962). The Stress-Dilatancy Relation for Static Equilibrium of an Assembly of Particles in Contact. *Proc. Royal Soc. London: Math., Phys. Eng. Scien.*, A269(1339), 500–527.

Rowe, P. W. (1969). The relation between the shear strength of sands in triaxial compression, plane strain and direct shear. *Géotechnique*, 19(1), 75–86.

Saada, AS, et Townsend, F. C. (1981). State of the art: laboratory strength testing of soils. *laboratory shear strength of soil, ASTM STP 740*, Philadelphia, PA., 7–77.

Salgado, R., et Randolph, M. F. (2001). Analysis of Cavity Expansion in Sand. *Int. J. Geomech.*, 1(2), 175–192.

Sammis, C. G., King, G., et Biegel, R. (1987). The kinematics of gouge deformation. *Pure Appl.*

Geophys., 125, 777–812.

Santamarina, J. C., et Cho, G. C. (2004). Soil behavior: The Role of Particle Shape. *In Advances in geotechnical engineering. The Skempton Conference.*, Thomas Telford, London, UK, 604–617.

Schanz, A., et Vermeer, T. P. (1996). Angle of friction and dilatancy of sand. *Géotechnique*, 46(1), 145–151.

Schofield, A. N., et Wroth, C. P. (1968). *Critical State Soil Mechanics.* McGraw-Hill, London, UK.

Seed, HB, et Idriss, I. (1971). Simplified procedure for evaluating soil liquefaction potential. *Journal Soil Mechanics Foundations Division*, 97, 1249–1273.

Seed, HB, et Lee, K. L. (1966). Liquefaction of saturated sands during cyclic loading. *Journal Soil Mechanics Foundations Division*, 92, 105–134.

Shibuya, S., Mitachi, T., et Tamate, S. (1997). Interpretation of direct shear testing of sands as quasi-simple shear. *Géotechnique*, 47(4), 769–790.

Simoni, A., et Houlsby, G. T. (2006). The direct shear strength and dilatancy of sand-gravel mixtures. *Geot. Geol. Eng.*, 24(3), 523–549.

Skempton, A. W. (1949). Alexandre Collin: a note on his pioneer work in soil mechanics. *Géotechnique*, 1(4), 216–221.

Skempton, A. W., et Bishop, A. W. (1950). The measurement of the shear strength of soils. *Géotechnique*, 2(2), 90–108.

Skinner, A. E. (1969). note on the influence of interparticle friction on the shearing strength of a random assembly of spherical particles. *Géotechnique*, 19(1), 150–157.

Stroud, M. A. (1971). *The behaviour of sand at low stress levels in the simple shear apparatus.* University of Cambridge, Cambridge, UK.

Sukumaran, B., et Ashmawy, A. (2001). Quantitative Characterization of the geometry of Discrete Particles. *Géotechnique*, 51(7), 619–627.

Tatsuoka, F., Nakamura, S., Huang, C. C., et Tani, K. (1990). Strength anisotropy and shear band direction in plane strain tests of sand. *Soils Found.*, 30(1), 35–54.

Taylor, D. W. (1948). *Fundamentals of soil mechanics.* John Wiley and Sons Inc., New York, US.

Terzaghi, K. (1920). Old earth-pressure theories and new test results. *Engineering News Record*, 85(14), 632–637.

Terzaghi, K. (1943). *Theoretical Soil Mechanics*. John Wiley and Sons, Inc., New York, US.

Terzaghi, K., et Peck, R. B. (1948). *Soil mechanics in engineering practice.* Wiley, New York.

Thornton, C. (2000). Numerical simulation of deviatoric shear deformation of granular media. *Géotechnique*, 50(1), 43–53.

Tokue, T. (1979). Deformation behaviours of dry sand under cyclic loading and a stress-dilatancy model. *Soils Found.*, 19(2), 63–78.

Vaid, Y. P., Byrne, P. M., et Hughes, J. M. o. (1981). Dilation Angle and Liquefaction Potential. *Proceedings on Recent Advances in Geotechnical Earthquake Engineering and Soil Dynamics*, St. Louis, Missouri, 161–165.

Vaid, Y. P., et Sasitharan, S. (1992). The strength and dilatancy of sand. *Can. Geot. J.*, 29, 522–526.

Veiskarami, M., Jahanandish, M., et Ghahramani, A. (2011). Prediction of the bearing capacity and load–displacement behavior of shallow foundations by the stress-level-based ZEL method. *Scientia Iranica*, 18(1), 16–27.

Vermeer, P. (1982). A five-constant model unifying well-established concepts. *Int. Workshop on Constitutive Behaviour of Soils*, Grenoble, Balkema, 175–197.

Vesic, A. S. (1972). Expansions of cavities in infinite soil mass. *J. Soil Mech. Foun. Eng., ASCE*, 98(3), 265–290.

Vesic, A. S. (1973). Analysis of ultimate loads of shallow foundations. *J. Soil Mech. Foun. Div., ASCE*, 99(1), 45–73.

Vesic, A. S., et Clough, G. W. (1968). Behaviour of granular materials under high stresses. *J. Soil Mech. Found. Div., ASCE*, 94(3), 661–688.

Wan, R. G., et Guo, P. J. (1998). A simple constitutive model for granular soils: Modified stress-dilatancy approach. *Comp. Geot.*, 22(2), 109–133.

Wan, R. G., et Guo, P. J. (1999). A pressure and density dependent dilatancy model for granular materials. *Soils Found.*, 39(6), 1–11.

Wan, R. G., et Guo, P. J. (2000). Effect of microstructure on undrained behavior of sands. Canadian Geotechnical Journal. *Can. Geot. J.*, 38, 16–28.

Wan, R. G., et Guo, P. J. (2001). Effect of fabric on strain localization of sands. *Proc. 1st. Asia-Pacific Conf. on Computational Mechanics*, Sydney, Australia, 503–508.

Wang, J., Dove, J. E., et Gutierrez, M. S. (2007). Discrete-continuum analysis of shear banding in the direct shear test. *Géotechnique*, 57(6), 513–526.

Wijewickreme, W. K. D. (1986). *Constant volume friction angle of granular materials.* M.Sc. Dissertation, University of British Columbia, Vancouver, Canada.

Wu, P. K., Matsushima, K., et Tatsuoka, F. (2008). (2008). Effects of specimen size and some other factors on the strength and deformation of granular soil in direct shear tests. *Geotech. Test. J., ASTM*, 31(1), 1–20.

Yamaguchi, H., Kimura, T., et Fujii, N. (1976). On the influence of progressive failure on the bearing capacity of shallow foundation in dense sand. *Soils Found.*, 16(4), 11–22.

Yoshimine, M., Ishihara, K., et Vargas, W. (1998). Effects of principal stress direction and intermediate principal on undrained shear behavior of sand. *Soils Found.*, 38(3), 178–188.

Youd, T. L. (1973). Factors controlling maximum and minimum densities of sands. Evaluation of Relative Density and its Role in Geotechnical Projects Involving Cohesionless Soils. *STP 523, ASTM International*, West Conshohocken, PA, 98–112.

Yu, H. S. (1990). *Cavity expansion theory and its application to the analysis of pressuremeters.* Ph.D. Dissertation, University of Oxford, Oxford, UK.

Yu, H. S., et Houlsby, G. T. (1991). Finite cavity expansion in dilatant soils: loading analysis. *Géotechnique*, 41(2), 173–183.

Yu, H. S., et Rowe, R. K. (1999). Plasticity solutions for soil behaviour around contracting cavities and tunnels. *J. Numer. Anal. Meth. Geomech.*, 23(12), 1245–1279.

Zelasko, J. S., Krizek, R. J., et Edil, T. B. (1975). Shear Behavior of Sands as a function of grain characteristics. *Proc. Istanbul Con. Soil Mech. Turkish National Soc. of Soil Mech. Found. Eng.*, Istanbul, Turkey, 55–64.

Zhang, L., et Thornton, C. (2007). A numerical examination of the direct shear test. *Géotechnique*, 57(4), 343–354.

Zienkiewicz, O. C., Humpheson, C., et Lewis, R. W. (1975). Associative and non-associative visco-plasticity and plasticity in soil mechanics. *Géotechnique*, 25(4), 671–689.